TECHNICAL REPORT No. 41

SYSTEMATIC ERRORS IN THE BAROCLINIC WAVES OF THE ECMWF MODEL

by

E. Klinker and M. Capaldo*

February 1984

*Present affiliation
Centro Nazionale Di Climatologia
e Meteorologia Aeronautica
Rome, Italy

C O N T E N T S

ABSTRACT

The space-time spectral analysis technique is used to investigate the forecast errors of the baroclinic waves in the ECMWF forecast model. The study concentrates on two groups of disturbances, the medium frequency baroclinic waves (MFBW: wavenumber 4 to7, period 3.6 to 10.3 days) and the high frequency baroclinic waves (HFBW: wavenumber 5 to 9, period 2.4 to 3.5 days).

Both mid-latitude wave types suffer a considerable weakening in the early stages of the forecast. The geographical distribution of this error shows the largest decrease over North America and the North Atlantic. A close connection between the forecast changes in the baroclinic waves and the time-mean state is indicated by the decrease of the baroclinicity of the mean flow over North America. In the Pacific region an increased baroclinicity seems to be responsible for increased wave activity in the high frequency range.

An increase of the SW to NE phase tilt of the MFBW's at low latitudes seems to be due to problems in the interaction of deep baroclinic waves with the tropical flow. In the vertical, the forward tilt of the temperature waves increases during the forecast.

1. INTRODUCTION

Space-time spectral analysis has become a widely used tool for studying the large scale travelling disturbances for both the observed and the simulated general circulation of the atmosphere. A review of the methods and applications by Hayashi (1981) demonstrates the power of this analysis to investigate the characteristics, structure and energetics of travelling waves in a wide range of time and space scales.

The application of the space-time decomposition technique to general circulation model output (Hayashi, 1974; Hayashi and Golder, 1977) and to observations or to both (e.g. Pratt, 1977 and 1979; Böttger and Fraedrich, 1980; Strauss and Shukla, 1981) reveals some differences in the transient wave statistics between models and the real atmosphere. However, wave statistics from the general circulation experiments may depart from those observed due to large changes in the mean zonal flow of the forecast as well as through differences in the treatment of the transient waves themselves. Compared to long integrations, the short to medium range forecast can be seen as a much closer realisation of real atmospheric wave activity. At the beginning of the forecast when the changes of the mean zonal flow are still rather small, it will be easier to understand the mechanisms which cause the differences in the wave statistics between the analysis and the forecast. To investigate these differences we will compare the space-time spectrum of forecast ensembles with the spectrum calculated from the corresponding analyses. We will spectrally analyse the ensembles of one day forecasts, two day forecasts etc; each of these ensembles can be thought of as a realisation of a model atmosphere, provided the forecasts are sufficiently accurate to give reasonable time continuity.

In Section 2 we describe the data for the study while Section 3 discusses the methodology. The time-mean state of the atmosphere and the changes in the forecast are discussed in Section 4. The results are presented in Sections 5 to 7. In Section 5 we examine the inconsistencies in successive forecasts. In Sections 6 and 7 the forecast errors for two wavenumber frequency groups (medium frequency baroclinic waves and high frequency baroclinic waves) are discussed in detail.

2. DATA

The data used in this study was extracted from the ECMWF analysis and forecast archive. The observational data set for the space-time decomposition consists of 112 initialized analyses valid for 12 GMT starting from 20 November and ending at 11 March for the two winter seasons 1980/81 and 1981/82. Some calculations have been extended to cover the 1982/83 winter as well. The initialized analysis is the final product of the ECMWF data assimilation system (Bengtsson et al. 1982). From this analysis the 10 day forecast is run operationally on a daily basis; major features of the forecast system are described in Hollingsworth et al. (1980). From the 10 day forecast sets, equal time steps verifying on the same analysis ensemble element number were selected to form a forecast ensemble of the same length as the analysis time series. The wavenumber-frequency analysis was carried out on 9 pressure levels (1000,850,700,500,400,300,200,100,50 mb) and on a latitude band from 25°N to 76°N in 3° intervals. This space domain will be sufficient to look at major features of the mid-latitude baroclinic waves in the northern hemisphere.

The data set for the space-time decomposition is not uniform throughout the period of investigation. A number of changes in the data assimilation system and in the forecast model have been made within the two winters and in the period which separates them. The effect of single changes in the data

assimilation or forecast system on the space-time analysis is difficult to assess, but from the results we will see that the major model errors for the baroclinic waves are very similiar in the two winters. This is not true for the ultra-long waves (to be discussed in a later paper), for which the model error has a large inter-annual variability. The reduction in the error of these waves between winter 1981/82 and in the previous one can probably be explained by the introduction of higher mountains in April 1981. Recent experiments (Wallace et al. 1983) at the ECMWF have shown that a further increase in the height of the models mountains reduces the errors in the ultra-long waves even more.

3. METHODOLOGY

As in many other investigations (e.g. Hayashi, 1974; Hayashi and Golder, 1977; Fraedrich and Böttger, 1978; Pratt, 1979; Strauss and Shukla, 1981; Mechoso and Hartmann, 1982) we will use the space and time decomposition technique proposed by Hayashi (1971). In this the disturbances, as defined by deviations from the zonal mean, are decomposed into progressive and retrogressive waves

$$W(x,t) = \sum_{k} \sum_{\omega} R_{k,\pm\omega} \cos (kx \pm \omega t + \phi_{k,\pm\omega})$$

where k is the zonal wavenumber and ω the frequency; $R_{k,-\omega}$, $\phi_{k,-\omega}$ and $R_{k,+\omega}$, $\phi_{k,-\omega}$ are the amplitude and phase angle of the progressive and retrogressive waves respectively. A brief description of the wavenumber-frequency analysis technique is given in appendix A. The interpretation of the amplitudes of progressive and retrogressive waves becomes difficult when a large standing part is present in the transient wave activity (Pratt, 1976). This affects mainly the ultra-long waves in the low frequency range. For the medium frequency and high frequency baroclinic waves discussed here, this problem is negligible as the standing part of the power spectrum is very small compared to the travelling part.

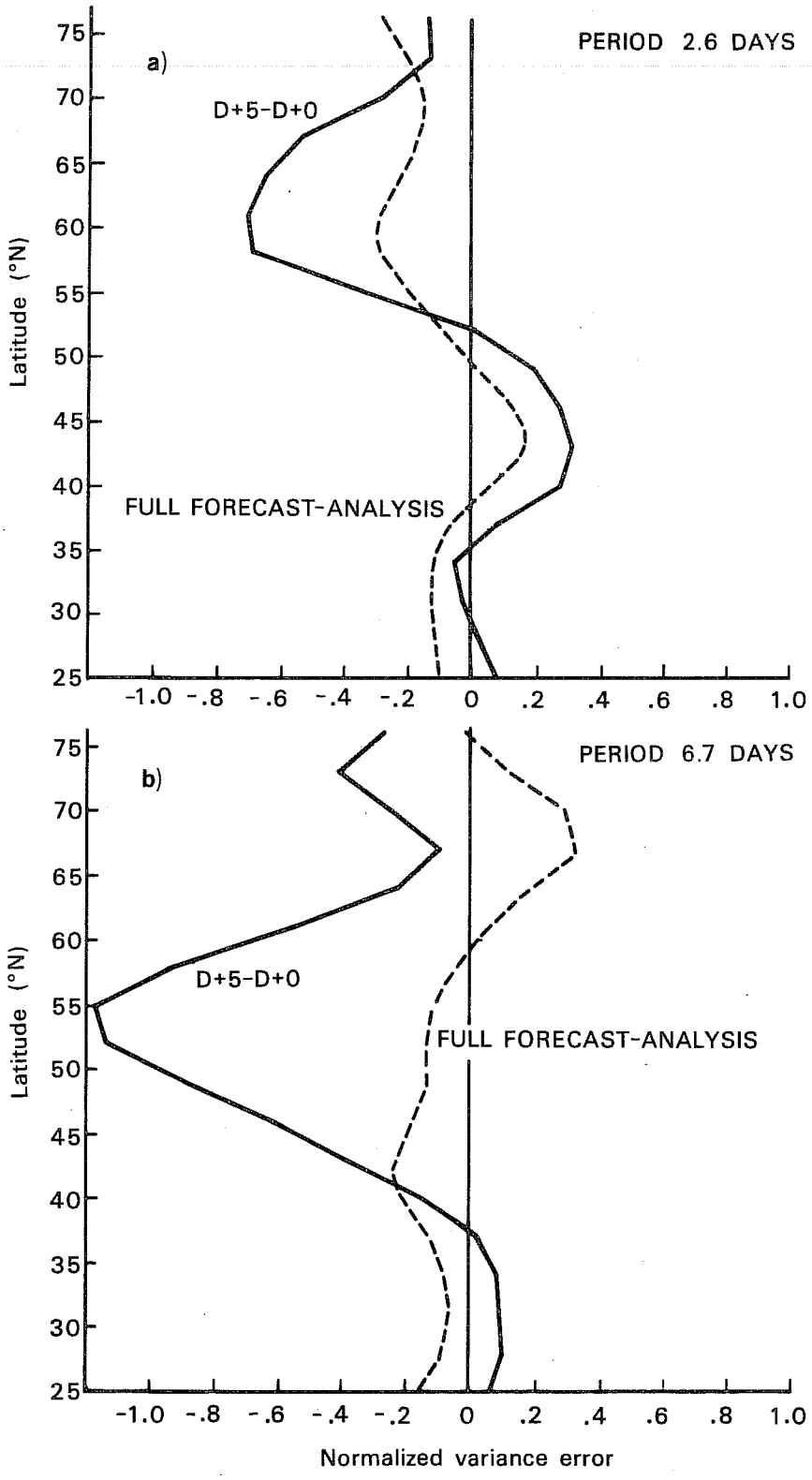

Fig. 1 Forecast error at 500 mb for the ensemble method and full forecast method (for the descriptions of these methods see text). Both panels show the forecast error (forecast-analysis) of the power spectrum integrated over wavenumber (4 to 9) and frequency. Upper panel mean period 2.6 days, lower panel mean period 6.7 days. Ensemble method: continuous line, full forecast method dashed line.

There are two useful ways of applying the space-time spectral analysis to a dataset which consists of a large number of daily forecasts and a continuous time series of analysis data. First the technique can be applied to single forecasts of 10 days duration and to the appropriate verifying analyses; here the time series contain 20 timesteps, each 12 hours apart. This procedure will result in a rather low spectral resolution in time. However, the significance of the spectral estimate can become very high when we average the raw spectrum over a large number of forecasts. This method will be used here only as a comparison to the main approach which we will follow in our investigation. In this technique the input for the space-time decomposition consists of an ensemble of equally advanced forecast steps. With a fairly long timeseries (112 days) which covers a little more than one season, the spectral resolution in time will be rather high. The significance of the spectral estimates is enlarged when we integrate over two spectral intervals which describe the medium frequency and high frequency baroclinic waves. With the calculation of the space-time spectrum for forecast ensembles of certain timesteps we can see changes in the transient waves which develop at different stages of the forecast.

Though the space-time spectral analysis uses the available 10 day forecast data differently in the two methods, major changes in the structure of the faster baroclinic waves during the forecast should affect the high resolution (ensemble method) and low resolution (full forecast method) time spectrum in a similiar way. In Fig. 1 we show the forecast error (forecast minus analysis) in two spectral intervals. Both graphs, the difference between the D+5 ensemble spectrum and the analysis spectrum (continuous line) and the difference between the 10 day forecast spectrum and the 10 day analysis spectrum (dashed line) are drawn with the same scale. To compare the power spectrum in one spectral interval of the low resolution spectrum with the corresponding band in the high resolution spectrum, we integrated the high

resolution spectrum over 11 single intervals. The comparison gives a fairly good agreement for shorter periods (2.6 days), as shown in Fig. 1a, but Fig. 1b shows a less satisfactory agreement for longer periods (6.7 days). The agreement of the two methods in the high frequency range supports our confidence in the results of the space-time spectral analysis of forecast ensembles. In the lower frequencies, where the two methods disagree, the spectrum of 10 day forecasts is very much affected by the short length of the time interval of 10 days and has, therfore, an influence on the variance in the longer periods.

Before we begin the detailed discussion of the ensemble spectral analysis, it is important to consider what kind of forecast errors we can detect when we compare the spectrum of one forecast ensemble with the spectrum of the initialized analysis. During the forecast the baroclinic waves may experience a systematic change in their amplitude, spatial phase structure or phase speed. Systematic amplitude changes will be seen as changes in the variance for particular wavenumber-frequency bands, whilst changes in the spatial phase structure can be detected by level to level cross-spectral analysis (see appendix A) or by latitude to latitude cross-spectral analysis. If the waves are generally too slow or too fast we will see a phase difference in the cross-spectral analysis between the forecast ensembles (D+X) and analysis ensembles.

Apart from the systematic errors, we can expect that the amplitudes and phases will undergo random changes in different forecasts. When the prediction range increases the forecasts diverge from each other and irregularities in the wave phases and amplitudes will enter the time series of the forecast ensemble. This will increase the noise level of the wavenumber-frequency spectrum and will have a smoothing effect where significant peaks are present in the spectrum of the analysis sample.

Generally the spectrum will have a trend towards a white noise spectrum with advancing forecast time.

4. TIME MEAN STATE

The development of baroclinic waves is closely related to the state of the mean zonal flow, as many theoretical investigations and numerical integrations have shown. This will be discussed in connection with the presentation of the results in Section 5. Therefore, when we describe the baroclinic disturbances in terms of deviations from the zonal mean, it is useful to know the time-mean and zonal-mean state for the period for which the spectral analysis has been carried out. In the discussion of the wavenumber-frequency analysis we can then refer to the structure of the mean state. We will be interested in the position of the disturbances relative to the main baroclinic zones of the mean field. Furthermore it will be important to see if changes of the baroclinic waves in the forecast are directly connected to changes in the mean fields. Our description of the mean state will be restricted to the temperature and the zonal component of the wind field. From the temperature field we have calculated the stability in terms of buoyancy frequency squared. The zonal and time averaged fields in the initialised analysis are very similiar in the two winters 1980/81 and 1981/82. As we also found a close agreement in the forecast errors of the mean fields for the two winters, we will present only the results for the second winter. The longitudinal variation of the time-mean flow, however, shows differences in the two winters which are worth showing as they reveal connections with the geographical distribution of the variance of the baroclinic waves (see Sections 6 and 7).

In the zonal mean temperature field (Fig. 2) we find a strong baroclinic zone around 30°N and so the thermal wind equation implies a large vertical increase of the mean zonal flow in this region. The tropopause is well

marked and shows the typical downward slope with increasing latitude. Examination of the difference pattern (D+3 minus D+0) reveals that there is mid-tropospheric cooling and warming near the surface. The mid-tropospheric cooling has a clear minimum at latitudes around 36° to 40°N and the largest temperature changes take place near the low latitude tropopause. Strong cooling in the stratosphere and warming of the upper troposphere indicates that the forecast shifts the tropopause slightly upwards; it also reduces the sharpness of the tropopause.

The stability in terms of buoyancy frequency squared (Fig. 3) is fairly uniform in most of the troposphere. An exception is the lower troposphere at higher latitudes where we have a very small vertical temperature gradient or a low level inversion; also the tropopause is indicated by a marked increase in stabilty. The mid-tropospheric cooling by day 3 leads to a destabilization of the lower troposphere and a more stable upper troposphere (Fig. 4). The stratospheric cooling has a destabilizing effect as well.

The configuration of the mean zonal flow is closely connected to the location and stucture of the baroclinic waves. Fig. 5 shows that the subtropical jet has a maximum above the major baroclinic zone at latitudes around 30° and the axis of the wind maximum tilts equatorward with height. The forecast changes of the mean zonal flow in the winter 1981/82 are almost identical to the errors in the previous winter 1980/81 (not shown here). The pattern of the difference between the forecast and the analysis indicates a poleward and upward shift of the subtropical jet. The geostrophic mean zonal flow has the same difference pattern indicating that the major changes of the zonal flow are coupled with the changes of the thermal structure via the thermal wind equation. The change of the mean zonal flow at middle latitudes has a barotropic part of nearly 1 m s^{-1} due to changes of the surface pressure (Arpe, 1983). The baroclinic changes correspond to an increase of the

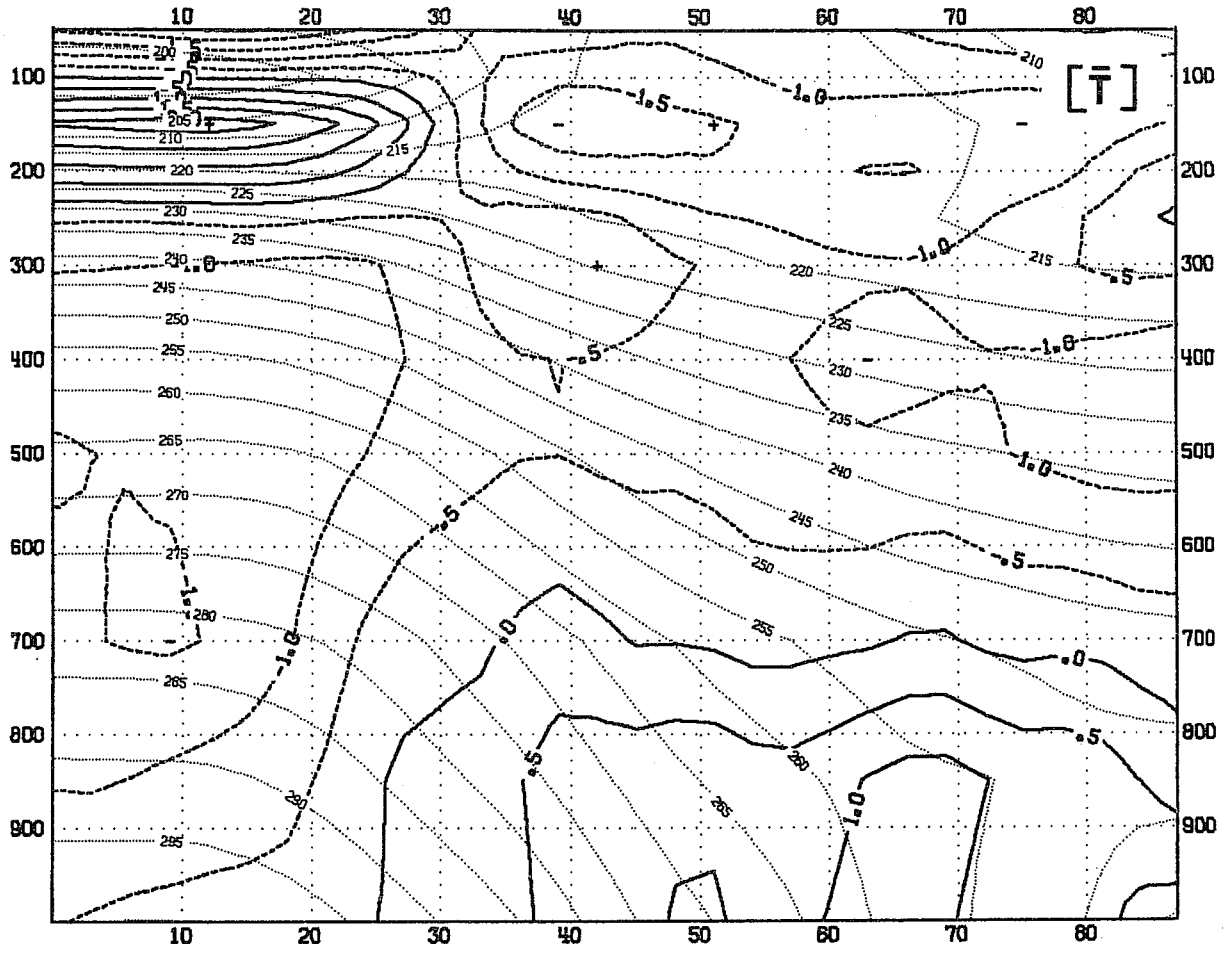

Fig. 2 Latitude-height plot of the zonal and time mean temperature in the initialized analysis (dotted lines) and the difference between the forecast and the analyses (D+3 - D+0, thicker lines). Time averaging period 112 days. Units: K.

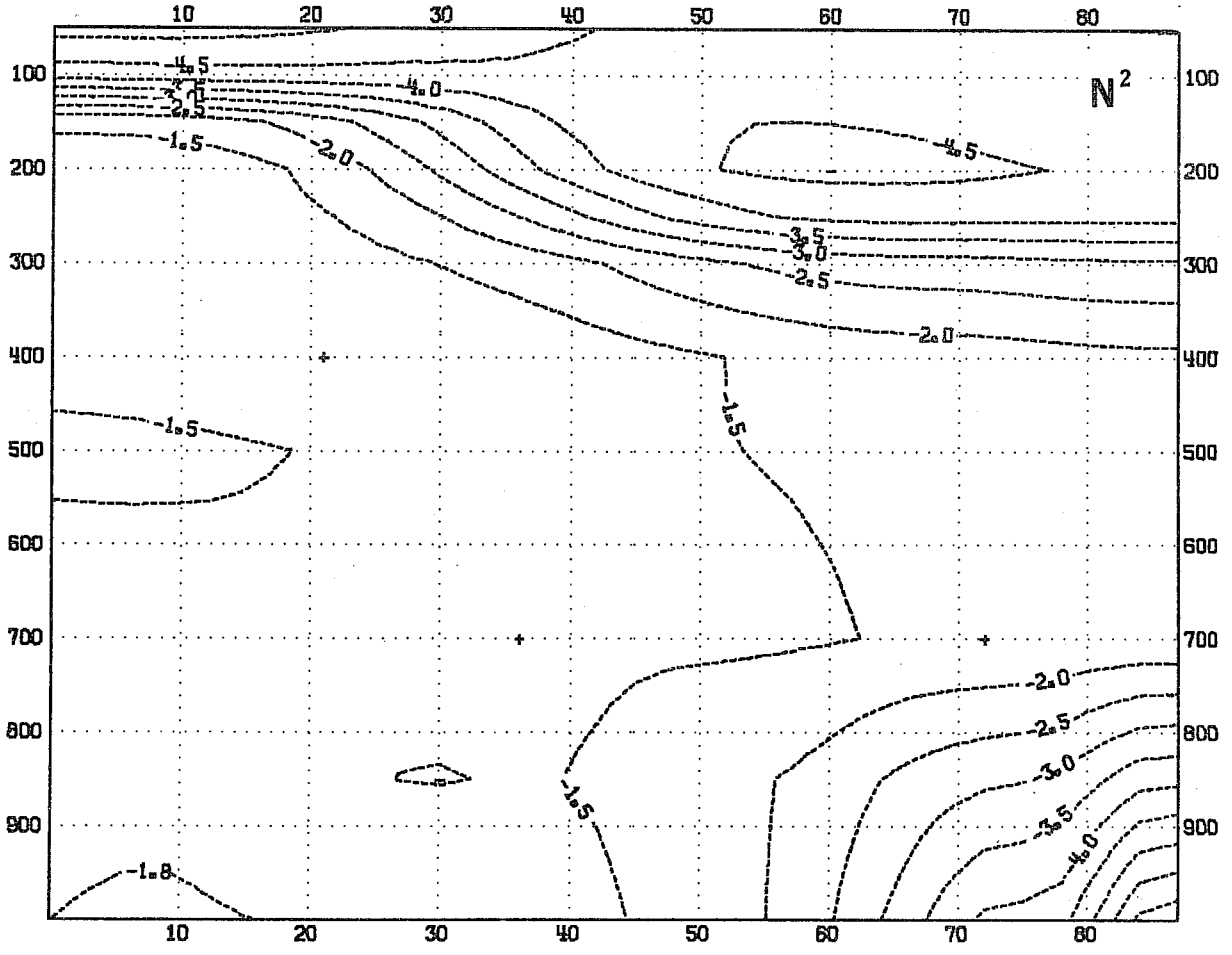

Fig. 3 Latitude-height plot of the stability in terms of buoyancy frequency squared (N^2) calculated from the zonal and time averaged temperature shown in Fig. 1. Winter 1981/82. Units: 10^{-4} s^{-2}

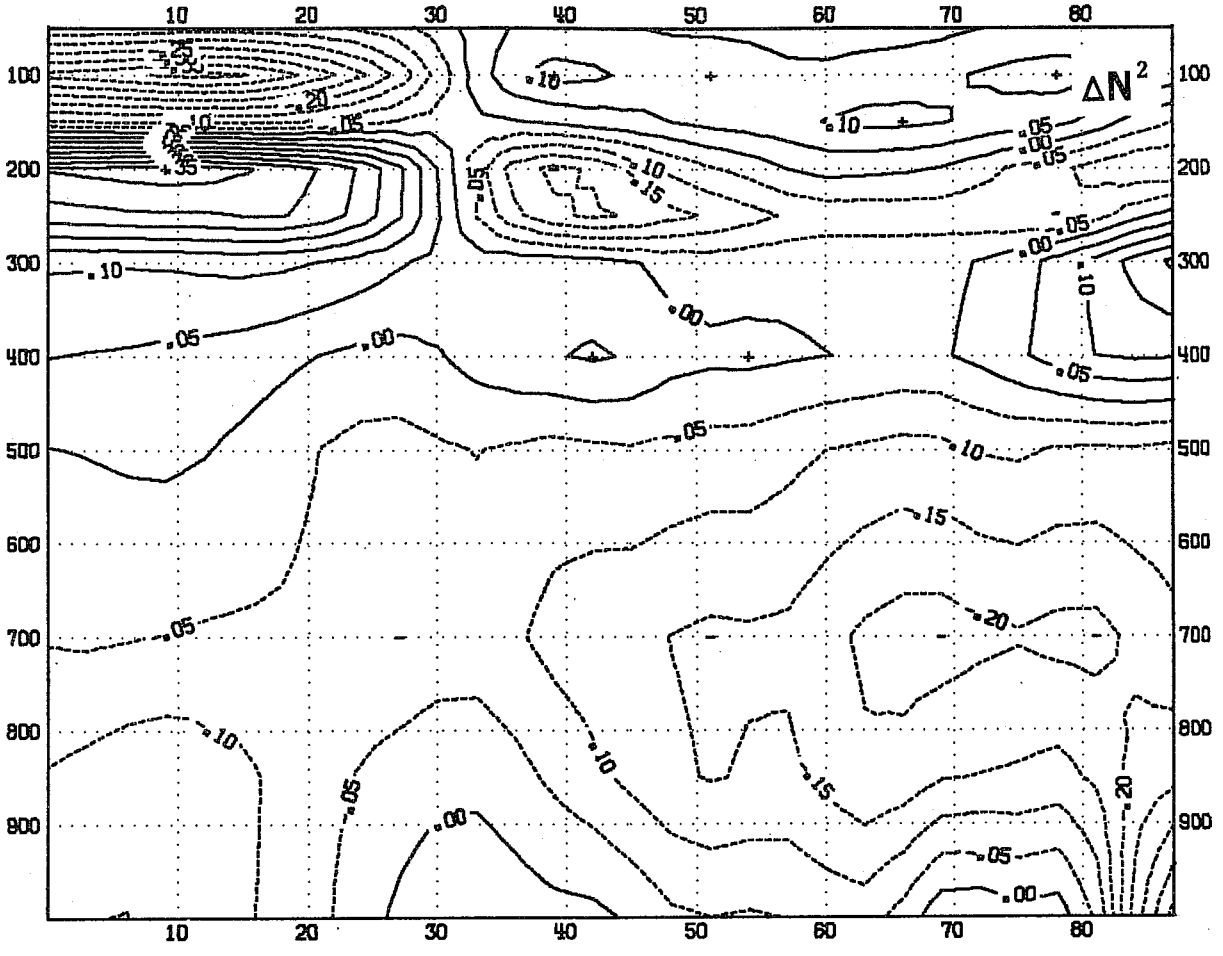

Fig. 4 Latitude-height plot of the difference between the forecast and the analysed (D+3 - D+0) stability N^2. Winter 1981/82. Units: $10^{-4}s^{-2}$.

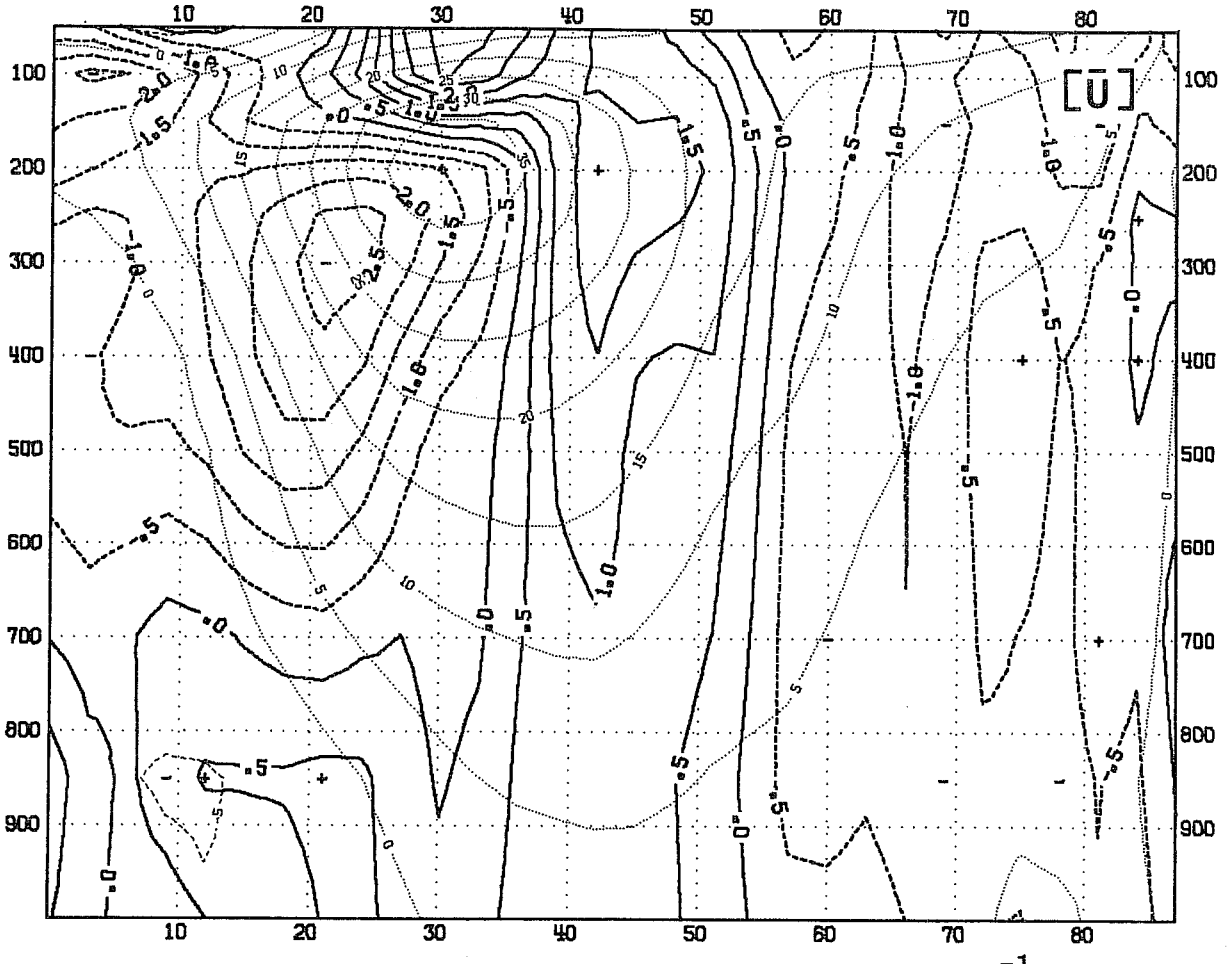

Fig. 5 As Fig. 2 except for the mean zonal wind. Units: ms^{-1}.

baroclinicity at middle latitudes and a decrease at lower latitudes.

The mean flow in the middle troposphere is illustrated by the time-mean geopotential height field at 500 mb (Figs. 6a and 7a). The major troughs over the east coasts of North America and Asia can be found in both winters. Over the west coast of North America the flow pattern is more zonal in the winter 1981/82 than in the previous winter, whereas over the Norwegian Sea a ridge is present in the winter 1981/82 whilst in 1980/81 the flow is more zonal in that region.

The pattern of the forecast error in the height field at 500 mb (Figs. 6b and 7b) has not changed since it was first reported by Hollingsworth et al. in 1980. Only the magnitude of this error has decreased due to improvements in the forecasting system (Arpe, 1983). The negative bias of the forecast over Alaska and the positive one over the Pacific extends the west Pacific frontal zone eastwards. The second persistent forecast error occurs over western Europe were we find another negative bias. Due to this change of the height field the flow directed into southern Europe is intensified. This is a particular feature of the early part of the forecast, since in the later stages the mean circulation changes to a more zonal flow.

5. THE GROWTH OF THE INCONSISTENCY OF SUCCESSIVE FORECASTS

In this section we will investigate the wavenumber-frequency spectrum of forecast ensembles to examine the growth of the noise level due to the inconsistency of successive forecasts. The two-sided spectrum is calculated for the initialized analysis and for three forecast ensembles (D+3,D+5,D+7). The spectral values are calculated for three latitudes 45°,50°, and 55°N. In the figures a cosine weighted mean for this latitude band is shown.

The wavenumber-frequency spectrum of the kinetic energy in the initialized

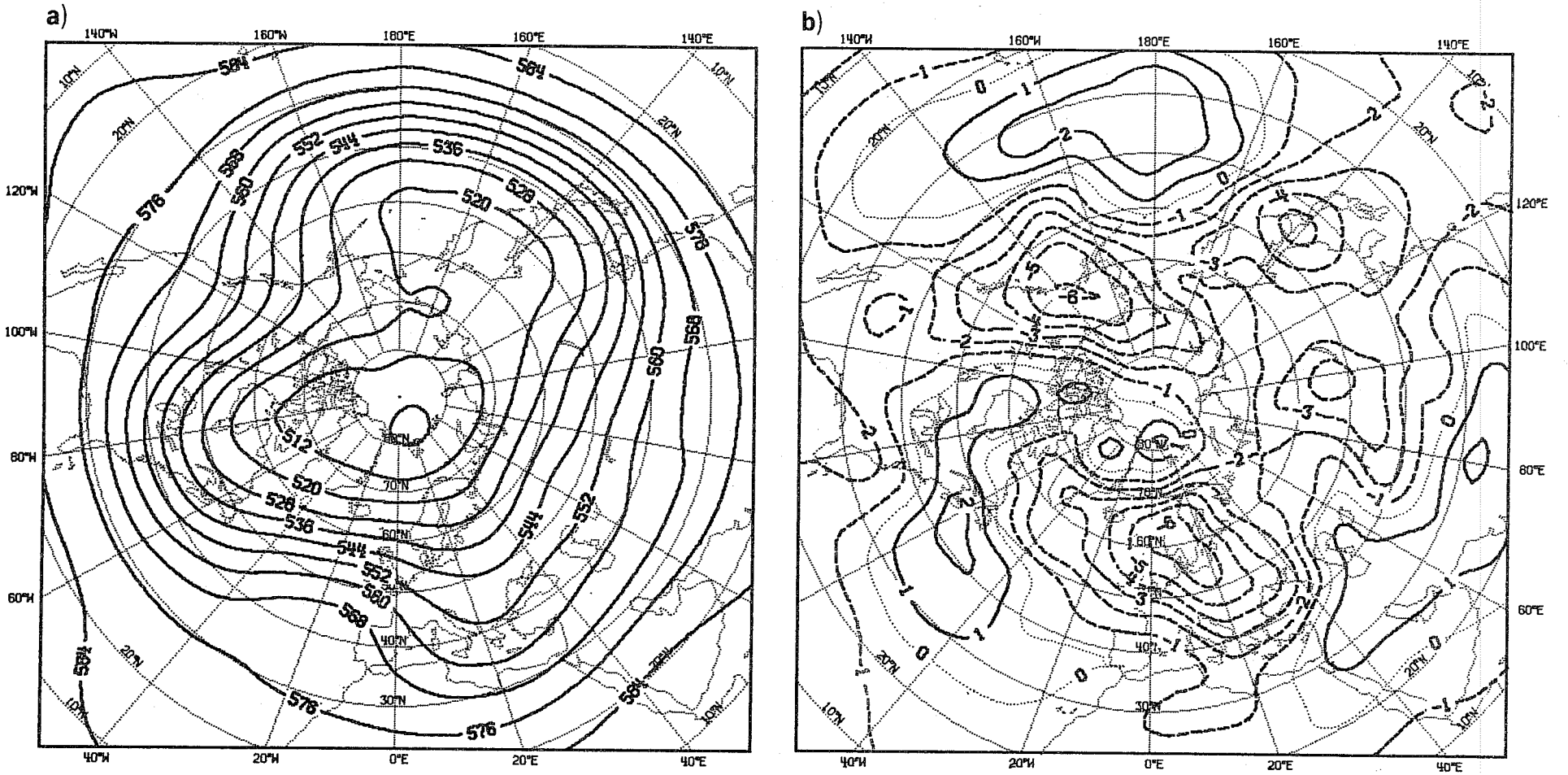

Fig. 6 Time mean of the 500 mb height field in the Northern Hemisphere for the winter 1980/81. (a) Analysis, (b) D+3 forecast-analysis. Units: 10m.

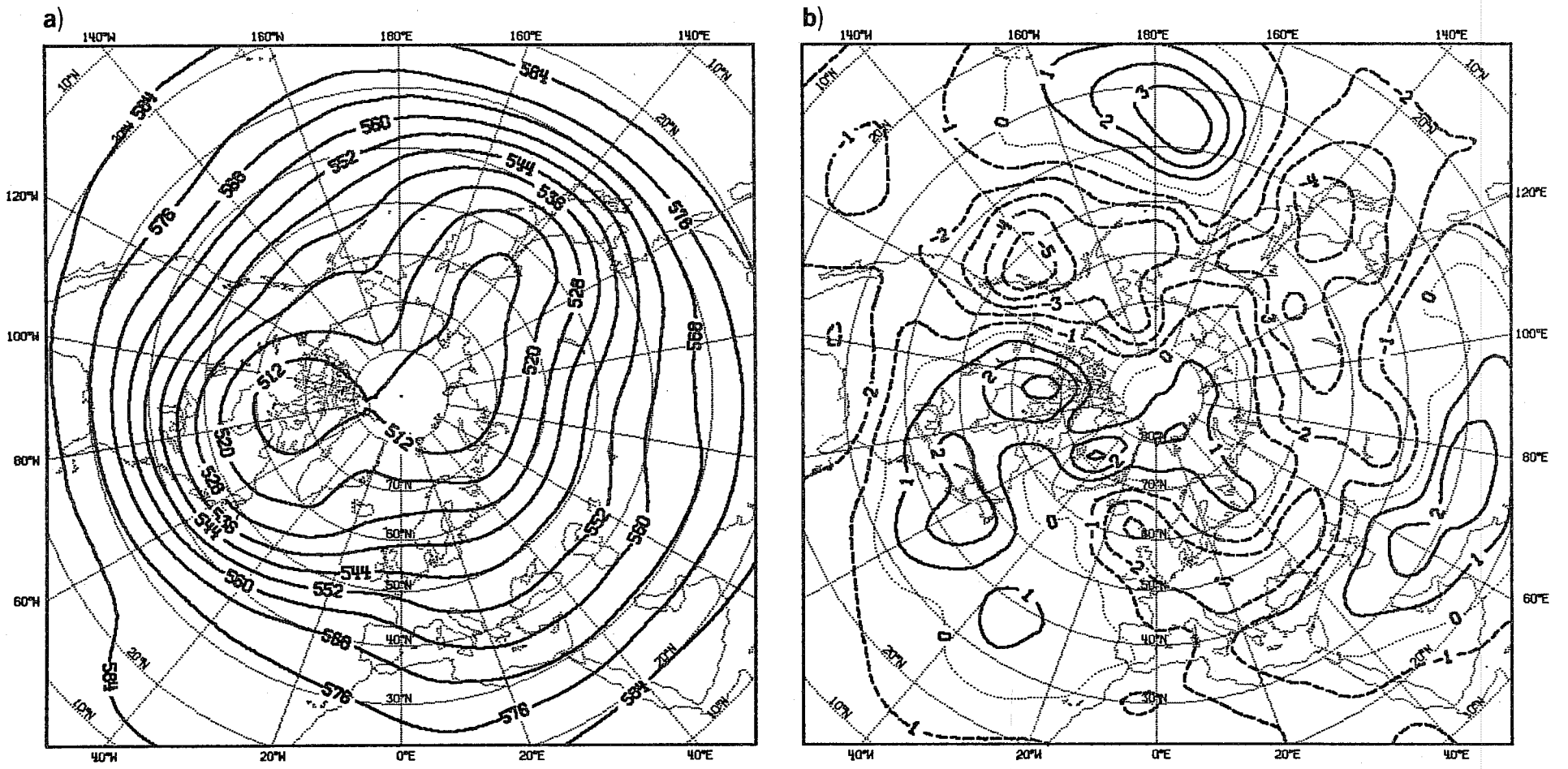

Fig. 7 The same as Fig. 6 except for the winter 1981/82.

analysis shows a distribution (Fig. 8a) similar to those found in other investigations (e.g. Hayashi and Golder, 1977; Böttger and Fraedrich, 1980) The maximum values of the spectral density are arranged along a line corresponding to the dispersion line determined from the Rossby formula $c=\bar{U}-\beta L^2/4\pi^2$ (Rossby, 1939) for a mean zonal wind between 15 and 20 m s^{-1}. In the winter of 1980/81, well separated peaks in the spectrum represent different types of wave motions. The ultra-long waves with wavenumbers 1 to 4 have their maximum variance in the low frequency region. At wavenumbers 5 and 6 two peaks appear in the medium frequency spectrum of the eastward travelling waves. The first maximum representing slowly moving baroclinic waves have a period of 12 days and the second maximum at higher frequencies represents the well-developed cyclones with a period of around 5 days. The more rapidly moving cyclones are seen as a variance peak at a period of 2.7 days. In the second winter the general distribution of the spectrum is very similiar to the previous one (Fig. 8b). However in the high frequency range, the maximum variance representing the rapidly moving cyclones is shifted to a longer period of 3.3 days. In the medium frequency range, the two maxima with periods of 10 and 5 days are not as well separated in 1981/82 as in 1980/81. The integration domain for the medium and high frequency baroclinic waves is marked by two boxes in Fig. 8.

When we compare the D+3 ensemble spectrum (Fig. 9) with the analysis spectrum we find a very good agreement in the overall structure. All major spectral peaks present in the analysis can be found in this forecast ensemble. For the baroclinic waves the general tendency during the first 3 days of the integration seems to be that they are weakened. This trend becomes very clear when the spectrum of the D+5 forecast ensemble is investigated (Fig. 10). A strong weakening has affected the medium and high frequency waves, whereas the ultra-long waves in the low frequency region have kept the same variance. In the negative frequency part, representing the

retrogressive waves, an increasing amount of variance indicates how the noise develops due to the growing inconsistency of successive days in the forecast ensemble. This process dominates the change from the D+5 to the D+7 forecast ensemble (Figs. 11a and 11b), causing most of the major spectral peaks of the baroclinic waves to disappear. We find that the time scale which is best handled by the model for later timesteps seems to be in the low frequency region.

The increase of the noise in the time series becomes very clear when we investigate the spectrum integrated over the range of baroclinic waves which are of interest here (wavenumbers 4 to 9). In Figs. 12a and 12b we have plotted the natural logarithm of the wavenumber integrated power spectrum. A small increase for the westward moving waves from D+0 to D+3, a larger one from D+3 to D+5 and an equal increase from D+5 to D+7 indicates an exponential growth of the noise due to the inconsistency in the forecast ensemble. The wavenumber integrated power spectrum also shows that the change in the low frequency region throughout the forecast period up to D+7 is rather small; the major decrease is found in the medium frequency band. These results indicate good consistency of the forecasts out to day 3.

In the following two sections we will focus our attention on changes which take place within the first 3 days of the forecast. For this forecast range the noise due to inconsistencies in the time series is low enough to see systematic changes in the structure of the waves.

6. SYSTEMATIC FORECAST ERRORS OF THE MEDIUM FREQUENCY BAROCLINIC WAVES

6.1 Three dimensional structure of wavenumber 6

To investigate the medium frequency baroclinic waves (MFBW's: wavenumbers 4 to 7 and periods from 3.6 to 10.2 days) we begin by selecting one wavenumber out of this group and we describe its structure in the latitude-height plane.

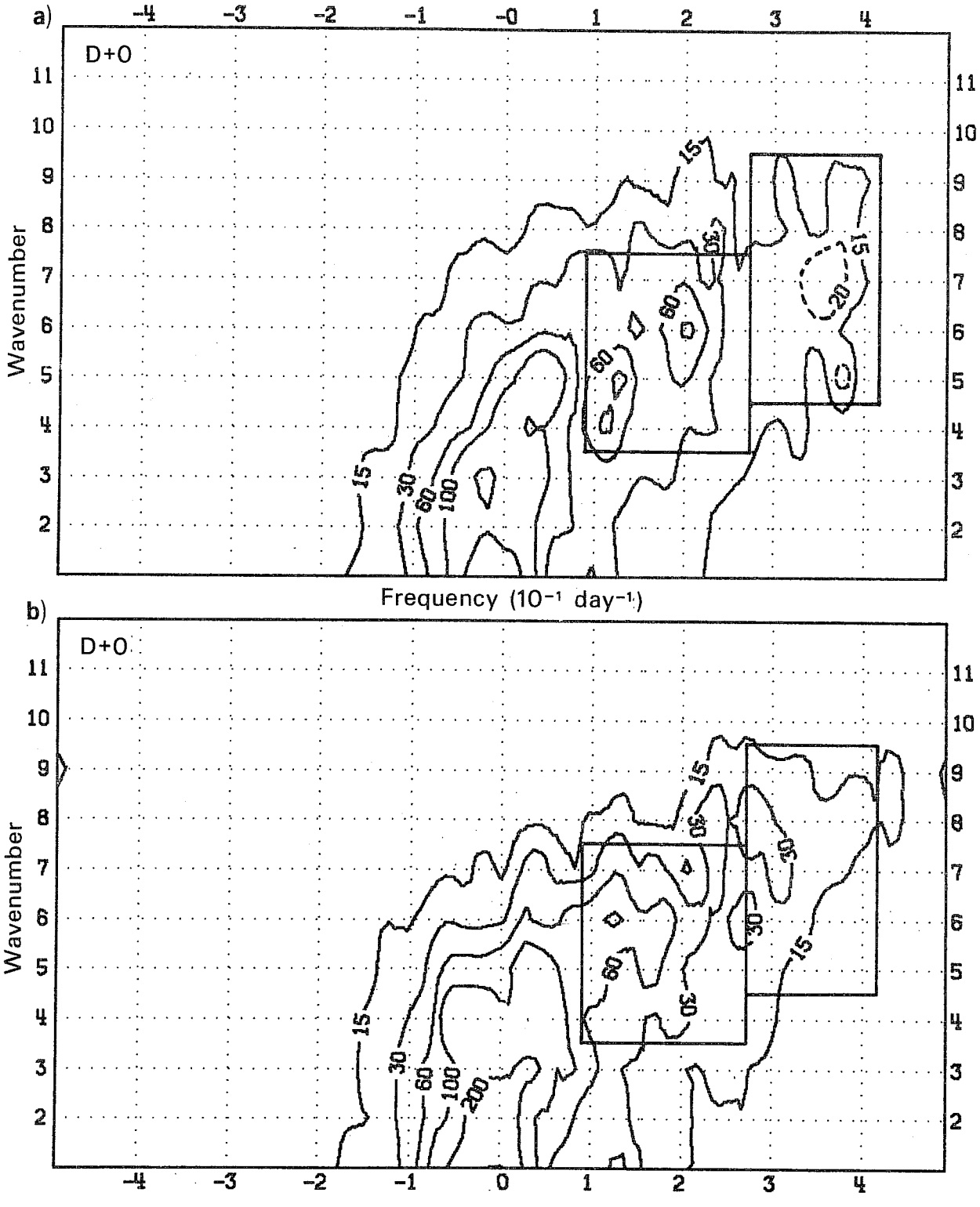

Fig. 8 Wavenumber-frequency spectrum of the kinetic energy at 500 mb in the initialized analysis. Power spectrum density values are averaged over three latitudes, 45°, 50°, and 55°N.
(a) Winter 1980/81 and (b) Winter 1981/82. Units: $m^2 s^{-2}$ day^{-1}.
The two boxes show the integration area for the medium frequency and the high frequency baroclinic waves.

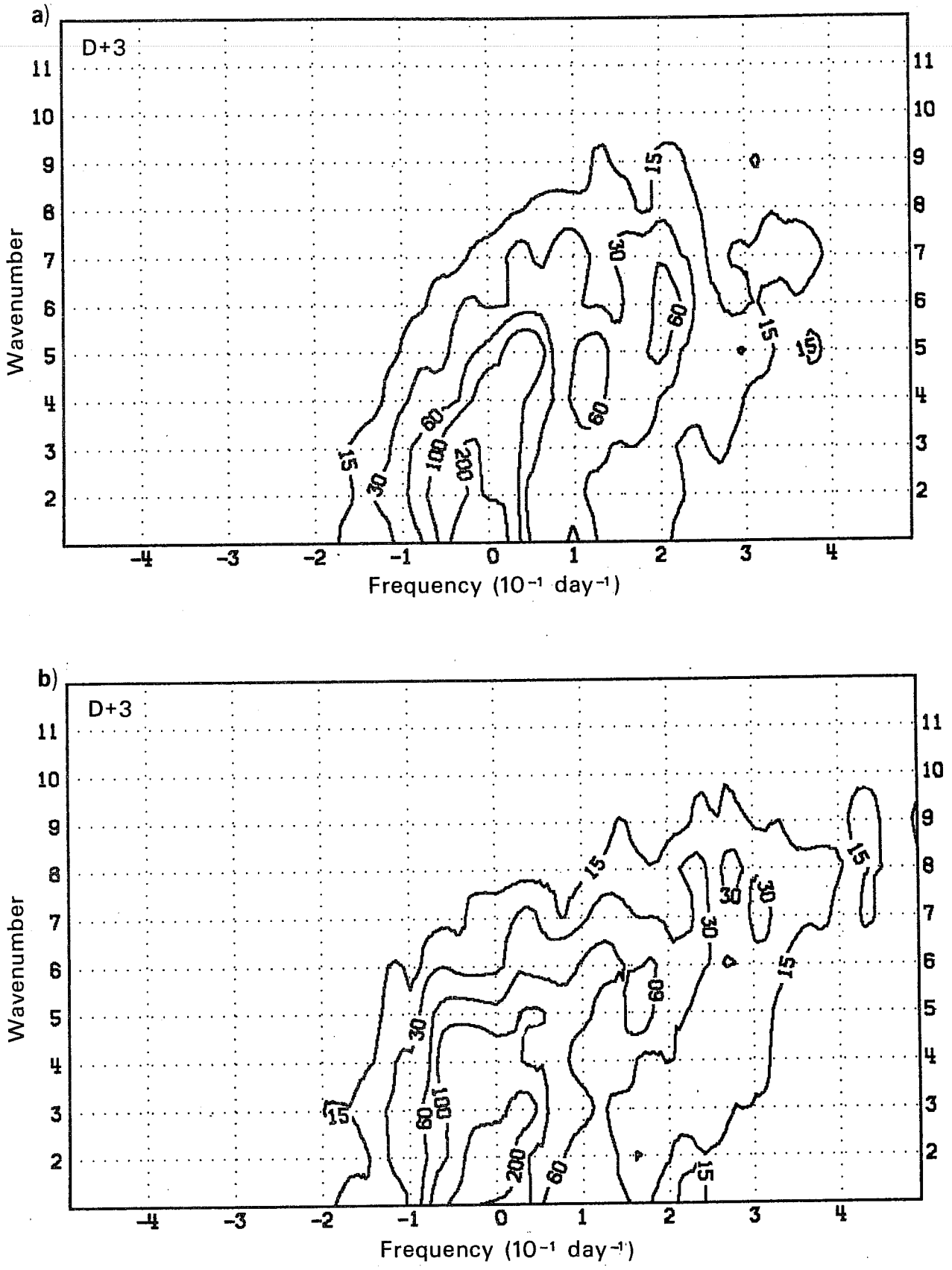

Fig. 9 the same as Fig. 8 except for the D+3 forecast ensemble.

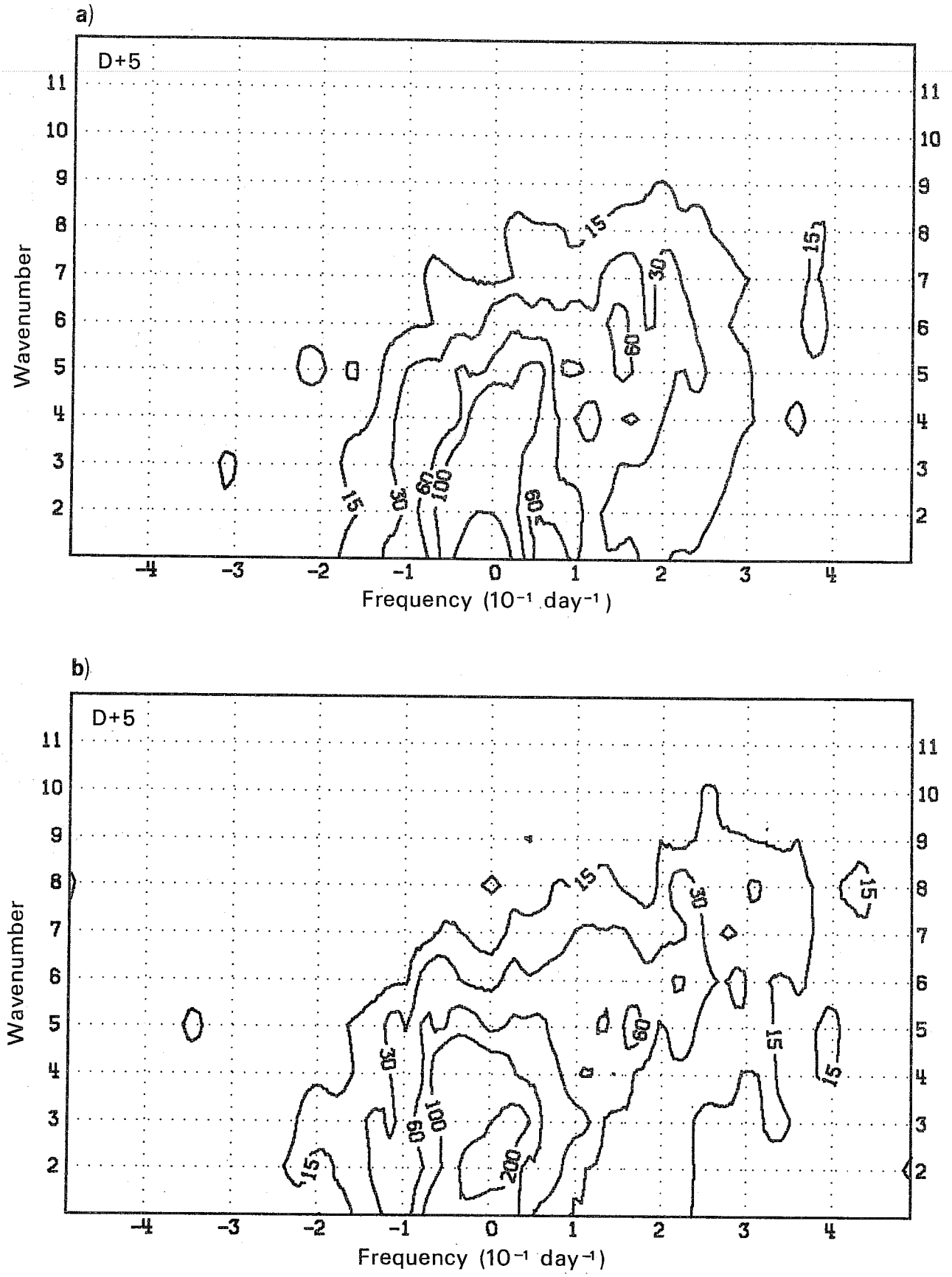

Fig. 10 The same as Fig. 8 except for the D+5 forecast ensemble.

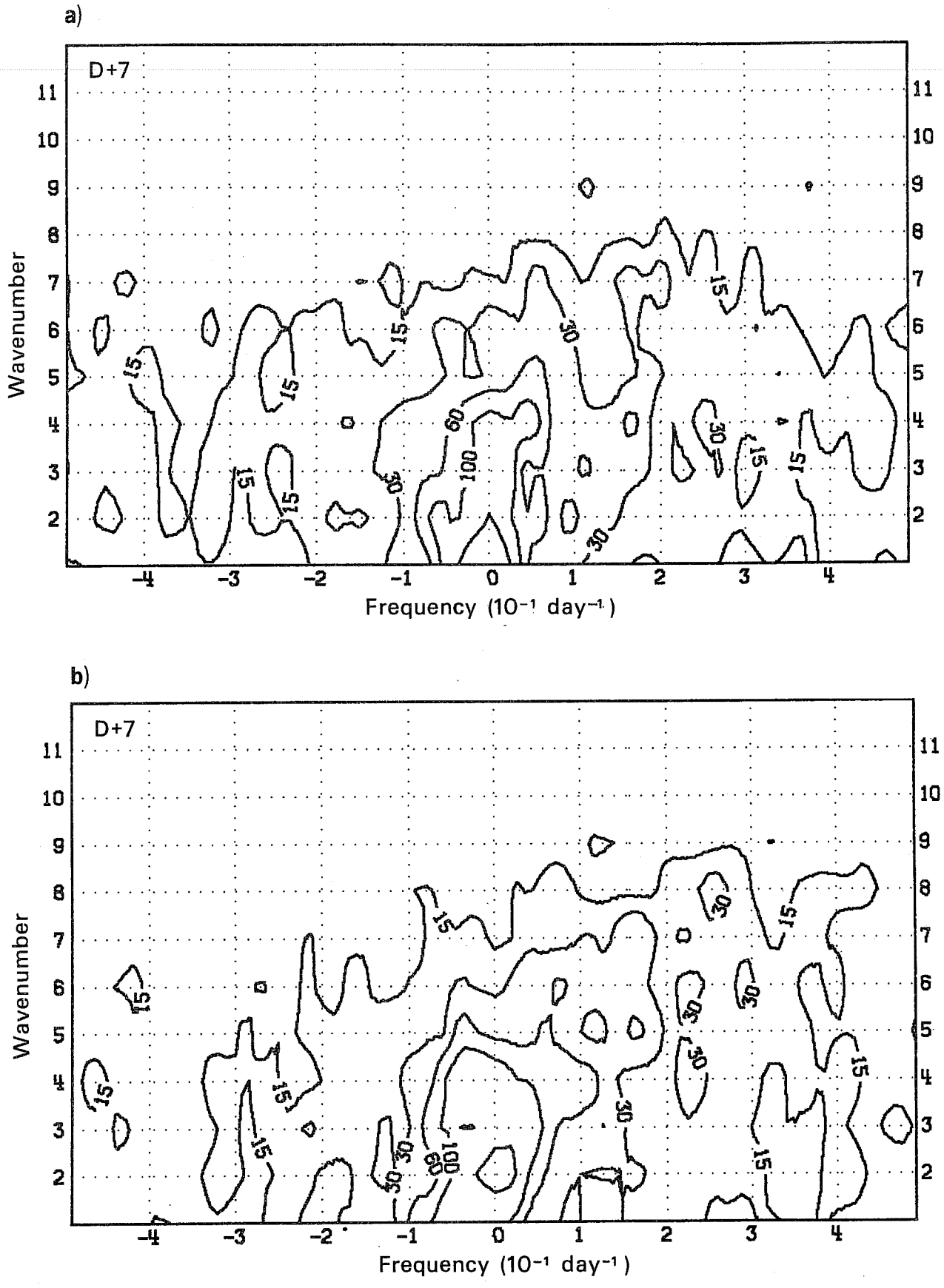

Fig. 11 The same as Fig. 8 except for the D+7 forecast ensemble.

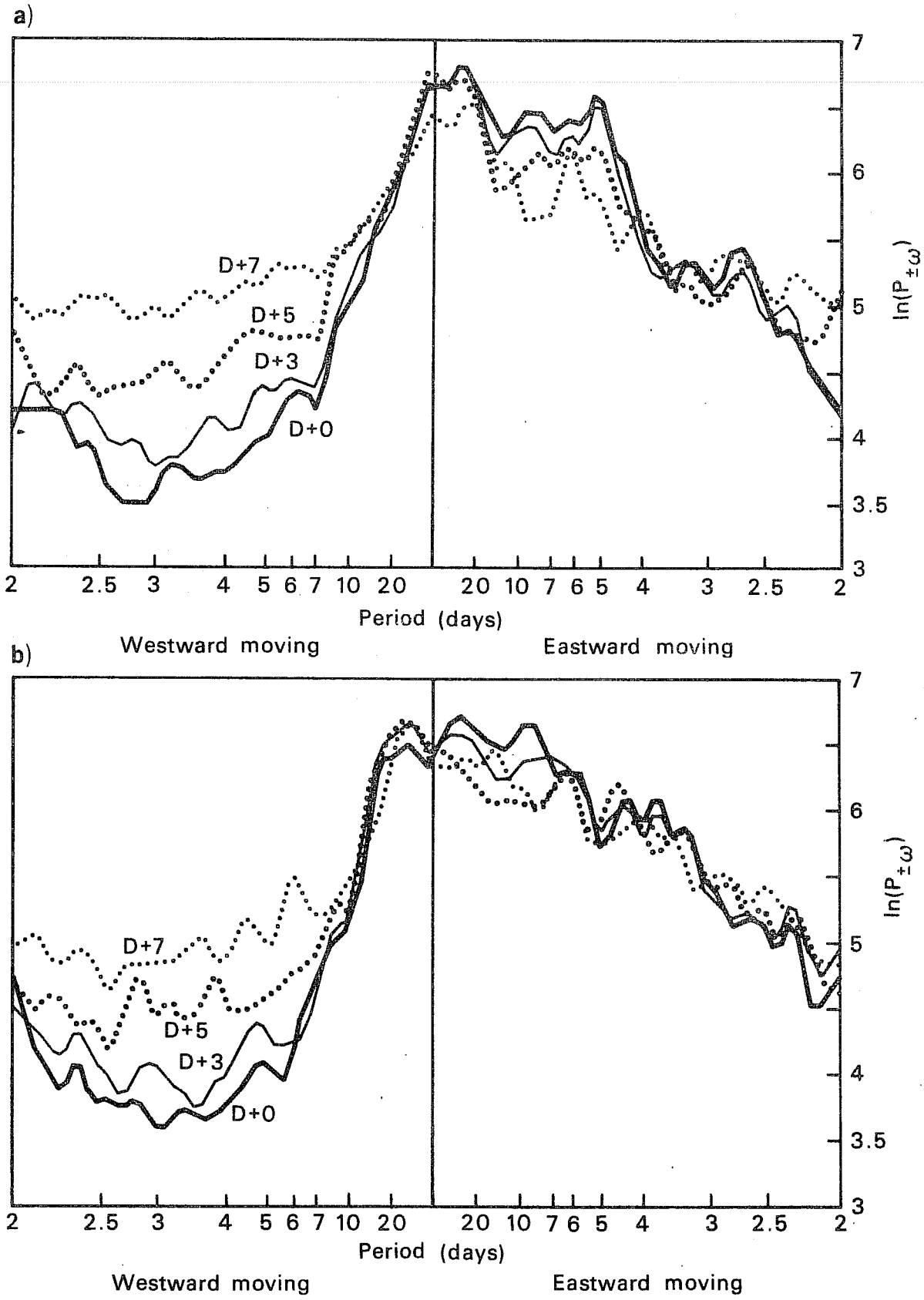

Fig. 12 Frequency spectrum of the kinetic energy integrated over wavenumbers 4 to 9 and averaged over 3 latitudes (45°, 50°, and 55°N). Spectral values are plotted on a logarithmic scale. The four graphs show the spectrum for the analysis (thick line) and the forecast ensembles D+3 (thin line), D+5 (thick dotted line) and D+7 (thin dotted line). (a) Winter 1980/81, (b) Winter 1981/82.

We can thereby compare the results from the initialized analysis with similiar investigations using analysed data or data taken from numerical models. A comparison with the wave structure found in theoretical models will also be made. We will then investigate the changes in the phase structure during the forecast, whereas changes in the amplitudes will be examined in the second part where we discuss the power spectrum integrated over the wavenumber-frequency group containing wavenumbers 4 to 7. We will focus our attention on the changes in the early part of the forecast where systematic changes seem to be larger than non-systematic ones.

6.1.1 Structure of wavenumber 6 in the meridional plane

For a more detailed description of the amplitude and phase structure of the medium frequency baroclinic waves, wavenumber 6 has been chosen because its variance is very close to the integrated variance over wavenumbers 4 to 7. In Fig. 13, which shows the variance of the geopotential wave in the latitude-height plane, we find the wavenumber 6 variance centred 12° poleward of the 300 mb subtropical jet (see Fig. 5). At lower levels the maximum zonal flow and the variance maximum of the wave are closer together as the jet has a considerable equatorward tilt with height. The variance structure in the latitude-height plane is very similiar in the two winters. A major maximum is found at 300 mb which is about 8 times as large as the secondary maximum near the surface. In the winter 1981/82 the wavenumber 6 disturbances of medium frequency are much stronger than in the previous winter.

The meridional scale of the observed wavenumber 6 is larger than the zonal scale and is as large as the scale of the zonal flow. Both the analytical β-plane solutions (Simmons, 1974) and numerical simulations of linear baroclinic waves on a sphere (Simmons and Hoskins, 1976) suggest a meridonal wave scale smaller than the scale of the zonal flow. However the meridional

wave scale found here agrees with the scale of the baroclinic waves as analysed in the GFDL general circulation model (Hayashi and Golder, 1977). The larger meridional scale indicated for the observed baroclinic waves is probably not in conflict with the theory, since the disturbances are not superimposed on a zonally symmetric flow but on a wave like time-mean flow. In particular the frontal zones over the Atlantic and the Pacific are at different latitudes, and the results presented here may thus show a meridional scale larger than that of individual disturbances. In addition, idealized models of baroclinic waves show some increase in meridional scale at upper levels in the non-linear regime (e.g. Simmons and Hoskins, 1978).

The three dimensional structure of the phase (Fig. 14) is almost the same in the two winter cases, with a predominantly westward tilt with height and a horizontal tilt which is largest (and directed from SW to NE) at low latitudes. For baroclinic waves with different wavenumbers the phase structure is not as consistent from one winter to the next as shown here for wavenumber 6. This is so especially in middle latitudes where the horizontal phase tilt for the single wavenumbers is often different in the two winters. The variability of the horizontal phase makes a comparison with theoretical studies very difficult. Simmons and Hoskins (1976) noticed that, in contrast to the uniformity of the eddy heat flux in all their experiments, horizontal momentum fluxes were sensitive to the mean zonal flow profile. As the horizontal eddy heat and eddy momentum fluxes are, to a good aproximation, proportional to the vertical and horizontal tilt of the geopotential wave (see formulae B4 and B5 of appendix B), their results are reflected in the varying horizontal phase tilt of observed baroclinic waves. However to the south of the variance maximum all baroclinic waves in the medium frequency range show a large SW/NE tilt which is consistent with both the theoretical result of Hollingsworth et al. (1976) for linear waves, and the more general results discussed by Edmon et al. (1980).

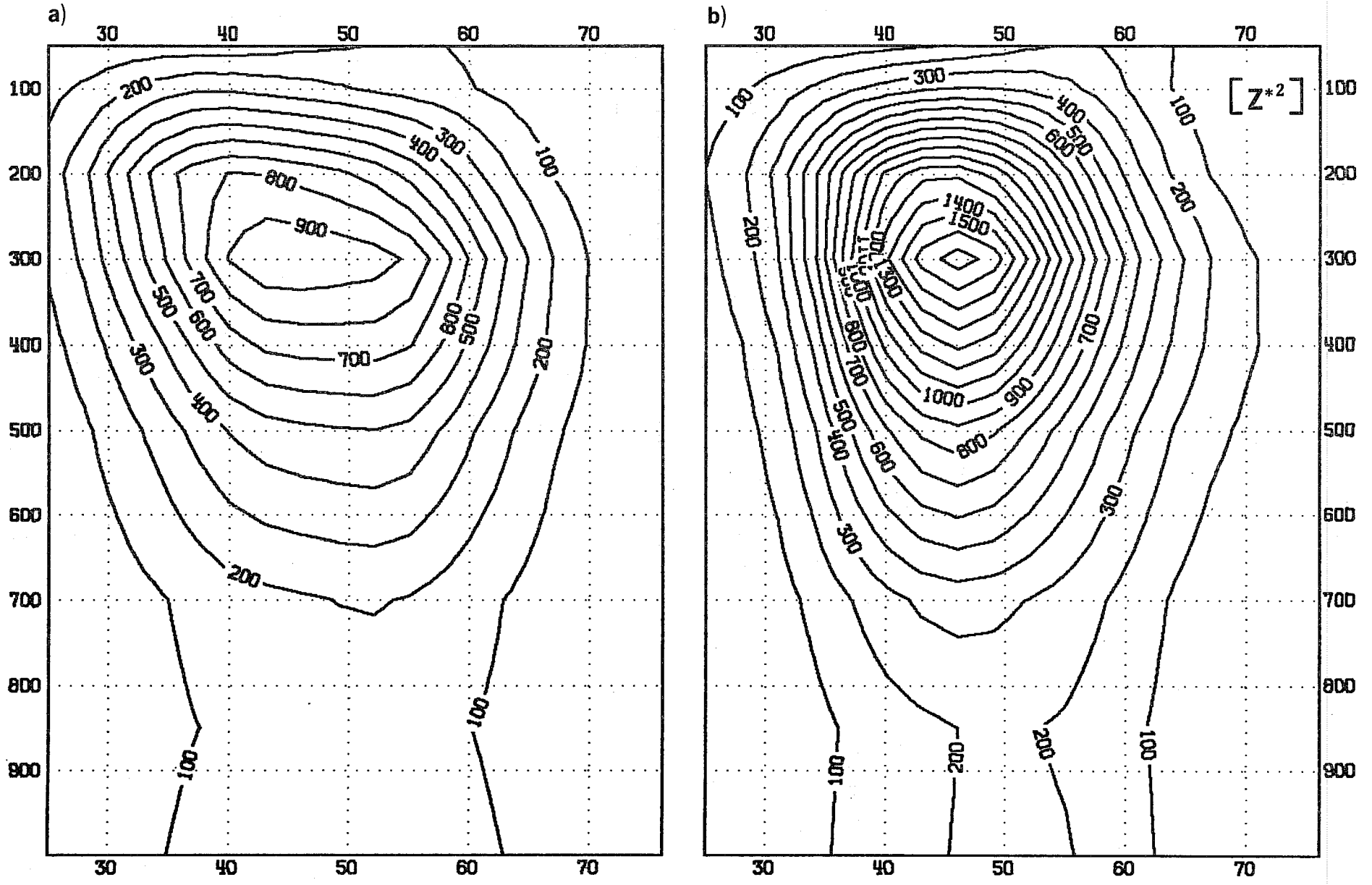

Fig. 13 Latitude-height plot of the geopotential height variance of wavenumber 6 in the medium frequency band (mean period 5.3 days), valid for the initialised analysis. Units : m^2. (a) Winter 1980/81 (b) Winter 1981/82.

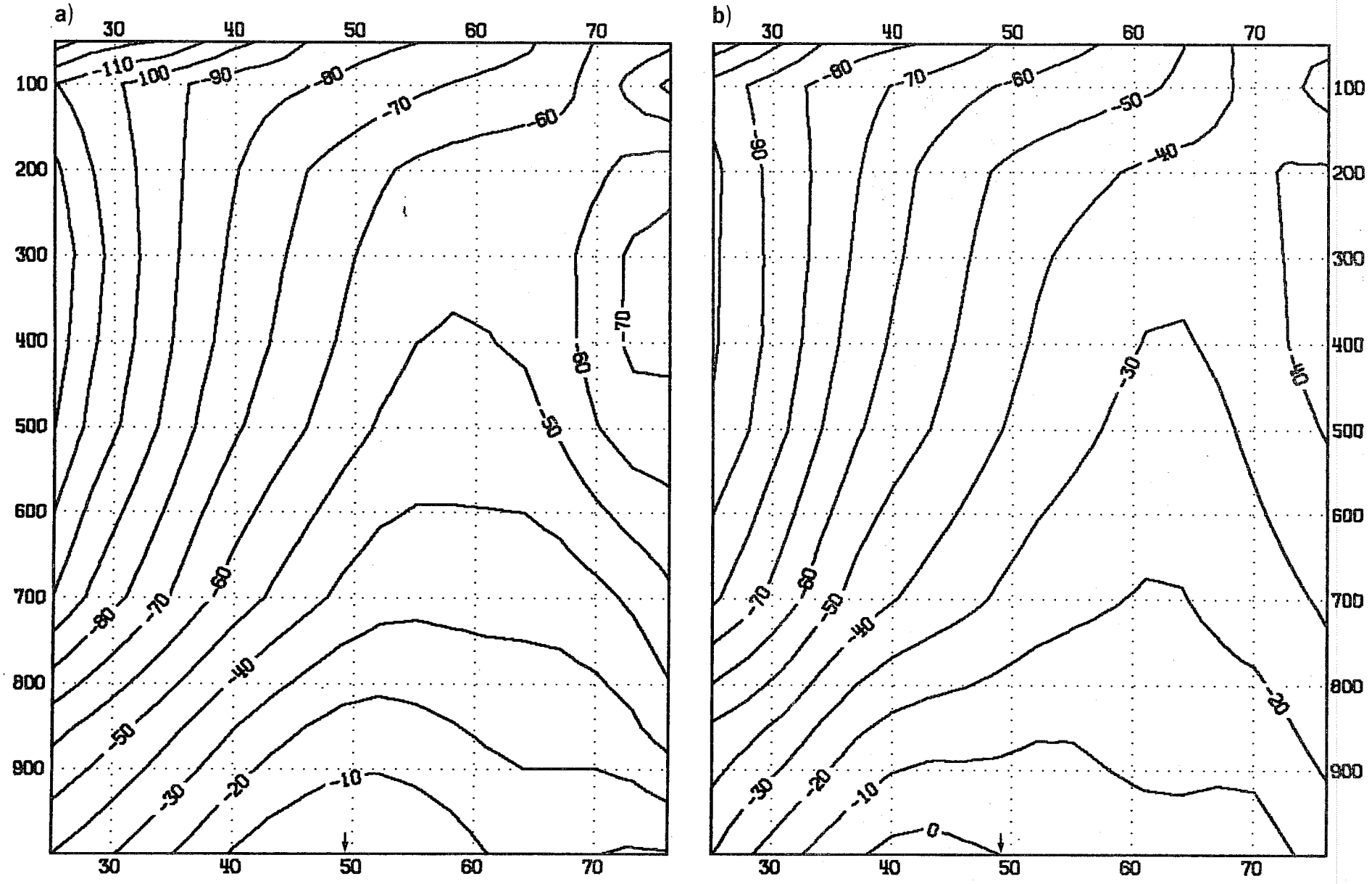

Fig. 14 Latitude-height plot of the geopotential height phase structure of wavenumber 6 in the medium frequency band (mean period 5.3 days), valid for the initialised analysis. Units : degrees. (a) Winter 1980/81 (b) Winter 1981/82 (↓: Reference point of phase calculation)

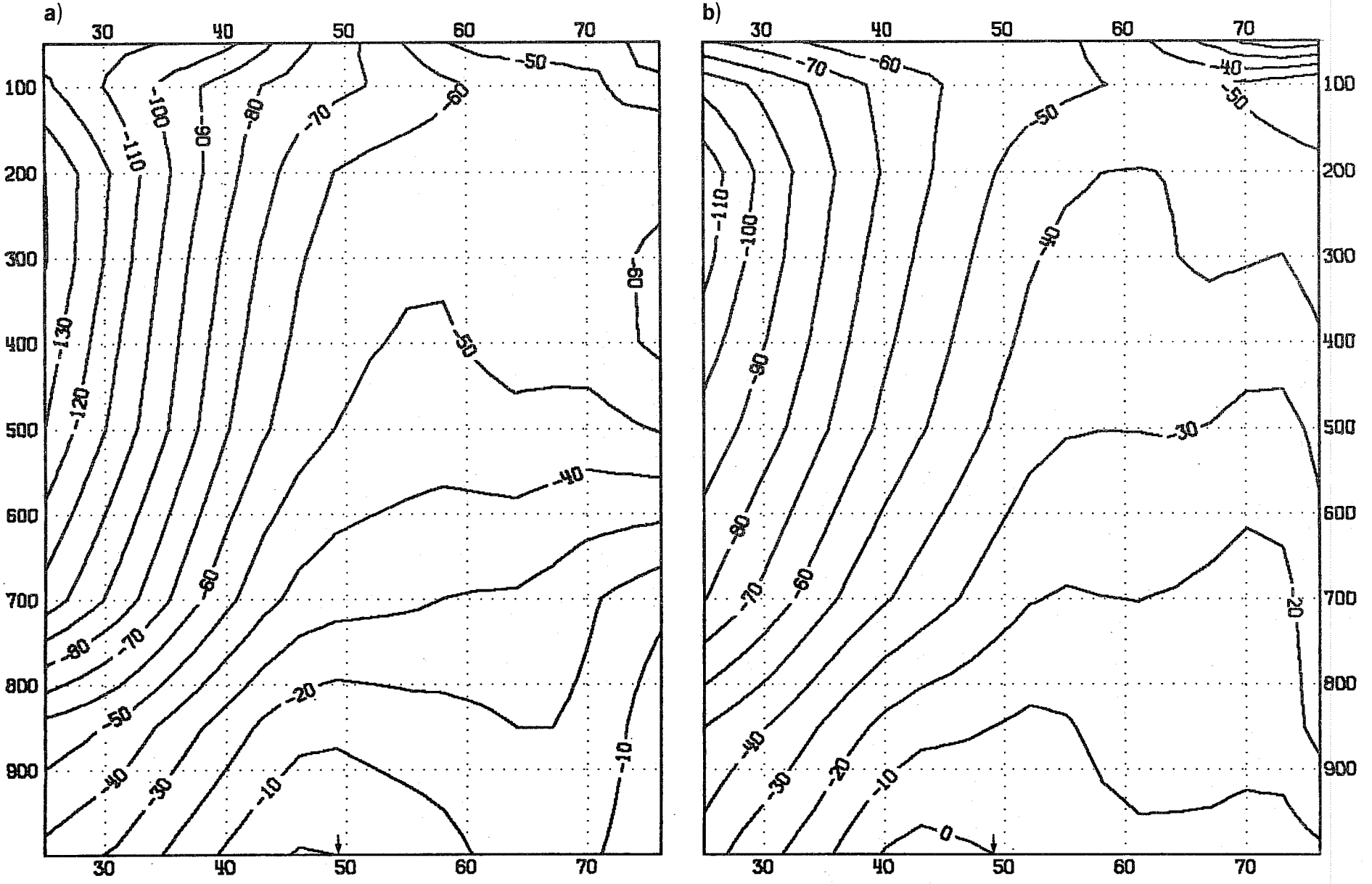

Fig. 15 The same as Fig. 14 except for the forecast ensemble D+3. (↓: Reference point of phase calculation)

In the D+3 forecast ensemble we notice that the phase structure has changed most, compared to the analysis, at low latitudes and upper levels (Fig. 15). Here the SW/NE phase tilt has increased. We will return to this point when the eddy momentum flux is discussed.

6.1.2 Vertical structure of wavenumber 6 in the zonal plane

In this section we will discuss the vertical structure of the wave with respect to geopotential height, temperature, zonal wind, meridional wind, and vertical velocity. The vertical phase lines of each variable and the phase difference between them will be investigated. For a better understanding of the relation between the variables we will make use of simple diagnostic equations we have derived in appendix B.

In Fig. 16 (winter 1980/81) and Fig. 17 (winter 1981/82) we show the vertical amplitude and phase structure for the geopotential height wave (wavenumber 6) as a mean over the latitude band from 43°N to 64°N. The vertical phase structure is determined by first calculating the phase difference between the temperature and each other variable at 500 mb. Then for all variables the vertical phase lines are continued upward and downward from 500 mb by adding the calculated phase differences between two adjacent levels. The quality of the phase calculation can be measured in terms of coherence. At 500 mb the coherence is a measure of reliability for the phase difference between the temperature and the other variables. At all other levels the coherence indicates the accuracy of the level to level phase increments for that variable.

Some general wave characteristics shown here for wavenumber 6 agree quite well with the structures derived from the linear theory of baroclinic waves (Charney, 1947; Eady, 1949; Green, 1960). Assuming a phase speed of 10 m s^{-1}

(which corresponds to a wavenumber 6 disturbance travelling eastward with a period of 5.3 days at 45°N), the steering level where the phase speed of the wave matches the mean zonal flow would be approximately at 600 mb. The β-effect acting on baroclinic waves distorts the vertical symmetry which exists for $\beta=0$. With respect to the steering level, the amplitude of the temperature wave is biased to lower levels and the vertical velocity wave to upper levels. The geopotential has a maximum at the lower boundary and at the tropopause (which acts as an imperfect upper lid to the baroclinic waves below). There is also a good qualitative agreement between observation and theory in the vertical phase structure. The geopotential tilts westward with height, and below 400 mb the temperature tilts forward with height. The vertical tilt of the vertical velocity is in the same direction as the tilt of the meridional wind. Though the tilt of the vertical velocity is smaller, we can expect some similarities in the poleward and upward eddy fluxes of heat.

The main discrepancy between linear theory and observation is that the theoretical upper level wave maximum is too weak. Though linear theory shows that a sharp tropopause can enhance the amplitude of the baroclinic waves at upper levels (Simmons and Hoskins, 1976), non-linear processes are required to explain upper level wave maxima which are larger than the surface maximum by a factor of at least 2 (Simmons and Hoskins, 1978). The relatively larger enhancement of upper level disturbances is also a function of the lifetime of the baroclinic waves. The mean zonal flow can be modified by a growing baroclinic wave in such a way that the growth rate near the surface decreases, thereby allowing the upper level part of the wave to attain larger amplitudes before all growth ceases at the mature stage (Gall, 1976). It seems that the well developed baroclinic waves with large amplitudes aloft are the major contributors to the variance in this wavenumber-frequency group.

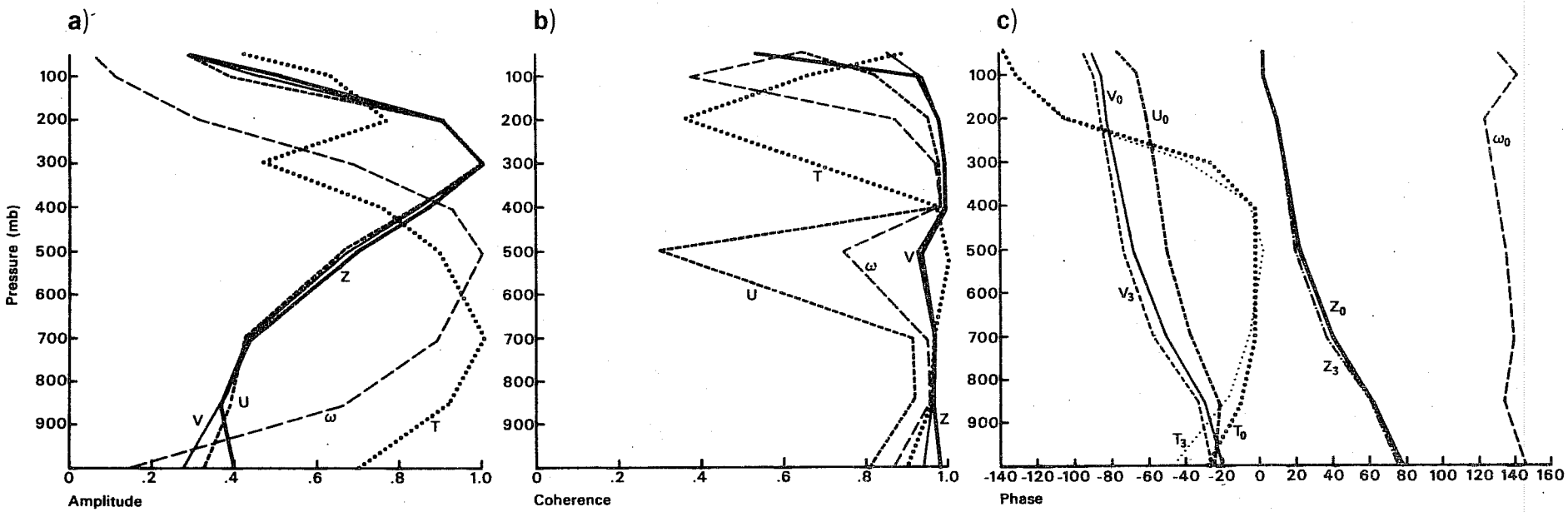

Fig. 16 Vertical structure of wavenumber 6 in the medium frequency band (mean period 5.3 days). Profiles of amplitude (a), normalized by the maximum value, coherence (b) and phase difference with respect to temperature at 500 mb (c). Spectral values are averaged over a latitude band from 43^{o}N to 64^{o}N. The graphs show the vertical structure of the geopotential height (Z), temperature (T), zonal wind (U), meridional wind (V) and vertical velocity (ω) for the initialized analysis. The phase structure is shown for the forecast ensemble D+3 as well. Winter 1980/81.

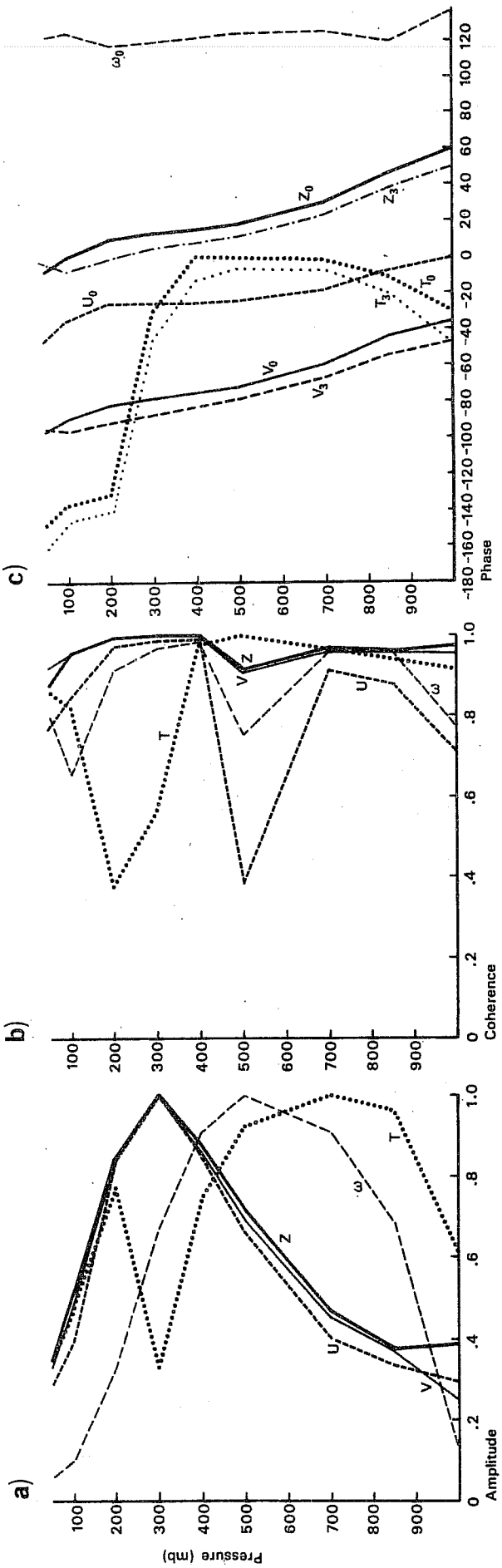

Fig. 17 The same as Fig. 16 except for the winter 1981/82.

The temperature wave has its major maximum at 700 mb and a minor one above the tropopause. The phase difference between the temperature and the geopotential is smallest in the middle troposphere, and a large phase change of the temperature wave occurs through the tropopause. The change of the amplitude of the geopotential height wave in the vertical is consitent with the vertical phase structure of the temperature wave and geopotential height wave for hydrostatic flow (see appendix B). A phase difference of less than 90 degrees between Z and T in the middle troposphere gives an increasing geopotential wave amplitude with height, whereas a phase difference of more than 90 degrees in the lower stratosphere accounts for the decrease of the geopotential wave with height. In this connection the minimum of the geopotential wave at 850 mb is consistent with the large phase difference between the temperature and the geopotential near the surface.

The close agreement of the vertical amplitude structure of the meridional wind and that of the geopotential indicates that the variance of the meridional wind is dominated by the geostrophic part. It is only near the surface that the structures (normalized by the maximum amplitude of Z and v) depart from each other; here friction has decreased the amplitude of the meridional wind. The large decrease of the meridional wind amplitude with height in the lower stratosphere is again in good agreement with the vertical phase structure. As expected from the thermal wind equation for waves (diagnostic formula B2 in appendix B), the meridional wind leads the temperature wave above the wind maximum.

The vertical profile of wavenumber 6 is very similiar to the profiles found by Hayashi and Golder (1977) in the GFDL general circulation model. Though they calculated the phases as differences with respect to temperature for all parameters and levels, instead of adding up phase differences from level to

level, their phase profiles are almost the same as found here. We also have a good agreement between the wave structure in our analysis and studies which are based on observational data (Hartmann, 1974; Böttger and Fraedrich, 1980).

The phase structure of the D+3 forecast ensemble was calculated in the same way as for the analysis. Additionally the phase difference between the D+3 disturbances and the disturbances in the analysis was determined by calculating the co-spectrum and quadrature spectrum between the travelling disturbances of the two ensembles. For the geopotential height this calculation shows that the wave in the forecast ensemble is slightly too slow (Fig. 16). For other wavenumbers in the medium frequency range which are not shown here, the phase lag was around 150 km after 3 days and 300 km after 5 days. We have checked the reliability of the calculation of the phase differences between the forecast and the analysis by an artificial change of the forecast ensemble. We repeated the calculation with an unchanged analysis ensemble but with a forecast ensemble starting and ending one day later. The phase difference is exactly as large as we would theoretically expect for a wave with a period of 5.3 days travelling eastward for one day.

An important feature of all baroclinic waves in the forecast is that the forward tilt of the temperature wave with height increases during the forecast. This error shown for wavenumber 6 is representative of the other wavenumbers as well. The phase change increases the poleward heat flux as the phase difference between the meridional wind and temperature becomes smaller in the lower troposphere. The phase difference between the geopotential and temperature becomes larger giving a more pronounced decrease of the geopotential wave amplitude with height near the surface.

6.2 Forecast errors in the medium frequency baroclinic waves: integrated results

In this section the variance of single variables and the cospectrum of pairs of varables, both integrated over wavenumbers 4 to 7 and frequencies from 1/10.2 to 1/5.2 (1/days), are investigated. By integrating over a region in the wavenumber-frequency domain we can improve the significance of our results (see appendix A). We will describe the latitude-height distribution of the variance for the initialized analysis and look at changes which arise during the forecast. Attention will be concentrated on the differences between the variance of the D+3 forcast ensemble and the variance of the initialized analyses.

6.2.1 Geopotential and temperature

The variance of the geopotential height (Fig. 18) has a meridional scale which is much larger than the scale of the mean zonal flow. The scale is also larger than the meridional scale of single waves as the latitude of the maximum amplitude varies markedly with wavenumber. Higher wavenumbers generally have their maximum amplitude at lower latitudes. The vertical profile of the variance is the same as we have shown in the single wave description of wavenumber 6 in the previous section (see Fig. 16); a major maximum is found at the tropopause and a minor one near the surface. The large decrease of the variance with height above the tropopause indicates that the MFBW's are not able to penetrate into the stratosphere. The distribution of the variance in the latitude-height plane is nearly the same in the two winters except that in the second winter the variance maximum tilts equatorward with height, whereas in the first one no tilt is observed.

The thermal structure of the MFBW group (Fig. 19) reveals one temperature maximum in the lower troposphere and one in the lower stratosphere. As we have shown for the vertical phase structure of wavenumber 6 (see Fig. 16),

the temperature wave and the geopotential height wave are nearly in phase in the middle troposphere. However, they are out of phase by more than 90 degrees above the variance maximum of the geopotential height wave. As we know from the hydrostatic equation for waves (diagnostic formula B1 in appendix B) this phase difference is necessary to explain the vertical decrease of the geopotential wave with height. In this sense the lower stratospheric temperature waves compensate the tropospheric temperature waves which account for the vertical increase of the geopotential height wave.

During the first 3 days of the forecast large changes in the vertical structure of the MFBW's take place (Fig. 20). A marked weakening of the upper level maximum is the dominant feature in both winters, with the largest reduction of the variance on the poleward side of the observed variance maximum. Up to D+3 the upper level maximum has decreased by 15%. In the same forecast period the near surface layer shows an increase in the variance which has almost the same relative magnitude. This positive deviation at low latitudes extends into upper levels as well. The weakening of the upper level maximum of the geopotential height wave continues up to D+5 (not shown here) with a further decrease of 15%. The decrease has also spread to lower levels and only a weak increase remains near the surface at middle latitudes. The hydrostatic equation (appendix B) relates the forecast errors of height waves to changes in the thermal structure of the waves. We find a decrease of the temperature variance in the middle troposphere and a weakening of the compensating temperature waves in the lower stratosphere as well (Fig. 21). These two changes in the variance of the temperature are closely coupled with the decrease of the geopotential height variance and should not be seen as separate processes.

The general tendency of the MFBW's in the ECMWF forecast model to have an upper level maximum which becomes too weak relative to the surface maximum

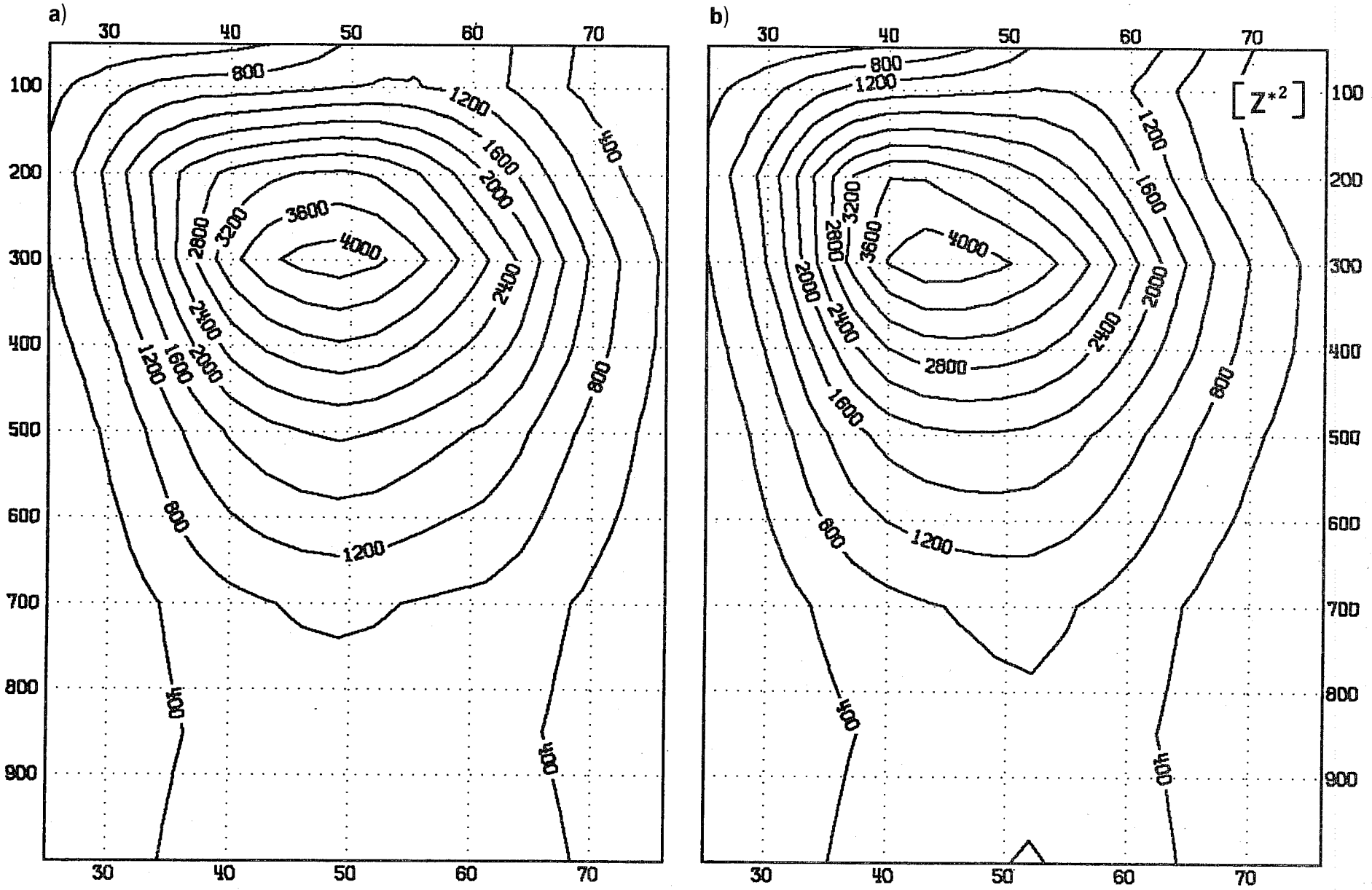

Fig. 18 Latitude-height section of the geopotential height variance for the MFBW's in the initialized analysis. Units: m^2. (a) Winter 1980/81, (b) Winter 1981/82.

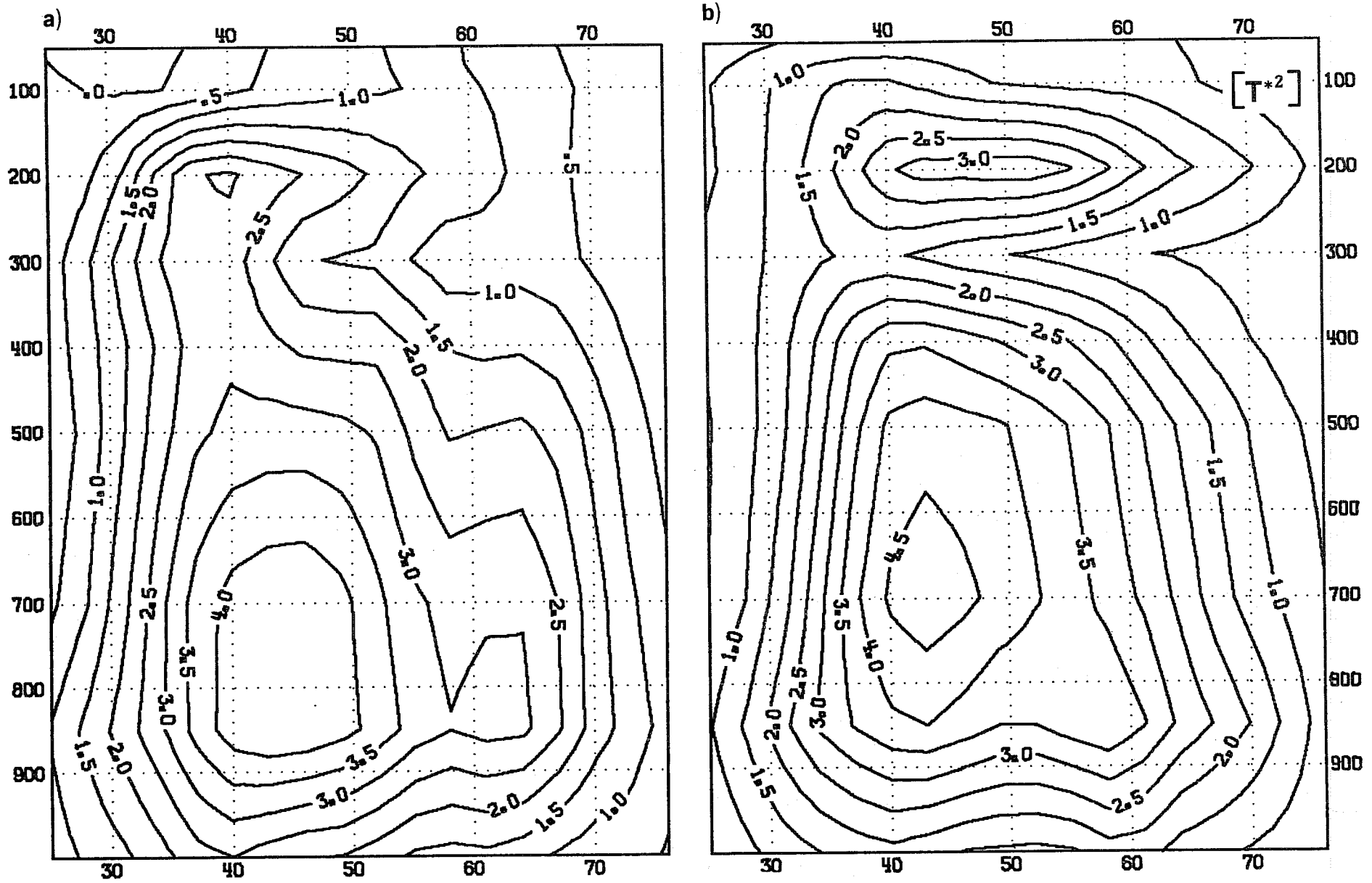

Fig. 19 Latitude-height section of the temperature variance for the MFBW's in the initialized analysis. Units: K^2. (a) Winter 1980/81, (b) Winter 1981/82.

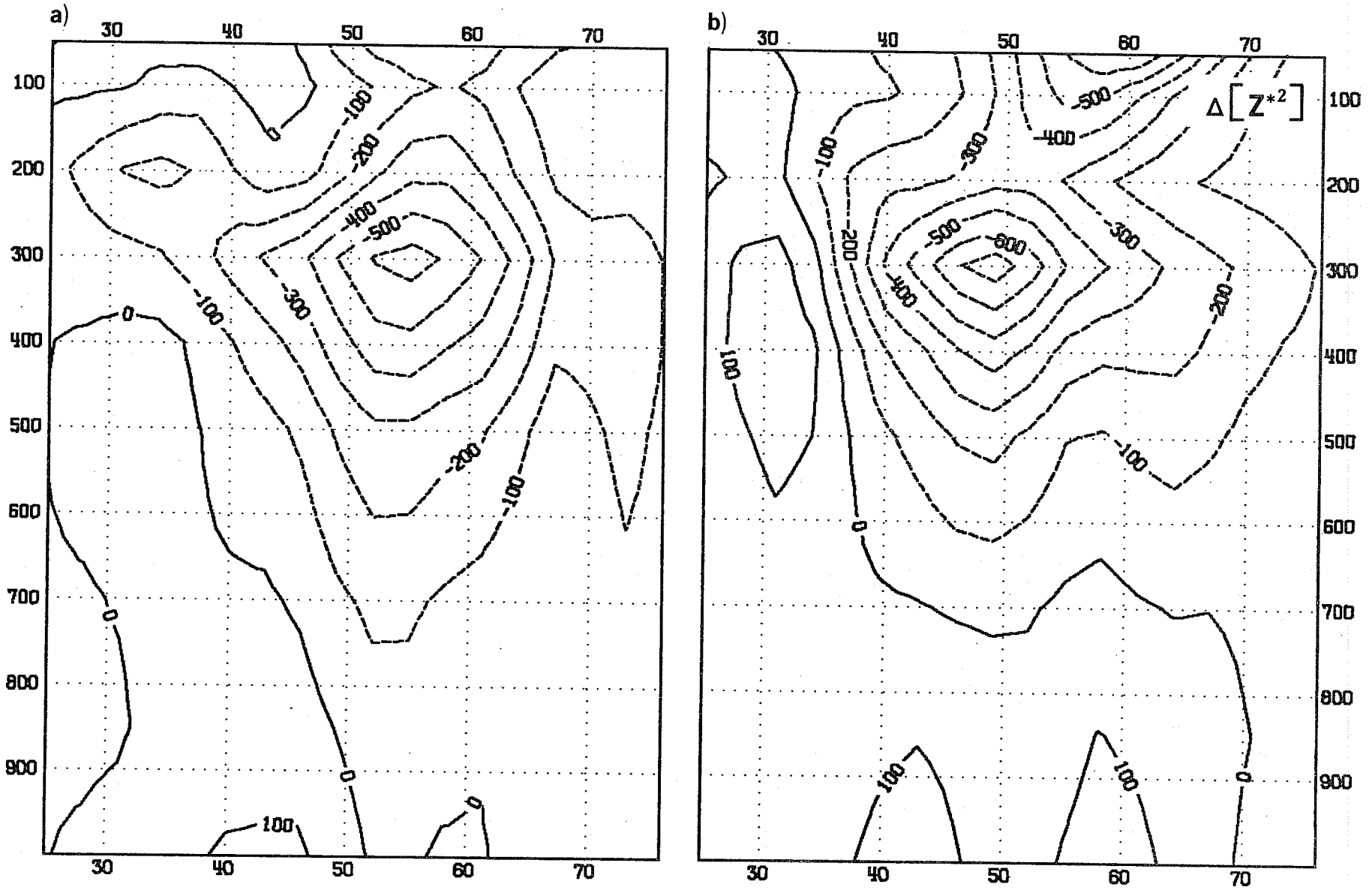

Fig. 20 Latitude-height section of the geopotential height variance error for the MFWB's. Forecast (D+3) - analysis. Units: m^2. (a) Winter 1980/81, (b) Winter 1981/82.

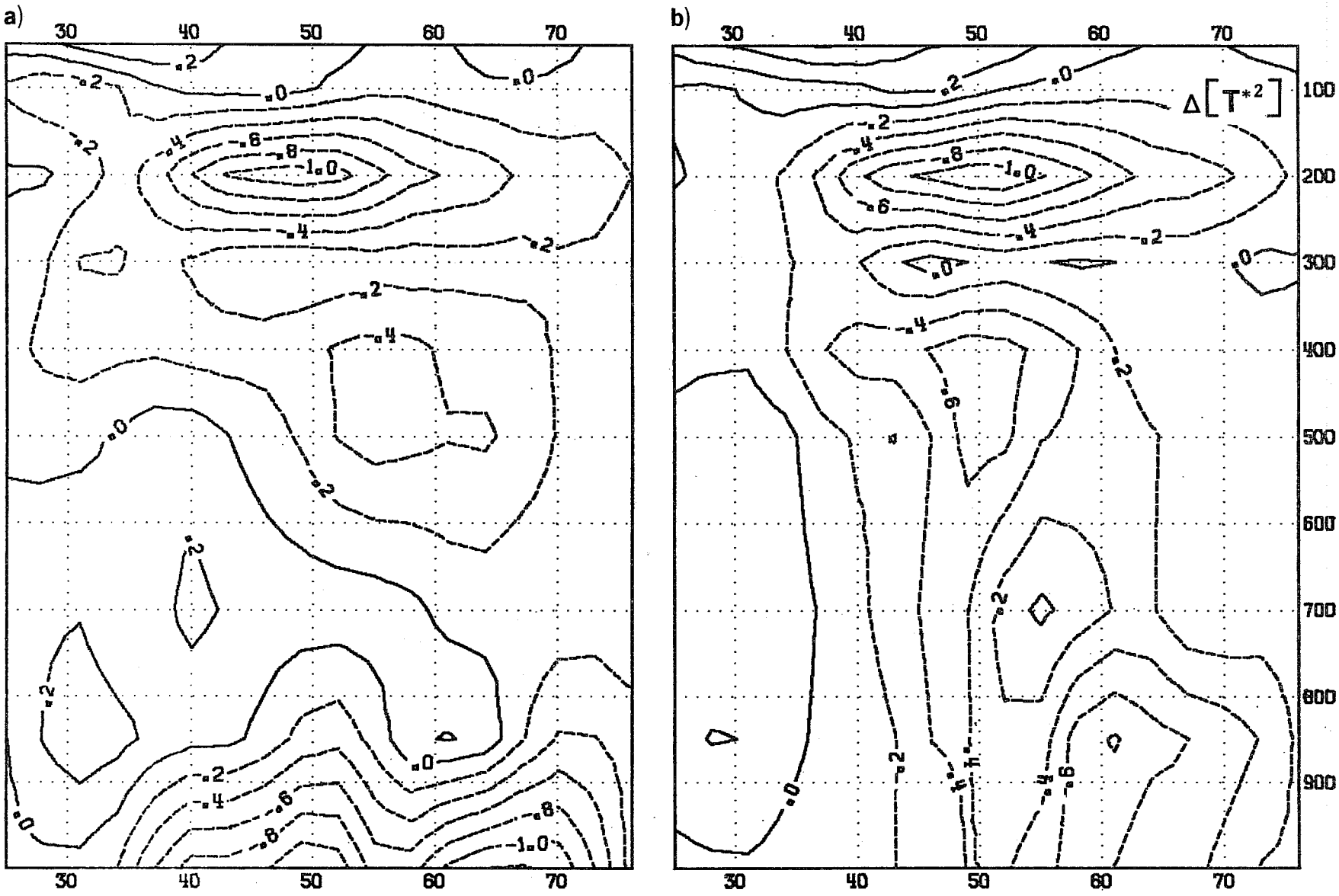

Fig. 21 Latitude-height section of the temperature variance error for the MFBW's. Forecast (D+3)- analysis. Units: K. (a) Winter 1980/81, (b) Winter 1981/82.

seems to be a common feature for other numerical integrations. Simmons and Hoskins (1978) performed some non-linear experiments to simulate the life cycle of baroclinic waves and found that the ratio of the upper level kinetic energy to the suface values was 5 to 1, whereas we found here a ratio of 8 to 1 in the initialized analyses. Too weak baroclinic waves in numerical integrations were also identified by Pratt (1979) when he compared observed variances with simulations from the NCAR and GFDL general circulation models. The underestimation of baroclinic wave amplitudes at upper levels was larger for the NCAR model than for the GFDL model. Pratt assumed that the differences could largely be attributed to the higher resolution of the GFDL model. The GFDL model had, however, a higher resolution in the vertical as well as in the horizontal, with five layers below 300 mb instead of three layers as in the NCAR model. As mentioned before, linear theory (Simmons and Hoskins, 1976) shows that the sharpness of the jet at the tropopause in the model can influence the upper level maximum of the baroclinic waves and we notice a reduced sharpness of the tropopause during the forecast (see Fig. 2). Compared to the NCAR and GFDL model the GLAS model is more successful in simulating the observed variance of the baroclinic waves (Strauss and Shukla, 1981). To what extent the ECMWF model error in the MFBW's is dependent on the model resolution is a question which could be answered by appropriate sensitivity experiments with higher vertical and/or horizontal resolution.

The changes of the MFBW's are consistent with the changes of the stability of the zonal mean state for the period under investigation. Below the tropopause a stabilisation of the mean state could be responsible for smaller growth rates at upper levels. However the stabilisation seems to be rather small. The destabilsation in the lower part of the troposphere would have the effect of enhancing the growth of baroclinic waves. This explanation for the overdevelopment near the surface is, however, not as straightforward as

it appears. The longitudinal contributions for the too high zonal mean temperatures come from large positive forecast errors at the lee side of the mountains (Arpe, 1983). In the discussion of the geopraphical distribution of the forecast errors for the MFBW's we will notice large longitudinal variation of the variance errors as well.

6.2.2 Horizontal eddy momentum flux

The height-latitude distribution of the integrated horizontal momentum flux is very similiar in the two winters (Fig. 22). The maximum poleward flux is located north of the subtropical jet which agrees with calculations by Hollingsworth et al. (1976) and with simulations of baroclinic waves by Simmons and Hoskins (1978).

The changes which arise in the forecast in the first 72 hours (Fig. 23) are very different in the two winter seasons. Only at low latitudes do the two winters show the same kind of change in the D+3 forecast ensemble. Examining the contributions from single wavenumbers to the change shown by the integrated values, we find similiar changes in the two winters for wavenumbers 4 and 6, whereas wavenumbers 5 and 7 are changed differently.

The horizontal momentum flux calculated from geostrophic winds (relation B4 in appendix B) is a function of the amplitude and the horizontal phase tilt of the geopotential height wave, giving a poleward momentum flux for a wave with a SW to NE tilt. We find good confirmation of this geostrophic relation in our analysis - Fig. 14 shows that the large SW/NE tilt of wavenumber 6 at low latitudes and high levels is associated with a poleward flux of momentum.

The same diagnostic formula also provides us with some information with which to understand the structural changes during the forecast. At low latitudes and upper levels where the eddy momentum flux increases, we find an increase

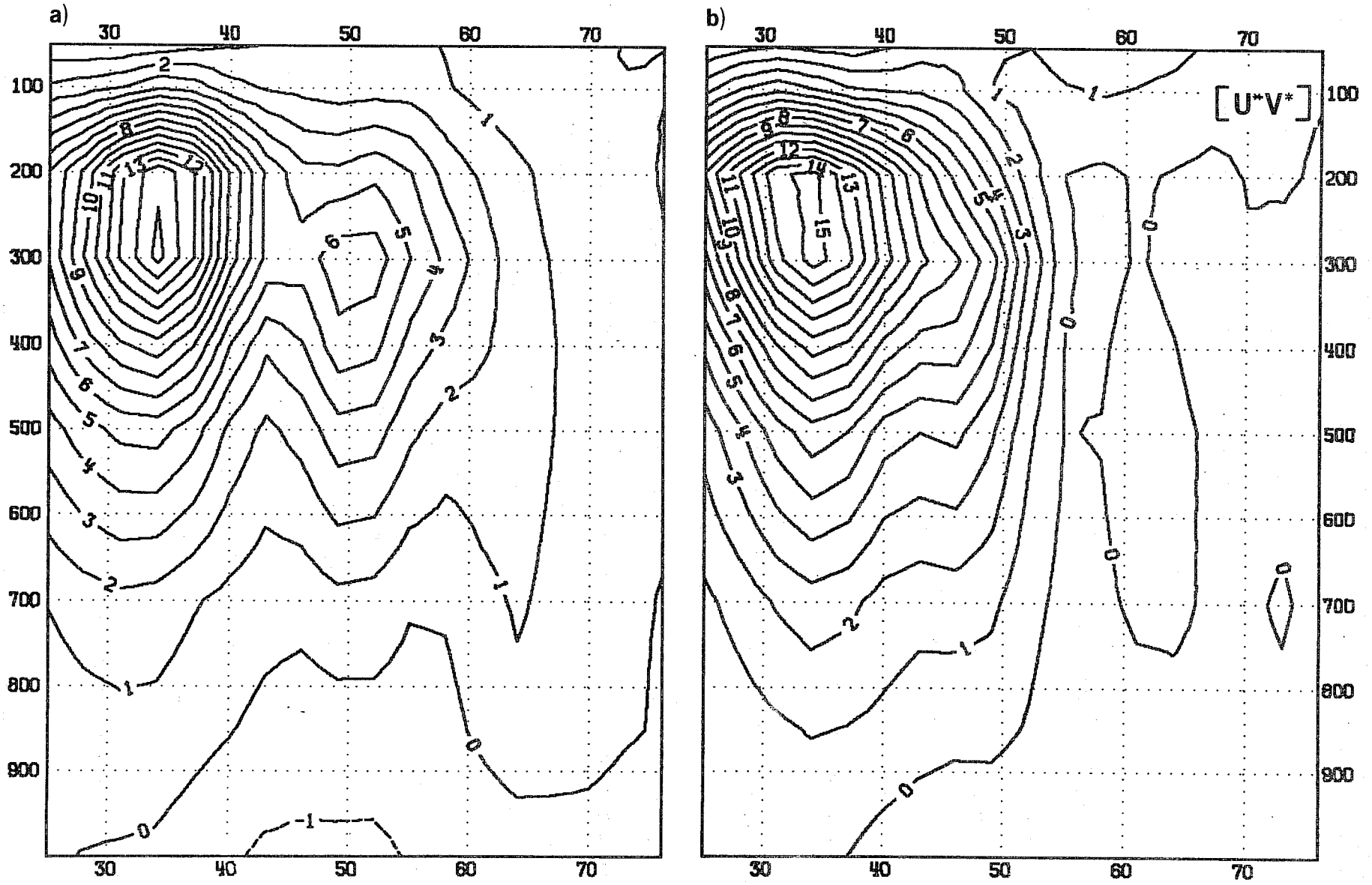

Fig. 22 Latitude-height section of the eddy momentum flux for the MFBW's in the initialised analysis. Units: $m^2 s^{-2}$. (a) Winter 1980/81, (b) Winter 1981/82.

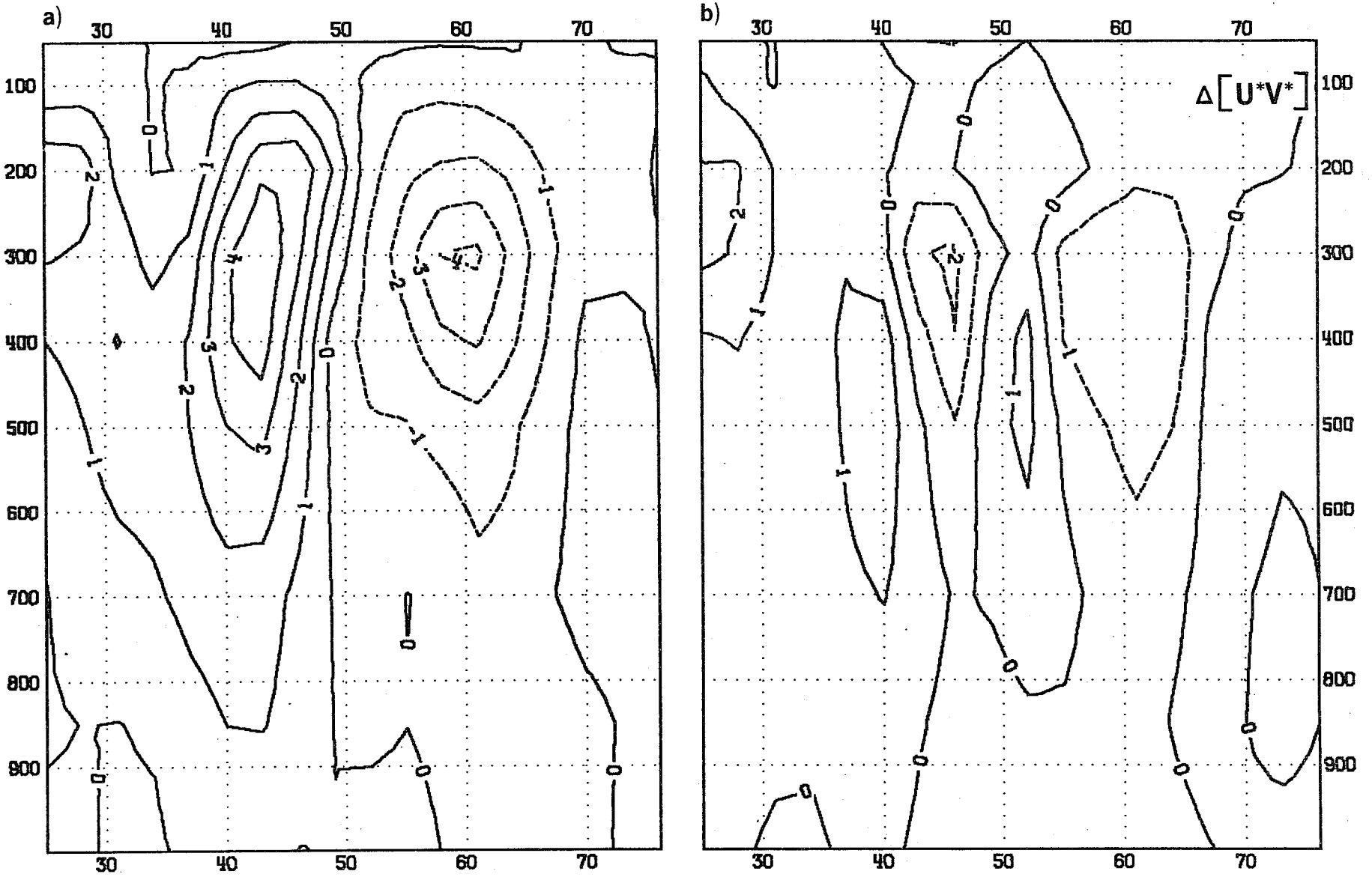

Fig. 23 Latitude-height section of the eddy momentum flux error for the MFBW's. Forecast (D+3) - analysis. Units: $m^2 s^{-2}$ (a) Winter 1980/81, (b) Winter 1981/82.

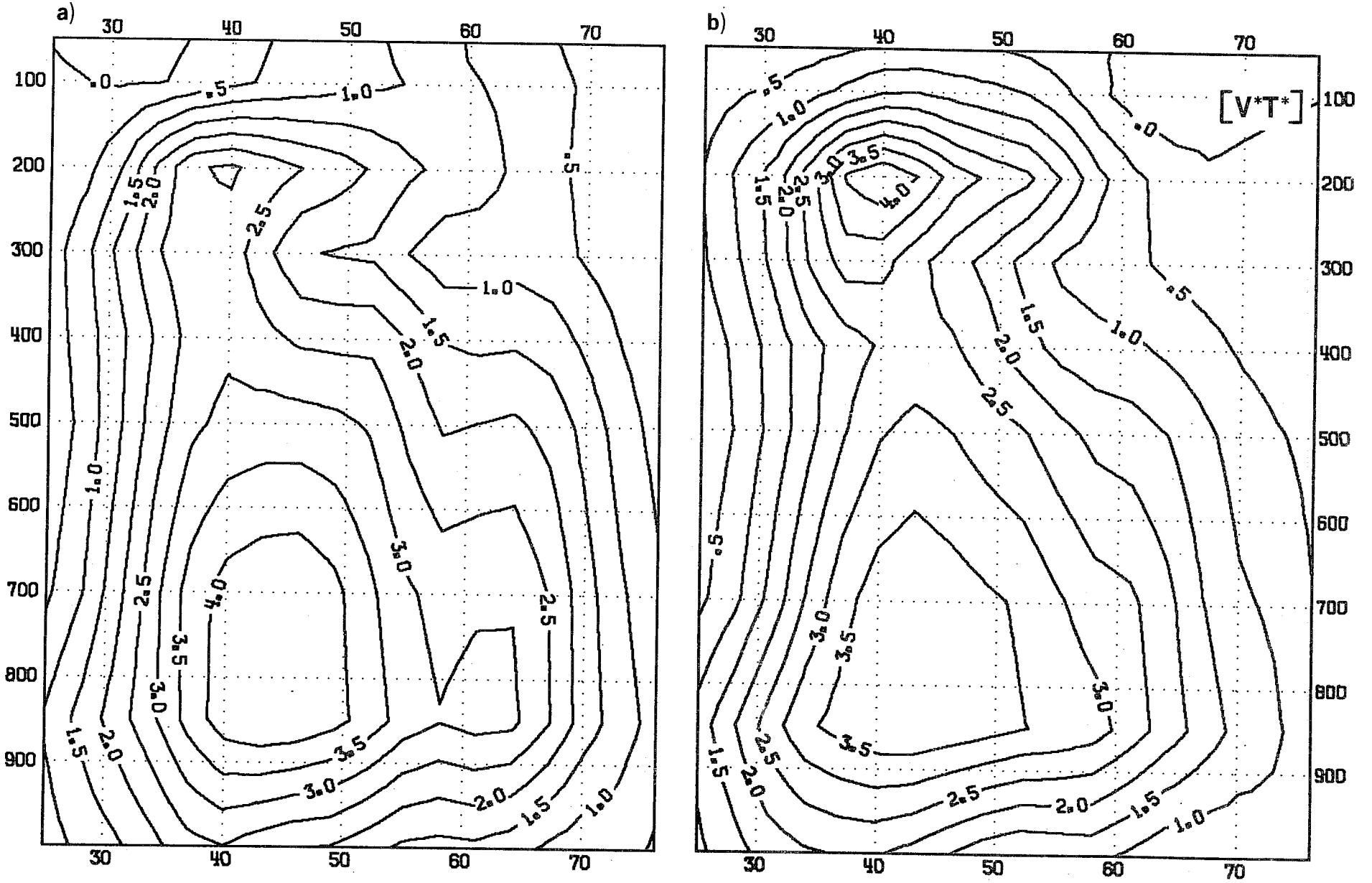

Fig. 24 Latitude-height section of the eddy heat flux for the MFBW's in the initialised analysis
Units: m s^{-1} K. (a) Winter 1980/81, (b) Winter 1981/82.

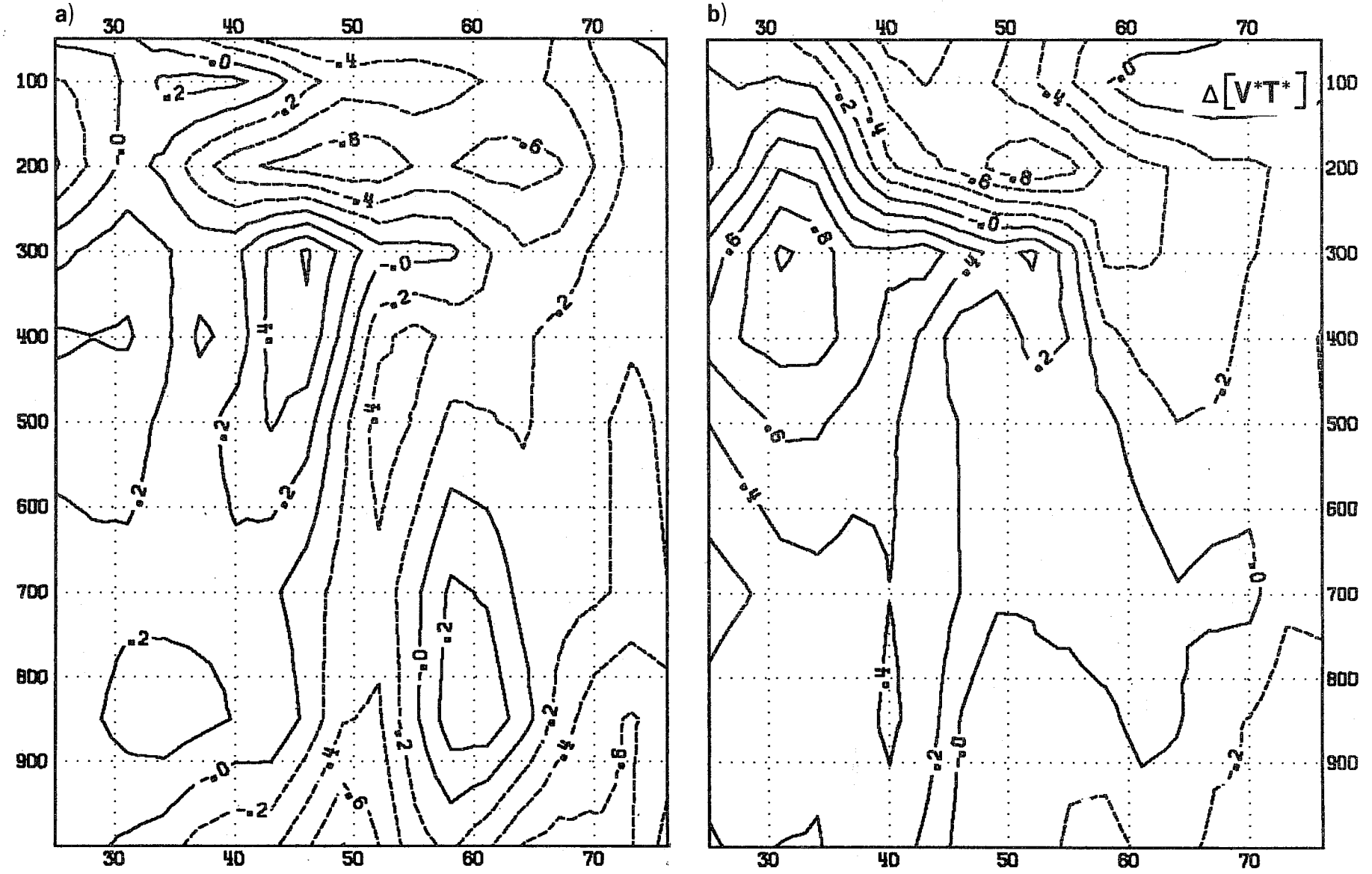

Fig. 25 Latitude-height section of the eddy heat flux error for the MFBW's. Forecast (D+3) - analysis. Units: m s^{-1} K. (a) Winter 1980/81, (b) Winter 1981/82.

of the SW/NE tilt as well. This change of the horizontal phase tilt is not only present for wavenumber 6 but for the other wavenumbers as well. One indication of an interaction process between the eddies and the zonal mean flow can be seen in the change of the mean zonal flow which has decreased at low latitudes and increased at middle latitudes (see Fig. 5). On the other hand there seems to be a close connection between the horizontal tilt and the interaction between the baroclinic waves at middle latitudes with the flow in the tropics. This suggests that the forcast errors in the tropics, which grow faster than at middle latitudes, can have an important effect on the interaction of the two regions. Haseler (1982) has shown in case studies that errors arising from the interaction of deep mid-latitude troughs with the tropics can have a significant impact on the subsequent evolution of the flow in extra-tropical regions. Haseler shows that initially the SW/NE tilt of the baroclinic waves increases too much, a result which agrees with the structural changes found here with the wavenumber-frequency analysis. The incorrect orientation of the troughs then leads to a spurious conversion from eddy to zonal kinetic energy. In other words the increased phase tilt may lead to a stronger barotropic damping of the baroclinic waves.

6.2.3 Horizontal eddy heat flux

The horizontal eddy heat flux (Fig. 24) is poleward almost everywhere in the latitude-height plane with a maximum flux near the latitude where the maximum of the temperature variance was found (Fig.19). In the vertical the analysis shows two maxima, one in the lower troposphere and one above the tropopause. The upper level maximum implies a counter gradient heat flux in the lower stratosphere. For both regions with large heat fluxes a small phase difference between v and T (see Fig. 16) indicates that the wave is fairly efficient at transporting heat poleward. In agreement with the diagnostic formula B5, the horizontal heat flux also corresponds to the vertical tilt of

the geopotential height wave (see Fig. 16) which is largest in the lower troposphere and above 300 mb.

The differences between the forecast ensemble and the analyses have some common features in the two winters. In both cases the upper level heat flux becomes weaker at high and middle latitudes (Fig. 25), and this is closely related to the decrease of the temperature variance in that region. At low latitudes we notice a positive deviation of the horizontal eddy heat flux where earlier we saw an increase of the SW/NE tilt of all waves (Fig. 15 shows this for wavenumber 6). With almost no phase change near the surface this means an increased vertical tilt of the geopotential height wave at low latitudes.

6.2.4 Vertical velocity and vertical eddy heat flux

The major vertical velocity variance maximum in the analysis (Fig. 26) is found 12 degrees south of the variance maximum of the geopotential height waves. The normal mode initialization scheme used at ECMWF (Temperton and Williamson, 1979) is applied in spherical geometry and does not zero the vertical velocity field at the outset. Leith (1980) has shown that if one starts from a state of linear balance on an f-plane (with vertical velocity initially zero), then the first iteration of the non-linear normal mode initialzation leads to a state satisfying the equations of quasi-geostrophic theory; in particular the vertical velocity satisfies the quasi-geostrophic omega equation. Our results for the vertical velocity suggest that, despite differences in technique, the operational initialization scheme produces vertical velocity fields in good agreement with Leith's results.

The spin-up process, which increases the vertical velocity mainly in the first 24 hours of the forecast, adds about 50% to the analysed variance up to D+3 (Fig. 27). This rather fast increase of the vertical velocity at the beginning of the forcast is an indication of significantly reduced divergent

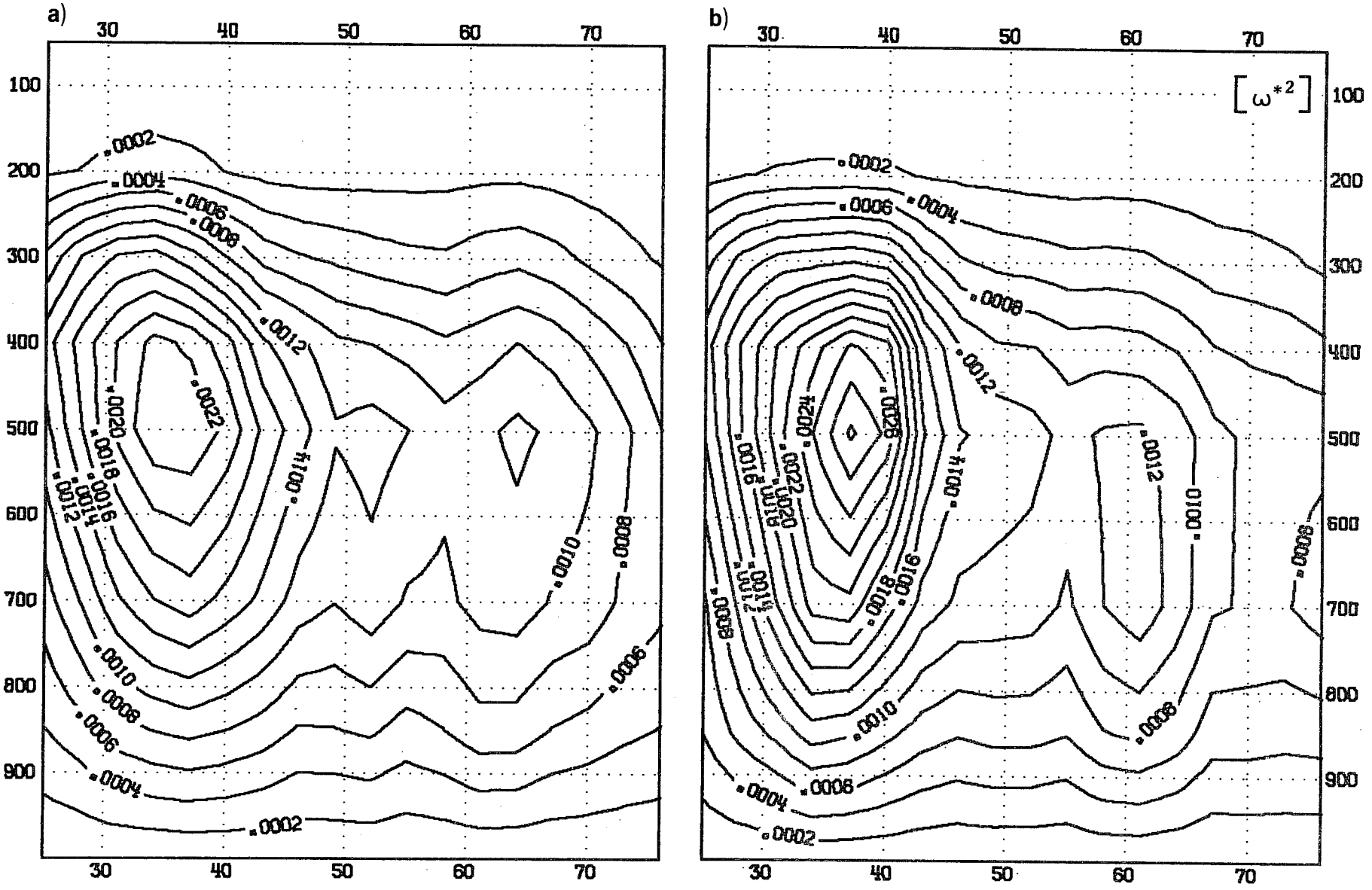

Fig. 26 Latitude-height section of the vertical wind variance for the MFBW's in the initialised analysis. Units: $Pa^2 s^{-2}$. (a) Winter 1980/81, (b) Winter 1981/82.

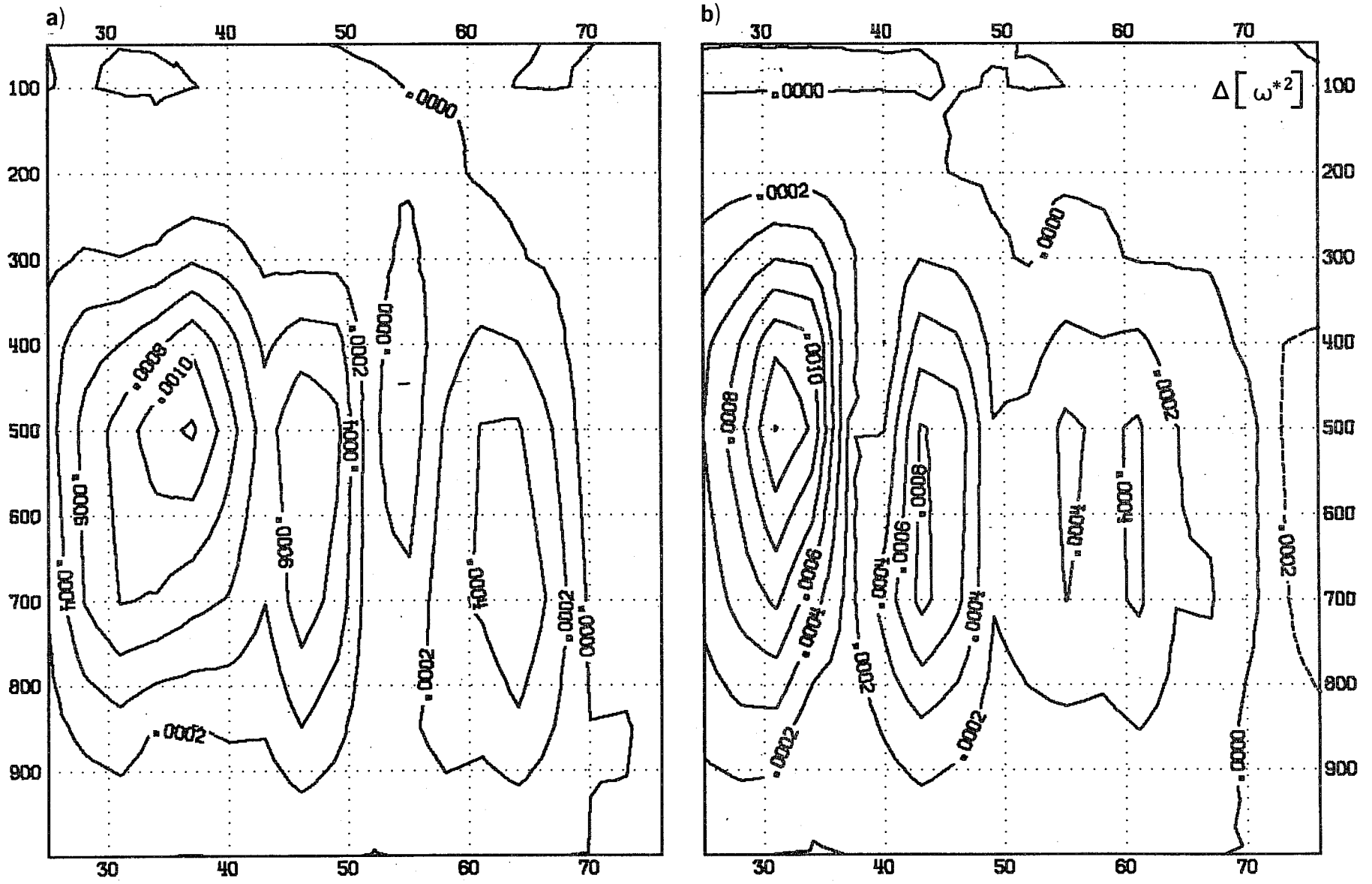

Fig. 27 Latitude-height section of the vertical wind variance error for the MFBW's. Forecast (D+3) - analysis. Units: $Pa^2\ s^{-2}$. (a) Winter 1980/81, (b) Winter 1981/82.

winds resulting from the adiabatic normal mode initialsation. Within 24 hours the forecast model generates reasonable vertical motion fields. Since September 1982 large scale diabatic forcing has been incorporated in the normal mode initialisation with the intent of reducing the suppression of divergent winds in the initial data (W. Wergen, pers. comm. 1983). From a comparison of the forecast errors in the winter 1982/83 (not shown here) with the previous two winters we can see a 75% reduction of the spin-up process for the scales of the MFBW's whereas the reduction is less for the smaller scales (HFBW's). This shows that the spatial filtering of the diabatic forcing in the diabatic initialization procedure leads to the result that the initialization is effectively adiabatic on the smaller scales. Calculations of the energy budgets (E. Oriol, pers. comm. 1983) support this result; they show that the spin-up process is still present but is weaker than with the adiabatic initialization.

From the single wavenumber representation (see Fig. 16) we have seen that the phase difference between upward motion and maximum temperature is almost 45 degrees in the middle troposphere. This gives a dominant upward directed eddy heat flux. In the vertical the maximum flux is found between the temperature and vertical velocity maximum. Looking at the vertical structure of the single wavenumber 6 (see Fig. 16), we see that upward motion occurs well to the east of the trough with only a small backward tilt in the vertical. From the phase difference of the geopotential and the vertical velocity we can expect an upward geopotential flux ($\overline{z'w'}$) at 700 mb and above and a downward flux at lower levels. Thus eddy kinetic energy is exported by pressure forces from the region where available potential energy is converted into eddy kinetic energy.

The spin-up process in the vertical velocity increases the vertical eddy flux of heat as well. Thus the baroclinic part of the energy cycle is

significantly enhanced at the beginning of the forecast, whilst a further increase follows in the later parts of the forecast (Arpe, 1983).

6.3 Geographical distribution of the forecast errors in the medium frequency baroclinic waves

The geographical distribution of the variance for the MFBW's shows two maxima of wave activity in the winter 1980/81 (Fig. 28). Both of them are located downstream of the two major troughs on the eastern coasts of North America and Asia. The MFBW's are more intense in the Atlantic than in the Pacific. A pronounced ridge is present in the time-mean height field over the western parts of North America and over the eastern Pacific (see Fig. 6) so that a clear minimum separates the Atlantic wave activity region from the one in the western Pacific. In the following winter (1981/82) the time-mean flow over the eastern Pacific and western parts of North America is much more zonal (see Fig. 7). In this situation the two regions of baroclinic wave activity are merged into one centred on the west coast of North America. In the North Atlantic the MFBW's are much weaker in this winter than in the previous one. Apart from the two winters examined in detail here, the cross-spectral analysis has also been calculated for the winter 1982/83. Comparing all three winters, the geographical distribution of the MFBW's have a larger annual variation than the high frequency group which corresponds more to the band passed filtered variance shown by Blackmon and Lau (1980).

Though the geographical distribution of the variance of the medium frequency baroclinic waves is different in the two winters, the forecast errors are very similiar in both cases (Fig. 29). In general the MFBW's are weakened in the forecast over North America and enhanced over SE Europe. When we compare the variance of other forecast ensembles (D+1 and D+5 not shown here) with the variance of the analyses we see that the geographically fixed error pattern is already established by day one. The negative error in the Atlantic region then increases very rapidly until D+5, whereas the positive

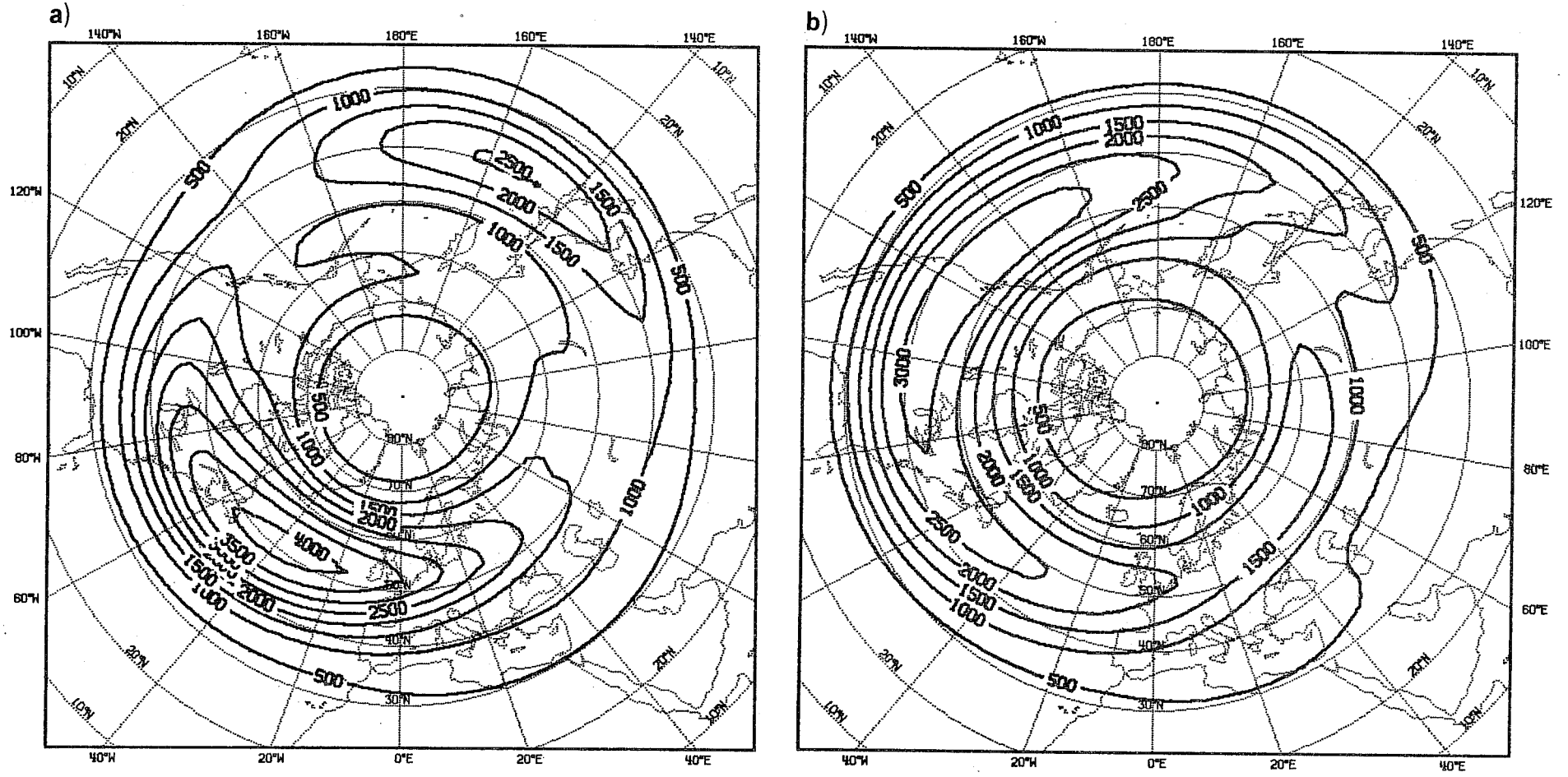

Fig. 28 Geographical distribution of the geopotential height variance for the MFBW's at 500 mb. Units: m^2. (a) Winter 1980/81, (b) Winter 1981/82.

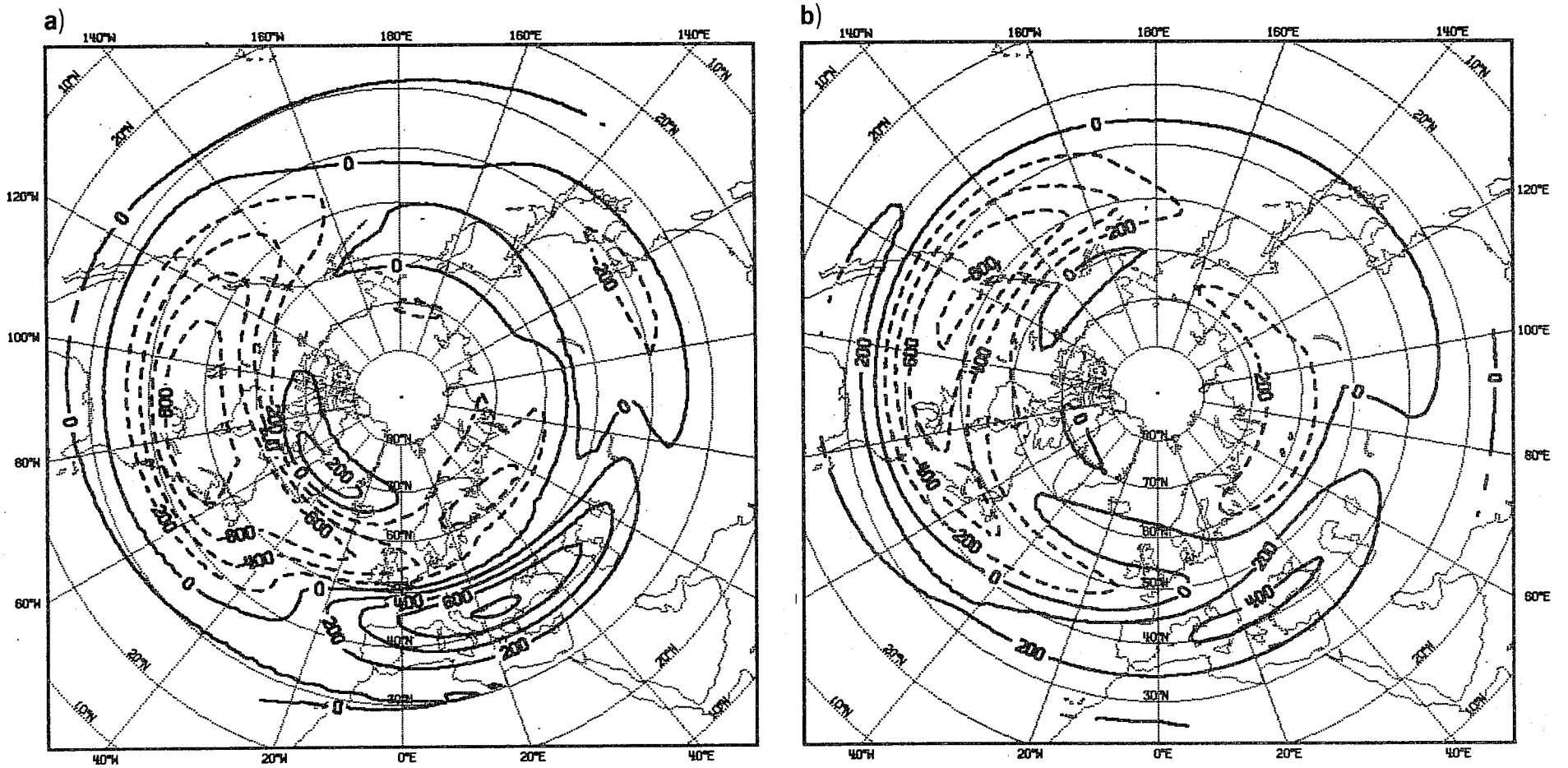

Fig. 29 Geographical distribution of the geopotential height variance error. (D+3 - D+0) for the MFBW's at 500 mb. Units: m^2. (a) Winter 1980/81, (b) Winter 1981/82.

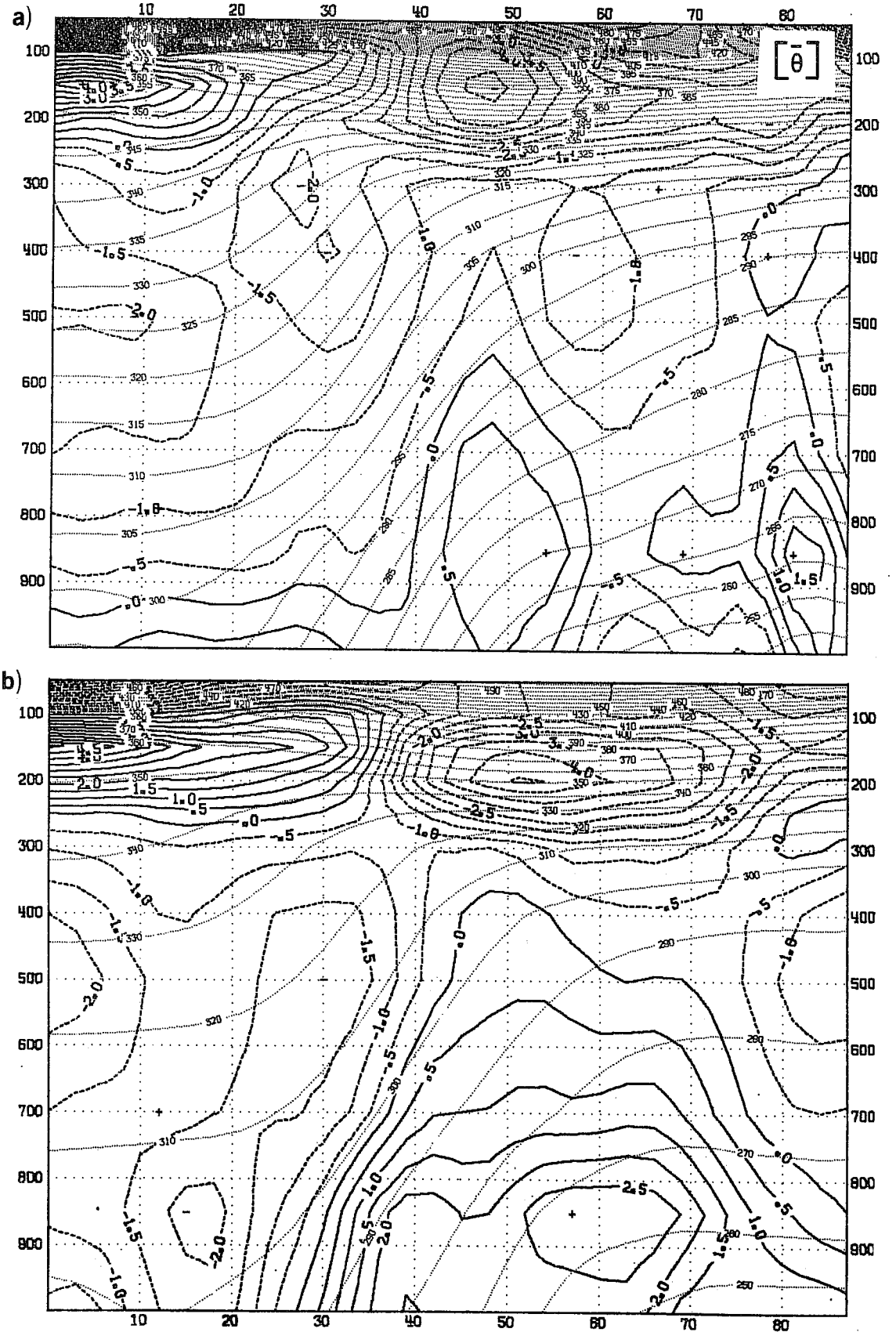

Fig. 30 Latitude-height plot of the mean time potential temperature in the initial analysis (dotted lines) and the difference between the forecast and the analysis (D+3 - D+0, thicker lines). Time averaging period 112 days. Units : K. a) Winter 1980/81 zonally averaged from 117° W to 90° W, b) Winter 1981/82 zonally averaged from 90° W to 60° W.

error over SE Europe has a much smaller growth rate. The difference maps of the variance for other levels (not presented here) indicate increased negative deviation of the forecast variance from the analysed variance with height. A corresponding error in the temperature variance suggests the baroclinic nature of the forecast error over North America.

The changes of the time-mean state in the forecast over North America are quite remarkable in this context. A warming over large areas of the North American continent and a cooling over Central America and the Caribbean has led to a decrease of the north-south temperature gradient at middle latitudes. The location of the largest reduction of the temperature gradient occurs in the eastern part of North America in the winter 1980/81 and in the central parts in the winter 1981/82. A vertical cross-section for the corresponding longitudes (Fig. 30) shows the difference between the time mean potential temperature of the forcast (D+3) and the analysis. A warming of low levels at high latitudes and a cooling of upper levels at low and middle latitudes has led to a decrease of the baroclinicity at middle latitudes where we find the decrease of the wave activity of the MFBW's. This warming of the lower levels is consistent with the error in the mean height field (Fig. 6) which produces too strong southerlies over North America by day 3.

For a zonal flow in thermal wind balance, the linearized equations for the potential temperature (θ) and quasi-geostrophic potential vorticity equation give an equation for the normal modes which relates the growth rate (σ) of the baroclinic waves to the meridional slope of the mean potential temperature ($-\bar{\theta}_y/\bar{\theta}_z$) and to the zonal slope of the wave potential temperature ($-\theta'_x/\theta'_z$)

$$\sigma = \frac{fk^2}{k^2+\ell^2} \frac{-\bar{\theta}_y/\bar{\theta}_z}{-\theta'_x/\theta'_z}$$

where k and l are the zonal and meridional wavenumbers, and x,y and z are the derivative indices. This relation indicates a decrease of the of the growth rate of the baroclinic waves when the vertical slope of the mean potential temperature field decreases and the slope of the temperature wave does not change. The decrease of the vertical slope of the temperature wave (see Fig. 16 and Fig. 17) would increase the growth rate, but this change is only present at lower levels.

Over SE Europe the variance increase of the MFBW's during the forecast has a larger barotropic part suggested by a smaller variation with height. The European forecast error pattern in the two winters compared here is also found in the winter 1982/83. Rather noticeable is the fact that the enhancement of the MFBW's in the winter 1980/81 is nearly double the size found in the two following winters. The forecast error in the time-mean field (see Figs. 6 and 7) over western Europe contributes to a strengthening of the mean flow from the Atlantic into southern Europe. It seems that the stronger flow across the Alps from NW to SE might be responsible for the enhancement of the MFBW's in that region. In the winter 1980/81 when the forecast error in the mean flow was largest, the increase of the MFBW's was double the size found in the following winter. It is also worth mentioning that in April 1981 the heights of the mountains in the model were increased, which may have contributed to an increased blocking effect over the Alps. But still we find that in many winter cases that almost stationary troughs over SE Europe start to travel eastward in the forecasts. The forecast error in the mean flow over the west coast of North America has a different relationship with the flow pattern; there we do not find such a significant increase of the flow over the mountains.

7. SYSTEMATIC FORECAST ERRORS OF HIGH FREQUENCY BAROCLINIC WAVES

The second wavenumber-frequency band to be studied contains the high frequency baroclinic waves (HFBW's: wavenumber 5 to 9 in a period range from 2.4 to 3.5 days). The vertical structure of the waves in this class is very similar to the structure of the medium frequency baroclinic waves. Therefore we will not discuss the details of the single wavenumber structure, but concentrate on the description of the wavenumber and frequency integrated variances and covariances.

7.1 Structure of the forecast error in the meridional plane

7.1.1 Geopotential and temperature

The meridional structure of the geopotential height variance shows that the latitudinal distribution of these waves can differ very much from one winter to the next (Fig. 31). While the main baroclinic wave activity in the winter 1981/82 is concentrated in middle latitudes, we see two latitude bands of maximum variance in the preceding winter. The ratio of the upper level and surface variance maxima is around 5 to 1 which is clearly smaller than that for the MFBW's where it was 8 to 1. The tendency for the higher wavenumbers (which are faster moving) to have smaller upper level maxima relative to the surface values has already been predicted by the linear theory of baroclinic waves (Gall, 1976). The large decrease of the variance with height above the 300 mb indicates that these waves are confined to the troposphere. This is also evident from the cross-spectral analysis of different levels. The level to level coherence of the disturbances drops sharply above 300 mb.

The differences in the meridional structure of the geopotential height disturbances in the two winters are reflected in the thermal structure (Fig. 32). A double maximum appears in the winter 1980/81 throughout the troposphere, whereas in the next winter two maxima are present only at lower levels. In both winters the compensating temperature variance at 200 mb has

the same magnitude as the tropospheric one.

Though the two winters have a different latitudinal distribution of baroclinic disturbances, the changes occuring in the forecast within the first 72 hours are remarkably similar. In both winters the geopotential height variance decreases at high and low latitudes (Fig. 33). In middle latitudes a small band of enhanced variance can be found which extends from the surface to the upper troposphere. This latitude dependent picture of changes during the forecast contrasts with the MFBW's which are weakened in a broad latitude band. The vertical structure of the differences indicates that this positive deviation has a large barotropic part. The baroclinic part becomes evident from the changes in the thermal structure of the HFBW's (Fig. 34). At the same latitude where the geopotential height waves are too strong, we find a well defined positive deviation of the temperature waves centred at 700 mb in both winters. The high and lower latitude negative deviations of the geopotential height waves are closely correlated to negative deviations of the temperature waves in the same latitude band. At 200 mb temperature has a compensating effect. Here the weakening of the temperature wave is especially strong.

7.1.2 Horizontal eddy flux of momentum and heat

Meridional cross-sections of the horizontal eddy fluxes of heat and momentum for the two wavenumber-frequency groups (MFBW's and HFBW's) have a very similar structure. Therefore we will show only the differences between the forecast and the analysis for the HFBW's. As for the MFBW's the forecast changes of the horizontal eddy momentum flux have a very small scale (Fig. 35). A common change for both winters, and for most of the single wavenumber contributions, seems to be a decrease of the northward momentum flux at middle latitudes and high levels, where the SW/NE tilt decreases or where the tilt may even reverse its sign. This implies an increased convergence of the

eddy momentum flux between 40°N and 45°N where we noticed an increase in the mean zonal wind (see Fig. 5).

The changes of the meridional heat flux during the forecast (Fig. 36) closely resemble the changes for the variances of the temperature and the meridional wind component, with a negative deviation at high and low latitudes and a pronounced positive deviation at middle latitudes (where the heat flux increases by nearly 30%).

7.1.3 Vertical velocity and vertical eddy heat flux

The structure of the vertical velocity in the band of HFBW's is almost identical to that of the MFBW's. Within the first 24 hours (not shown here) the vertical velocity increases over a large latitude band due to the spin-up of the divergent winds. For more advanced forecast steps the difference pattern between the forecast and the analysis has changed (Fig.37), which we did not see for the MFBW's. The positive deviation is concentrated on a small latitude band which coincides with the position of the positive error of the geopotential height and temperature waves.

The vertical eddy heat flux has a similar error structure as the vertical velocity. A large increase of the upward eddy heat flux is the main change in the the D+3 forecast (Fig. 38). As for the vertical velocity itself, this deviation is restricted to a rather small latitude band compared to the changes we saw in the MFBW band. A weak decrease of the upward eddy heat flux is seen at higher latitudes.

7.2 Geographical distribution of the forecast errors in the high frequencies

In the winter 1980/81 the HFBW's have maximum variance in the North Atlantic around 58°N and in the Pacific at a much lower latitude of 36°N (Fig. 39a). In this geographical distribution the high frequency baroclinic waves

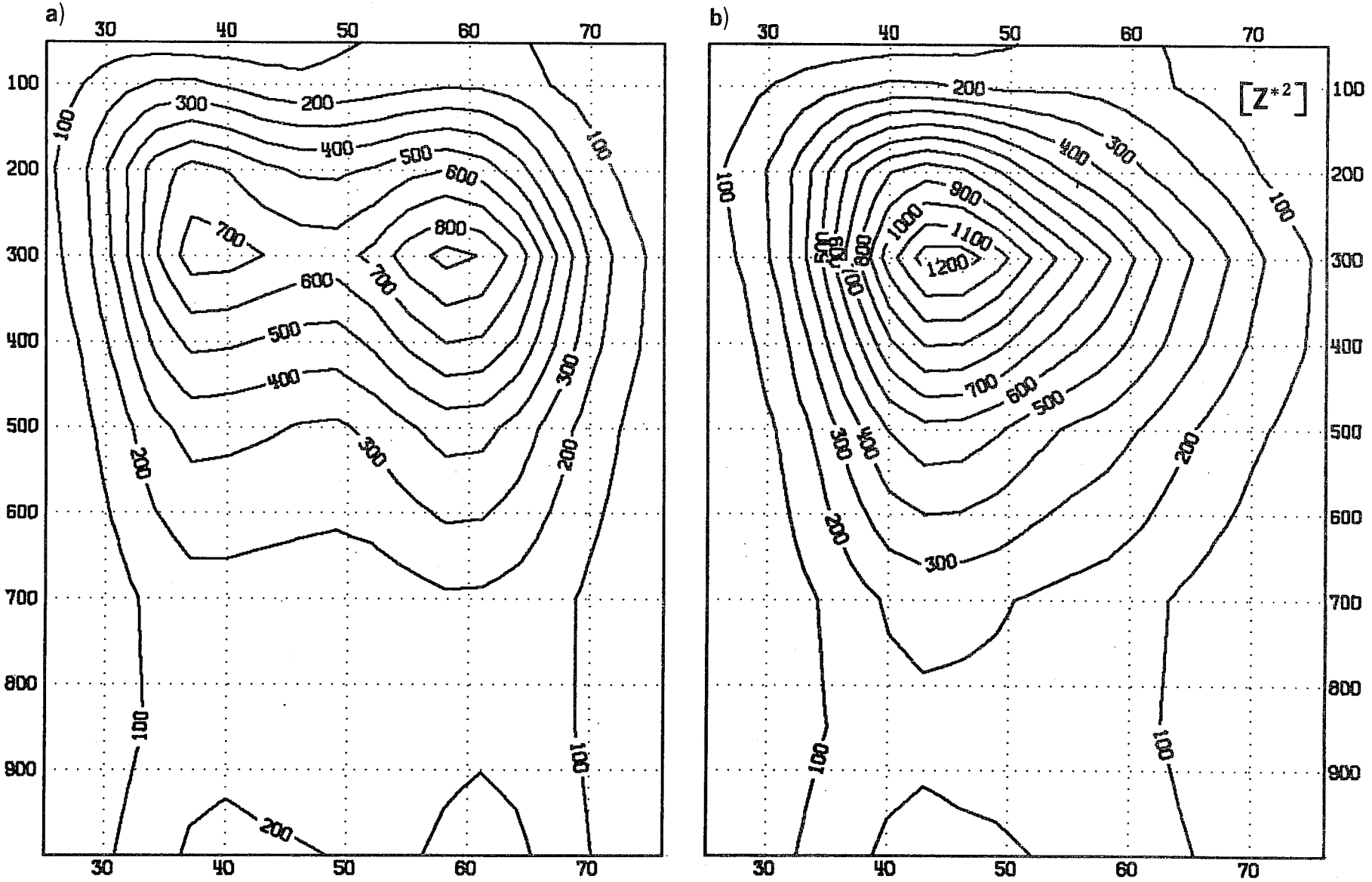

Fig. 31 Latitude-height section of the geopotential height variance for the HFBW's in the initialised analysis. Units: m^2. (a) Winter 1980/81, (b) Winter 1981/82.

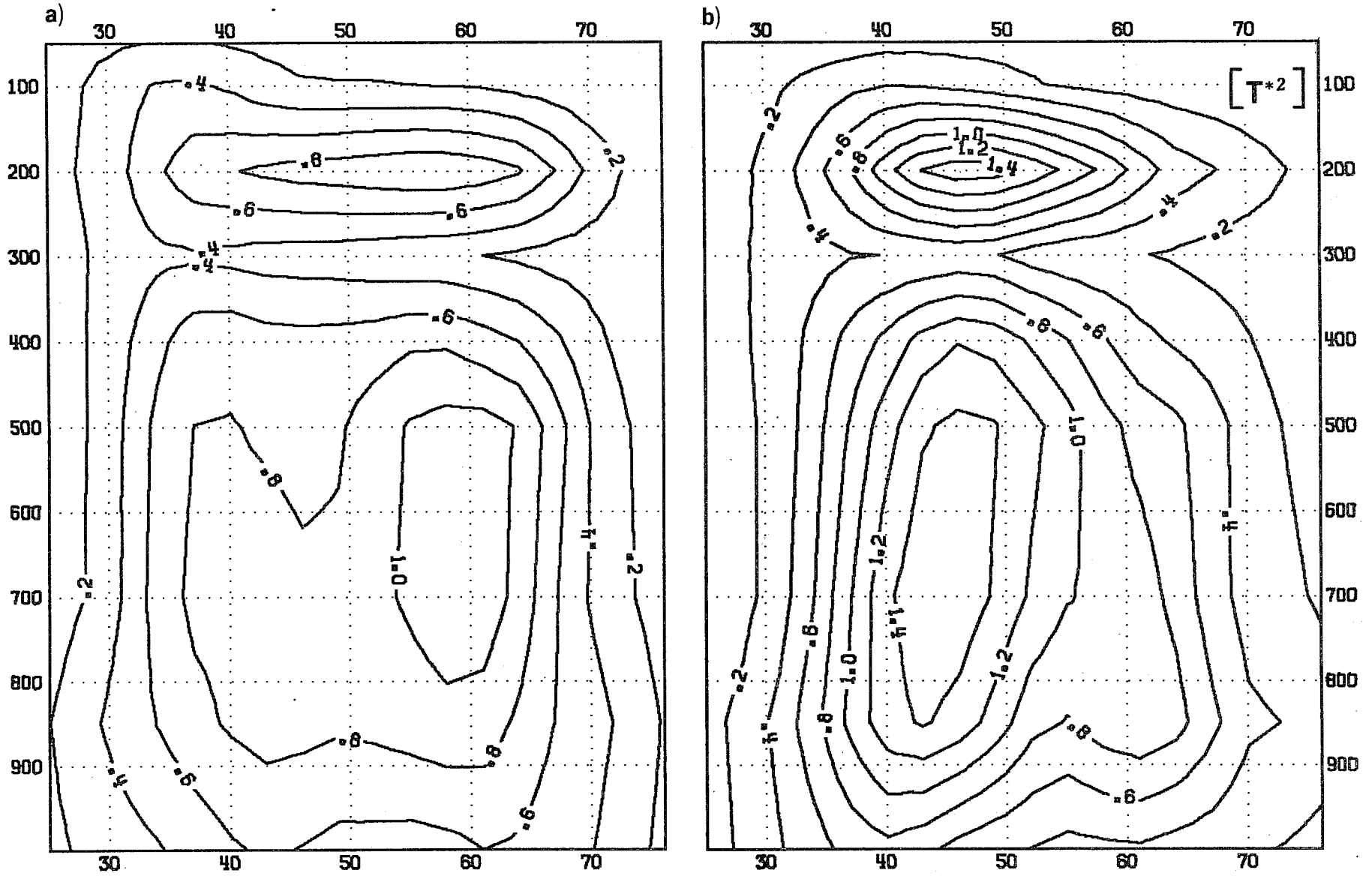

Fig. 32 Latitude-height section of the temperature variance for the HFBW's in the initialised analysis. Units: K. (a) Winter 1980/81, (b) Winter 1981/82.

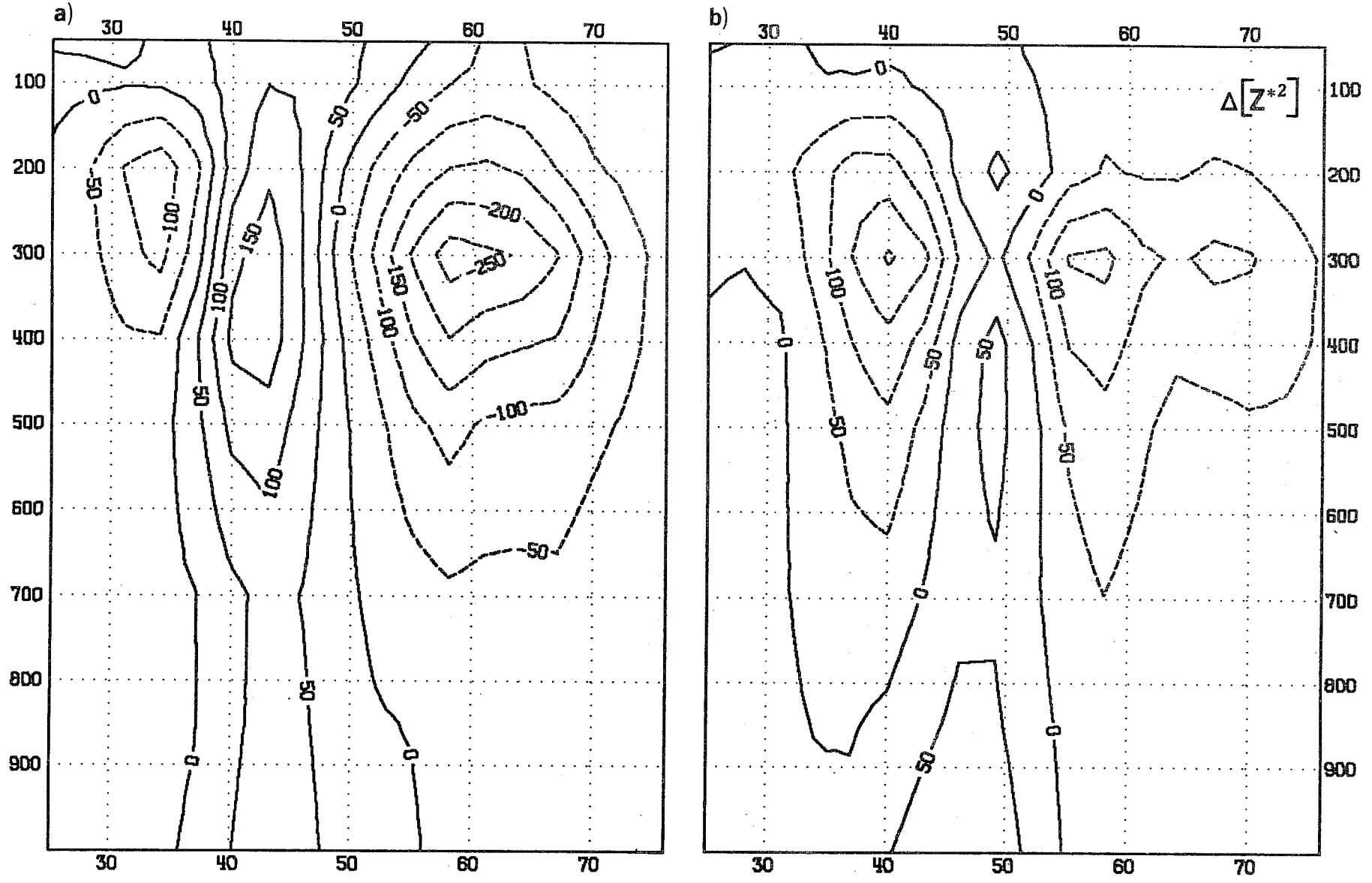

Fig. 33 Latitude-height section of the geopotential height variance error for the HFBW's. Forecast (D+3) - analysis. Units m^2. (a) Winter 1980/81, (b) Winter 1981/82.

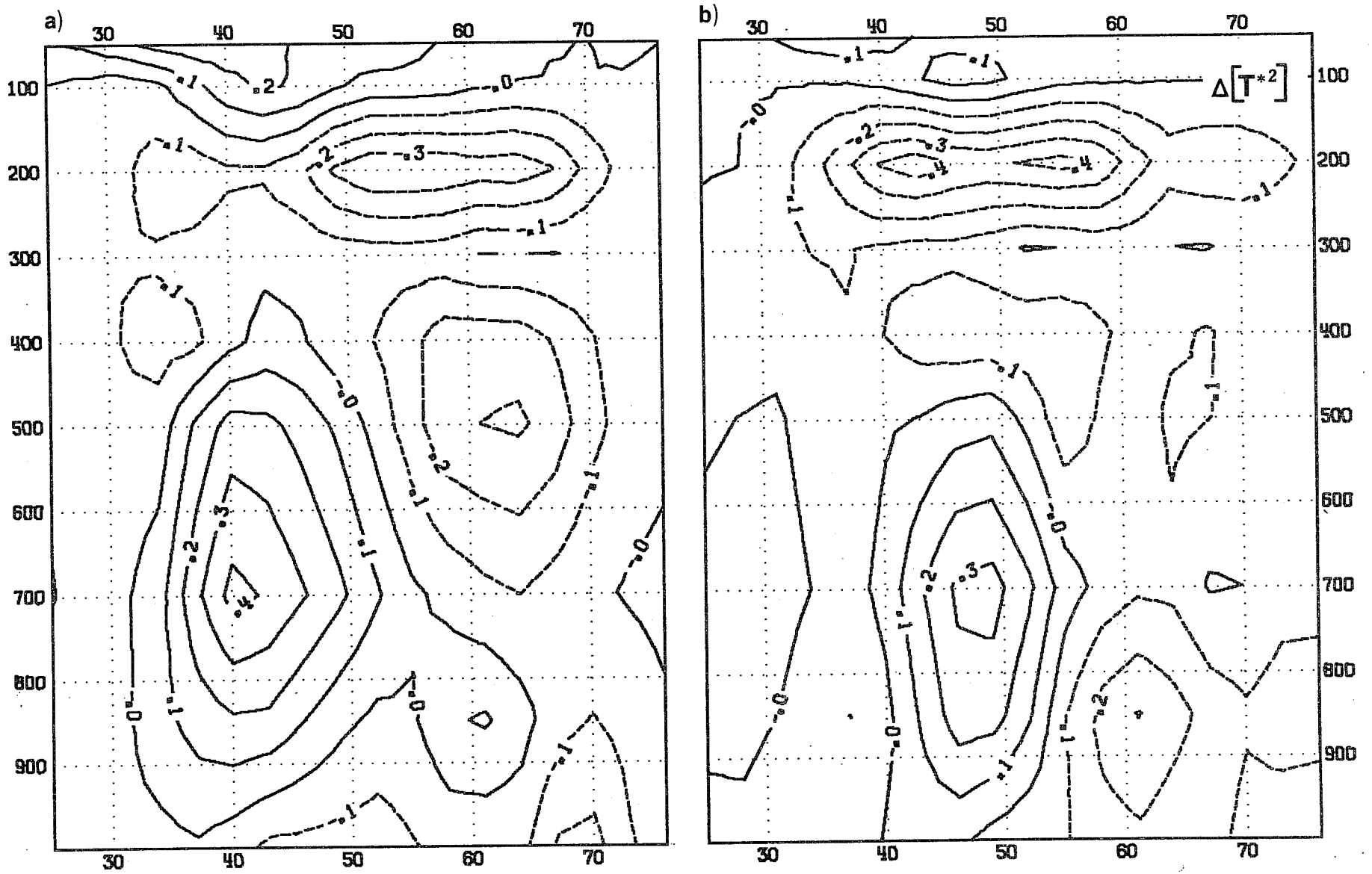

Fig. 34 Latitude-height section of the temperature variance error for the HFBW's. Forecast (D+3) - analysis. Units: K. (a) Winter 1980/81, (b) Winter 1981/82.

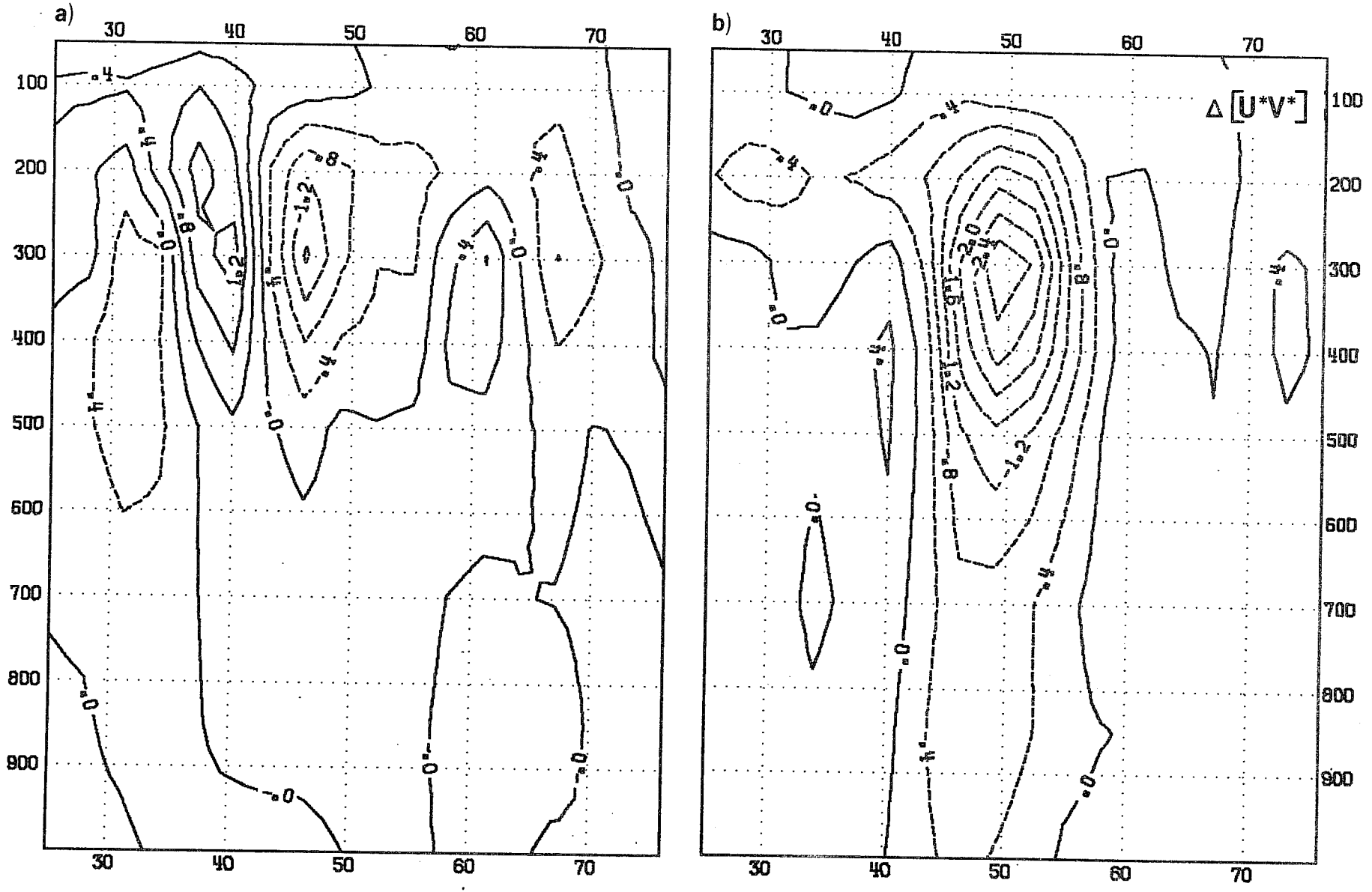

Fig. 35 Latitude-height section of the eddy momentum flux error for the HFBW's. Forecast (D+3) - analysis. Units: $m^2 s^{-2}$. (a) Winter 1980/81, (b) Winter 1981/82.

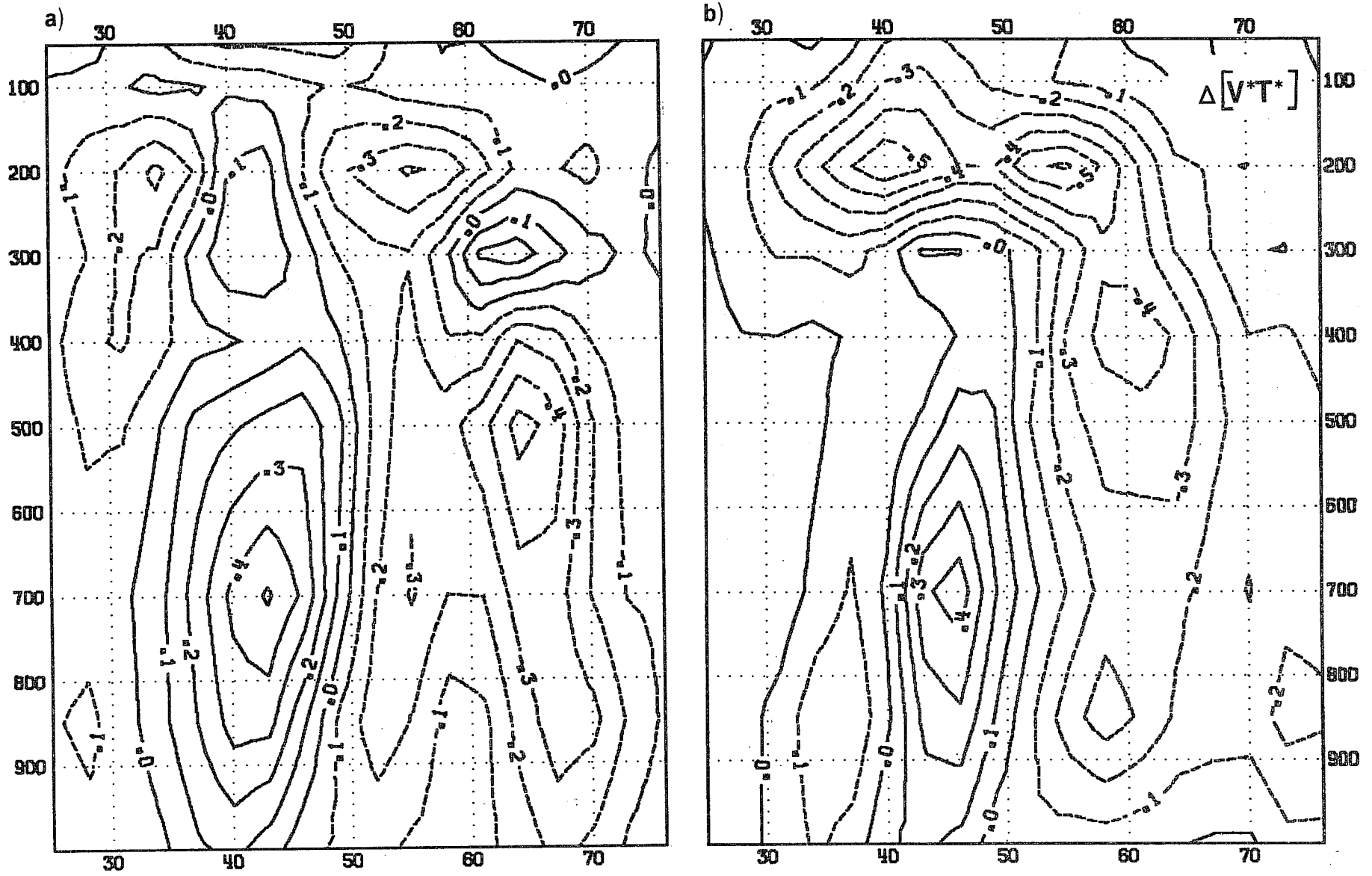

Fig. 36 Latitude-height section of the horizontal eddy heat flux error for the HFBW's. Forecast (D+3) - analysis. Units: m s^{-2} K. (a) Winter 1980/81, (b) Winter 1981/82.

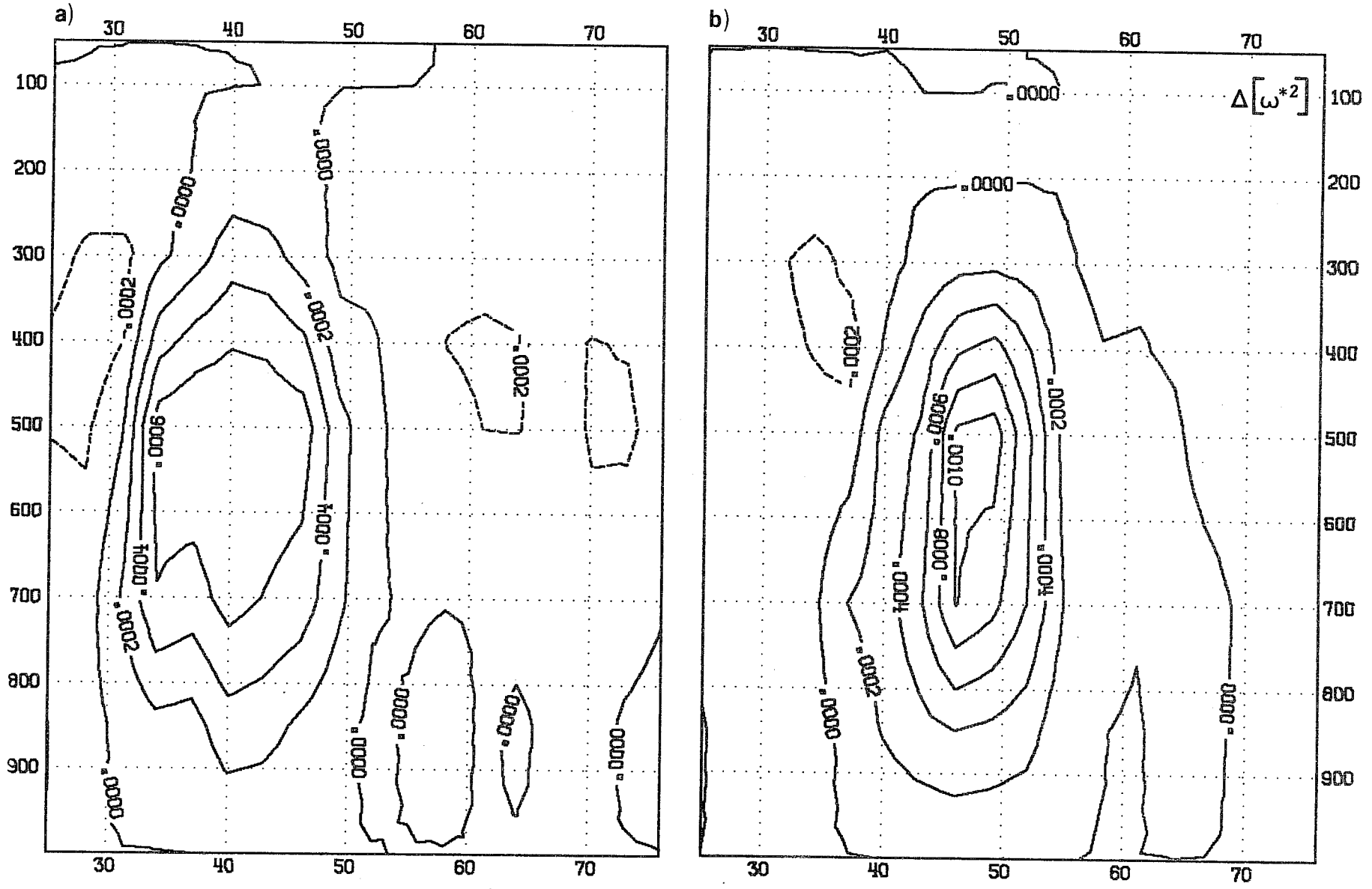

Fig. 37 Latitude-height section of the vertical wind variance error for the HFBW's. Forecast (D+3) - analysis. Units: Pa^2. (a) Winter 1980/81, (b) winter 1981/82.

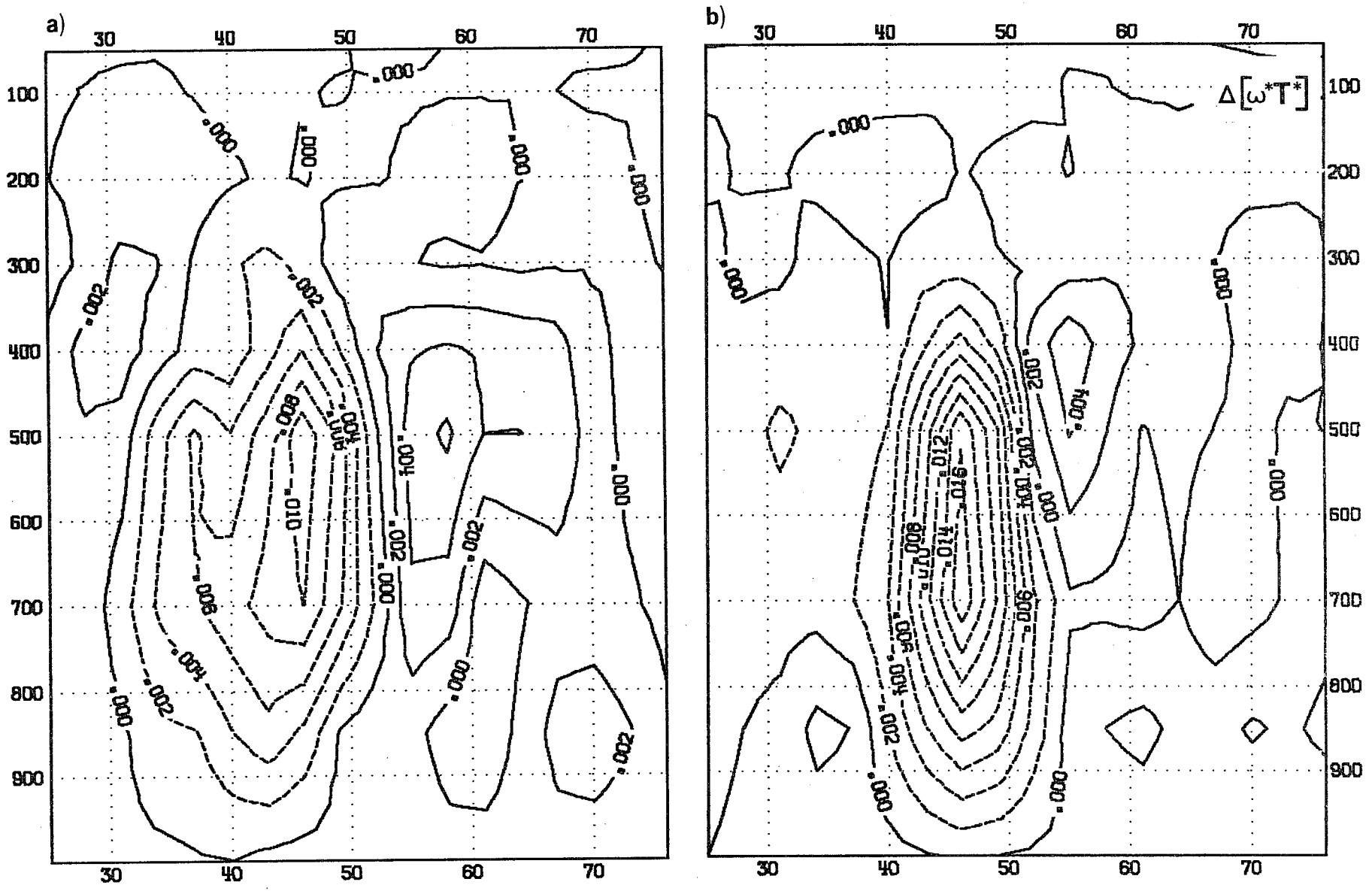

Fig. 38 Latitude-height section of the vertical eddy heat flux error for the HFBW's in the initialised analysis. Units Pa s^{-1}. (a) Winter 1980/81, (b) Winter 1981/82.

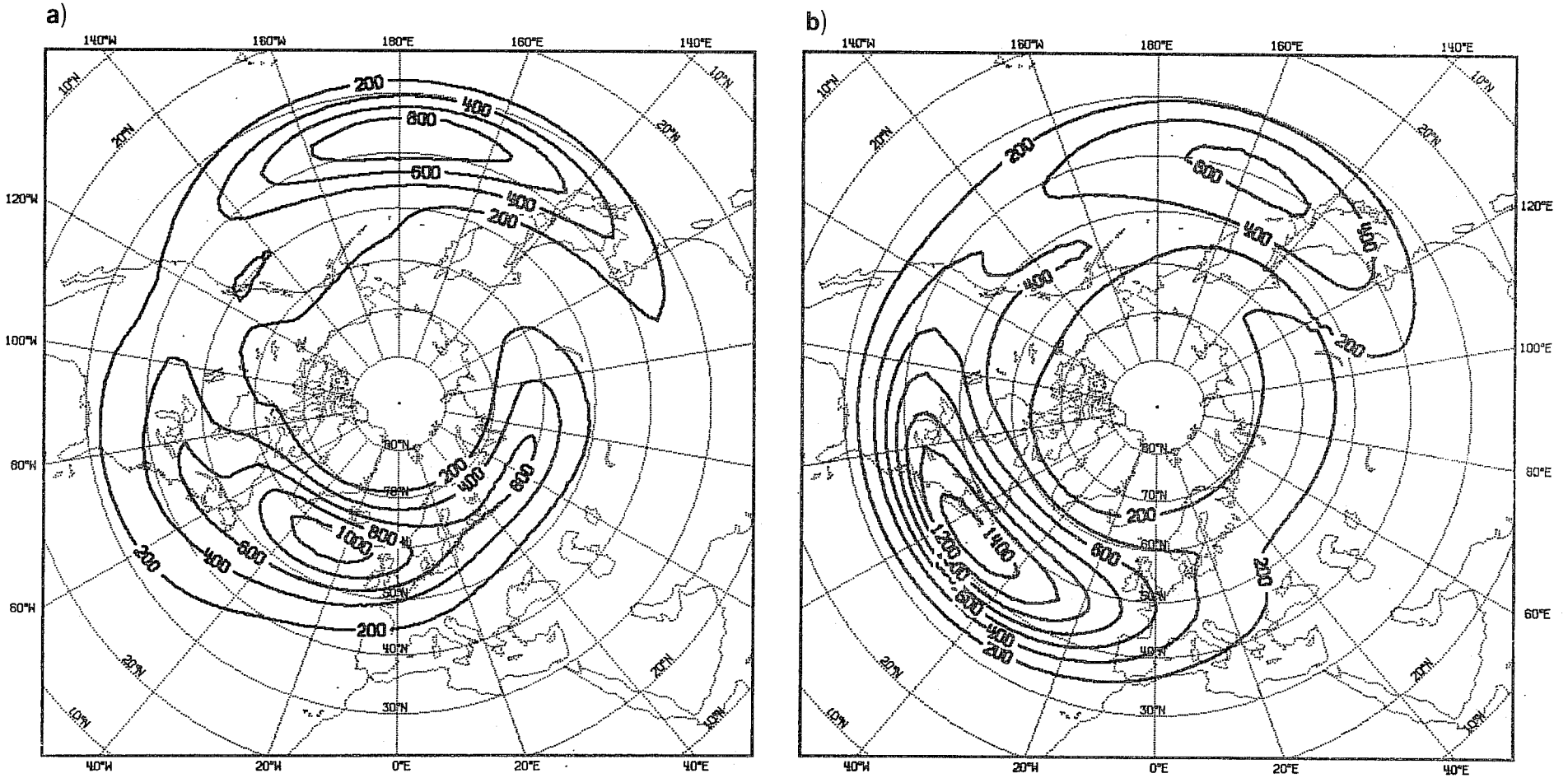

Fig. 39 Geographical distribution of the geopotential height variance for the HFBW's at 500 mb. Units: m^2. (a) Winter 1980/81, (b) Winter 1981/82.

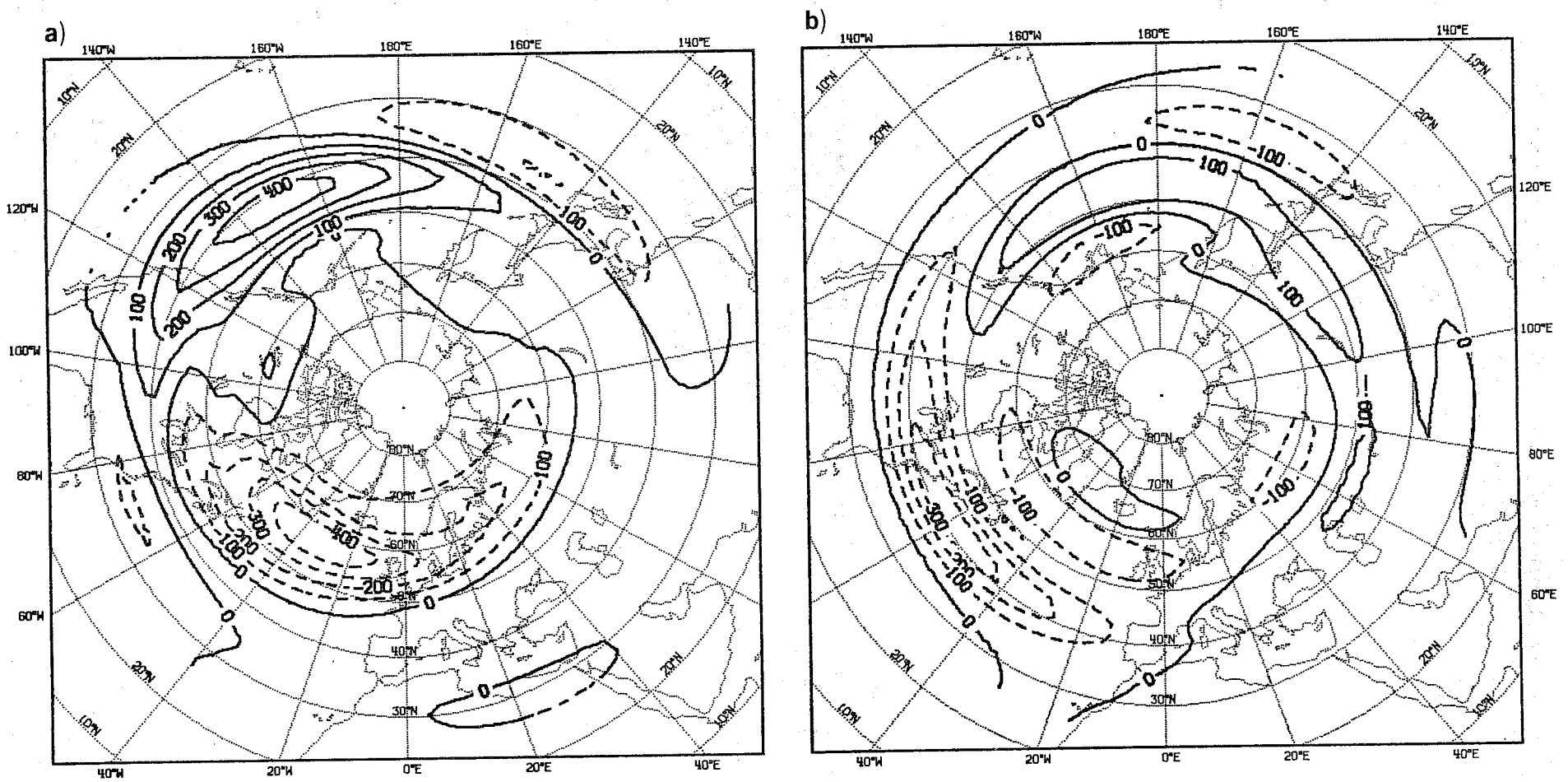

Fig. 40 Geographical distribution of the geopotential height variance error for the HFBW's at 500 mb. Units: m^2. (a) Winter 1980/81, (b) Winter 1981/82.

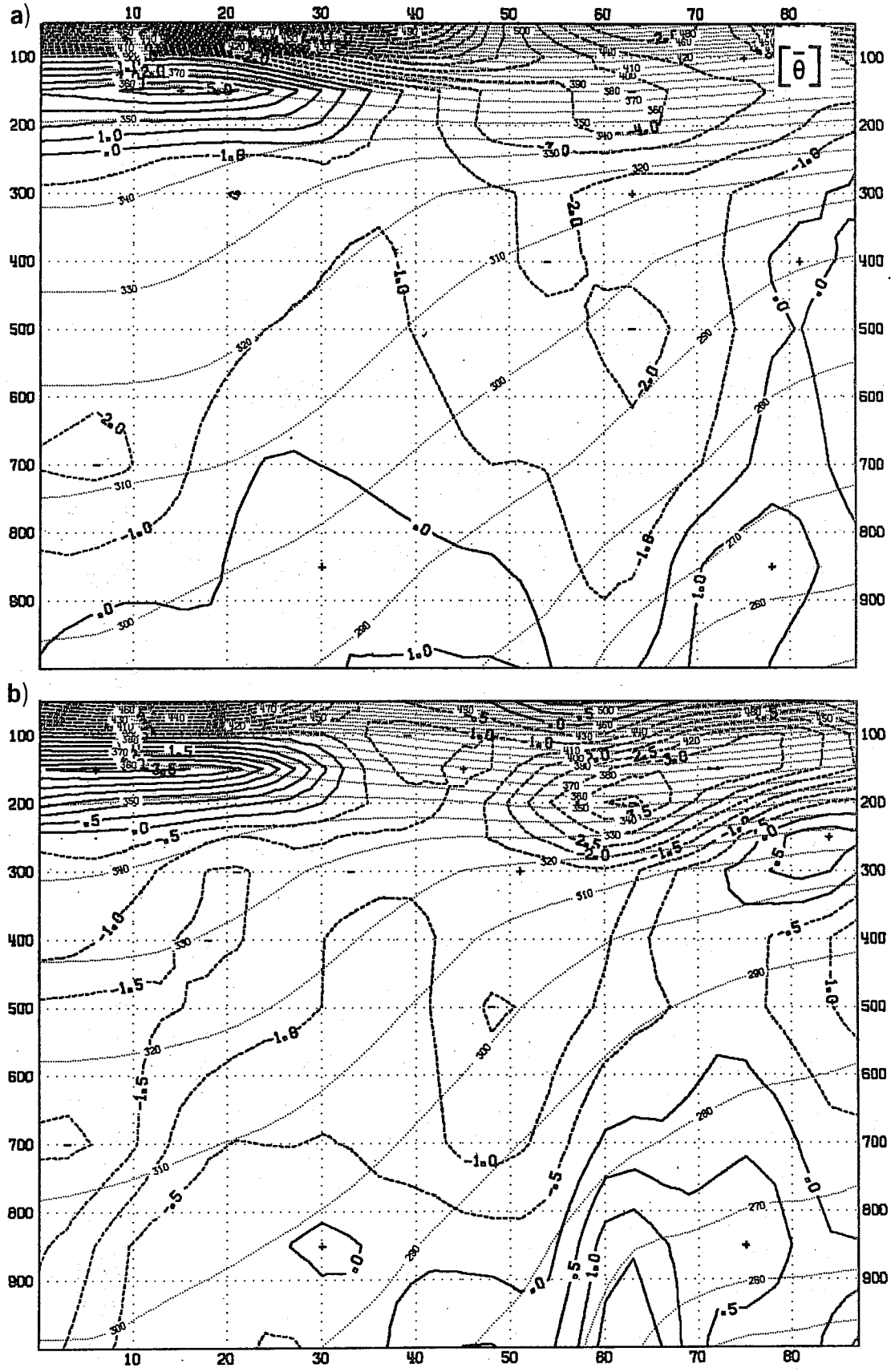

Fig. 41 Latitude height plot of the time mean potential temperature in the initialised analysis (dotted lines) and the difference between the forecast and the analysis (D+3 - D+0, thicker lines). Zonally averaged from 159° W to 120° W. Time averaging period 112 days. Units : K. a)Winter 1980/81, b) Winter 1981/82.

coincide with the two major storm tracks connected with the baroclinic zones on the eastern sides of the continents. In connection with the Atlantic storm track, some disturbances develop over the eastern parts of North America and some penetrate deep into northern parts of Russia. In the following winter the mean frontal zone (see Figs. 6 and 7) is further to the south in the Atlantic region (Fig. 39b) and the high frequency baroclinic waves are found at much lower latitudes. A ridge in the mean flow over northern Europe seems to have blocked the migration of the high frequency waves into the northern parts of Russia for this winter. In the Pacific the baroclinic waves are weaker in 1981/82 than in 1980/81, coinciding with a weaker baroclinicity in the later winter. The geographical distribution of the HFBW's variance depicts the major storm tracks over the oceans. The variance pattern is similar to the bandpass filtered variance in Blackmon and Lau (1980), who considered a period from 2.5 to 6.0 days compared to 2.4 to 3.5 days used here.

In both winters a weakening of the HFBW's in the forecast occurs downstream of the continental regions (Fig. 40). The baroclinicity of the time-mean flow on the eastern coast of both Asia and North America becomes weaker in the forecast. This effect is most pronounced downstream of the North American continent where we found the largest decrease in the baroclinicity (see Fig. 30). The North American error pattern is already established in the difference between the D+1 forecast and the analysis. The latitudinal structure of the time-mean temperature change in the forecast over North America is closely connnected to the changes on the HFBW's in the forecast further downstream.

In the winter 1980/81 the baroclinicity in the forecast is weakening over a broad latitude band from 30°N to 60°N over North America. In this case the HFBW's become weaker in the forecast where we found the maximum variance in

the analyses to the SE of Greenland. In the following winter the major decrease in the horizontal temperature gradient over North America occurs around 36°N (see Fig. 30b). The weakening of the HFBW's is split into two regions on both sides of the analysed variance maximum at 45°N whereby the largest decrease occurs downstream of the large change in the baroclinicity.

In contrast to the change of the time-mean temperature over the continent, the baroclinicty over the North Pacific and North Atlantic is increased (Fig. 41 for the Pacific). Maximum cooling at 60°N and warming or less cooling around 35°N is responsible for this change. The decrease of the baroclinicity on the east coast of Asia and the increase further downstream seems to have a damping effect on the baroclinic waves in the western Pacific and an enhancing one in the east Pacific.

8. SUMMARY AND CONCLUSIONS

Space-time decomposition has been applied to time series of forecast ensembles and of initialized analyses. The calculated power spectrum was then integrated over two regions in the wavenumber-frequency domain which represent the strong baroclinic waves moving eastward with a mean period of 5.3 days (MFBW) and the high frequency baroclinic waves with a period of 2.8 days (HFBW). The three-dimensional structure of these waves was discussed in detail and compared with theory and model simulations.

The main aim of this investigation is to identify the forecast errors which appear as changes of the travelling baroclinic waves. The MFBW's undergo a considerable weakening which amounts to 15% by D+3 and 30% by D+5. The maximum decrease occurs at 300 mb where these waves have maximum amplitudes. The under-forecasting of the upper level wave maximum seems to be a problem for other models as well. Linear theory shows that this might be the consequence of a low resolution near the tropopause. Other contributions

to the weakening of these waves at upper levels may come from the mid-tropospheric cooling, which leads to a stabilisation of the upper troposphere, and secondly from an enhanced barotropic damping associated with inaccurate meridional phase tilts. It seems desirable to test these hypotheses by suitable sensitivity experiments.

The influence of the time-mean flow can be seen very clearly when we compare the geographical disturbution of the time-mean forecast error with the forecast errors of the travelling baroclinic waves. The main centre of weakening of these waves is found over North America, where the baroclinicity of the time-mean flow decreases due to low level warming in high latitudes and upper level cooling in middle latitudes. The second persistent forecast error for the MFBW's occurs over SE Europe, where a significant increase in the variance during the forecast has taken place in three successive winters so far. Stationary troughs over SE Europe in the analyses tend to propagate slowly eastward in the forecast.

The three dimensional phase structure of the baroclinic waves is changed in two important ways during the forecast. In the horizontal the MFBW's increase their SW to NE tilt at low latitudes. Consequently the poleward eddy momentum flux increases in these latitudes and leads to a spurious conversion from eddy kinetic energy to zonal kinetic energy. The interaction of the MFBW's with the tropical flow seems to be responsible for this error. In the vertical the forward tilt of the temperature wave is increased at low levels. This is a forecast error we found for all baroclinic waves.

Cross-spectral analysis between the forecast ensemble and the analysis shows that the baroclinic waves are generally too slow. This can be seen by a growth of the phase lag between forecast and analysis with increasing forecast range. The MFBW's are lagging by around 150 km at day 3 and by

300 km at day 5. Comparative experiments (Girard and Jarraud, 1982) have shown that the phase error is significantly smaller in the ECMWF spectral model (operational since April 1983) than in the gridpoint model.

The high frequency baroclinic waves with a mean period of 2.8 days are weakened at higher and lower latitudes, whereas at middle latitudes a region of over-development in the forecast is seen in the two winters examined here and in the winter 1982/83 as well. The geographical distribution of this forecast error is likely to be closely connnected to the changes in the mean flow. As these waves are faster than the MFBW's their main weakening occurs further downstream from the region were we found a decrease of the baroclinicity. The largest reduction in the variance of the HFBW's during the forecast occurs over the North Atlantic.

A clearly persistent error for all winters is the east-west dipole error structure in the Pacific. A less baroclinic flow near the east Asian coast leads to a weakening of the downstream developments in the west Pacific. Increased baroclinicity over the central Pacific has the effect of a much stronger development of the high frequency baroclinic waves in the eastern part of the Pacific. When these waves decelerate in a later stage of their life cycle they seem to contribute to the negative deviation of the time-mean height of the analysis over Alaska. The forecast error in the time-mean flow contributes to an erroneously large poleward flux of heat over North America. This could explain the decrease in the baroclinicity of the flow over North America, where we find smaller growth rates of the baroclinic waves. However, errors in the diabatic forcing are also very likely to cause that kind of deviations in the mean fields.

The results show a close connection between the errors in the time-mean flow and the errors in the travelling baroclinic waves. However it is still

difficult to be sure which error is the primary one. From our analysis it seems that the different evolution of the baroclinicity over land and ocean is probably the primary error which then cause changes in the baroclinic waves.

The forecast error pattern of the baroclinic waves has only a small inter-annual variation in the northern hemisphere. The largest differences are closely connected to the two main frontal zones and the major storm tracks. So far the detailed examination of forecast errors for the baroclinic has been restricted to the northern hemisphere. The time-spectral computations, however, have been done for the southern hemisphere as well. There we found a much higher inter-annual variability in the geographical distribution of the forecast errors in the scales of baroclinic waves compared to those in the northern hemisphere. In the zonal mean statistics the baroclinic waves of the southern hemisphere are weakened even more than in the northern hemisphere.

Acknowledgements

The wavenumber-frequency analysis of forecast ensembles was proposed by A. Hollingsworth. His helpful suggestions and comments throughout this work are gratefully acknowledged. We are very grateful to K. Arpe for his support during the implementation of the package and for his suggestions for this report. We also wish to thank A. Simmons and R. Riddaway for their comments on the final draft.

REFERENCES

Arpe, K. 1983: Diagnostic evaluation of analysis and forecasts: Climate of the model. ECMWF seminar/workshop on interpretation of numerical weather prediction products, 13-17 September 1982, Reading, England, 99-140.pp.

Bengtsson, L., Kanamitsu, M., Kållberg. P and Uppala, S. 1982: FGGE 4-dimensional data assimilation at ECMWF. Bull.Am.Met.Soc., 63, 29-43.

Blackmon, M.L. and Lau,N.-C. 1980: Regional characteristics of the northern hemisphere wintertime circulation: A comparison of the simulation of the GFDL general circulation model with observations. J.Atmos.Sci., 37, 497-514.

Böttger, H. and Fraedrich, K. 1980: Disturbances in the wavenumber-frequency domain observed along 50°N. Contrib.Atmos.Phys., 53, 90-105.

Charney, J.G. 1947: The dynamics of long waves in a baroclinic westerly current. J.Meteor., 4, 135-162.

Eady, E.T. 1949: Long waves and cyclone waves. Tellus, 1, No.3, 33-52.

Edmon,Jr, H.J., B.J. Hoskins, and M.E. McIntyre, 1980: Eliassen-Palm cross-sections for the troposphere. J.Atmos.Sci., 37, 2600-2616.

Fraedrich, K. and Böttger, H. 1978: A wavenumber-frequency analysis of the 500 mb geopotential at 50°N. J.Atmos.Sci., 35, 745-750.

Girard C. and Jarraud M., 1982: Short and medium range forecast differences between a spectral and grid point model. An extensive quasi-operational comparison. ECMWF Tech.Rep.No.32, 176 pp.

Goodman, N.R., 1957: On the joint estimation of the spectra, cospectrum and quadrature spectrum of a two-dimensional stationary Gaussian process. Sci.Pap.No.10, Engineering Statistics Lab., College of Engineering, New York University.

Green, J.S.A. 1960: A problem in baroclinic instability. Quart.J.Roy.Meteor.Soc., 86, 237-251.

Gall, R. 1976: Structural changes of growing baroclinic waves. J.Atmos.Sci., 33, 374-390.

Haseler, J. 1982: An investigation of the impact at middle and high latitudes of tropical forecast errors. ECMWF Tech.Rep.No.31, 42 pp.

Hartmann, D.L. 1974: Time spectral analysis of mid-latitude disturbances. Mon.Wea.Rev., 102, 348-362.

Hayashi, Y. 1971: A generalized method of resolving disturbances into progressive and retrogressive waves by space Fourier and time cross-spectral analysis. J.Meteor.Soc.Japan, 49, 125-128.

Hayashi, Y. 1974: Spectral analysis of tropical disturbances appearing in a GFDL general circulation model. J.Atmos.Sci., 31, 180-218.

Hayashi, Y. 1979: A generalized method of resolving transient disturbances into standing and traveling waves by space-time spectral analysis. J.Atmos.Sci., 36, 1017-1029.

Hayashi, Y. 1982: Space-time spectral analysis and its applications to atmospheric waves. J.Meteor.Soc.Japan, 60, 156-171.

Hayashi, Y. and Golder, D.G. 1977: Space-time spectral analysis of mid-latitude disturbances appearing in a GFDL general circulation model. J.Atmos.Sci., 34, 237-262.

Hollingsworth, A., Arpe, K. Tiedtke, M., Capaldo, M. and Savijärvi, H. 1980: The performance of a medium-range forecast model in winter - impact of physical parameterizations. Mon.Wea.Rev., 108, 1736-1773.

Hollingsworth, A., Simmons, A.J. and Hoskins, B.J. 1976: The effect of spherical geometry on momentum transports in simple baroclinic flows. Quart.J.Roy.Meteor.Soc., 102, 901-911.

Hoskins, B.J. and Heckley, W.A. 1981: Cold and warm fronts in baroclinic waves. Quart.J.Roy.Meteor.Soc., 107, 79-90.

Julian, P.R. 1975: Comments on the determination of significance levels of the coherence statistic. J.Atmos.Sci., 32, 836-837.

Leith C.E. 1980: Nonlinear normal mode initialization and quasi-geostrophic theory. J.Atmos.Sci., 37, 958-968.

Mechoso, C,R. and Hartmann D.L. 1982: An observational study of traveling planetary waves in the southern hemisphere. J.Atmos.Sci., 39, 1921-1935.

Pratt, R.W. 1976: The interpretation of space-time spectral quantities. J.Atmos.Sci., 33, 1060-1066.

Pratt, R.W. 1977: Space-time kinetic energy spectra in mid-latitudes. J.Atmos.Sci., 34, 1054-1057.

Pratt, R.W. 1979: A space-time spectral comparison of the NCAR and GFDL general circulation models to the atmosphere. J.Atmos.Sci., 36, 1681-1691.

Rossby, C.G. 1939: Relation between variations in the intensity of the zonal circulation of the atmosphere and the displacements of the semi-permanent centres of action. J.Marine Res., 2, 38-55.

Simmons, A.J. 1974: The meridional scale of baroclinic waves. J.Atmos.Sci., 31, 1515-1525.

Simmons, A.J. and Hoskins B.J. 1976: Baroclinic instability on the sphere: Normal modes of the primitive and quasi-geostrophic equations. J.Atmos.Sci., 33, 1454-1477.

Simmons, A.J. and Hoskins B.J. 1978: The life cycles of some nonlinear baroclinic waves. J.Atmos.Sci., 35, 414-432.

Straus, D.M. and Shukla J. 1981: Space-time spectral structure of a GLAS general circulation model and a comparison with observations. J.Atmos.Sci., 38, 902-917.

Temperton,C. and Williamson, D.L. 1979: Normal mode initialization for a multi level grid point model. ECMWF Tech.Rep.No.11. 90 pp.

Wallace, J.M., Tibaldi, S. and Simmons, A.J. 1983: Reduction of systematic forecast errors in the ECMWF model through the introduction of an envelope orography. Quart.J.Roy.Soc., 109, 683-717.

APPENDIX A

Space-time spectral analysis

The travelling disturbances on latitude circles can be expressed in terms of amplitudes and phases of progressive and retrogressive waves

$$W(x,t) = \sum_k W_k(x,t)$$

$$W_k(x,t) = \sum_\omega R_{k,\pm\omega} \cos(kx \pm \omega t + \phi_{k,\pm\omega}) \tag{A1}$$

where k is the wavenumber, ω frequency, $R_{k,\pm\omega}$ amplitude, $\phi_{k,\pm\omega}$ phase of the progressive ($-\omega$) and retrogressive ($+\omega$) waves. The last equation can be rewritten as a sum of space sine and cosine contributions with time dependent coefficients.

$$W_k(x,t) = C_k(t)\cos kx + S_k(t)\sin kx \tag{A2}$$

Following Hayashi (1971) the two sided space-time power spectrum is then

$$P_{\pm\omega} = \frac{1}{2} R^2_{k,\pm\omega}$$

$$= \frac{1}{4} \left\{P_\omega(C_k) + P_\omega(S_k) \pm 2Q_\omega(C_k,S_k)\right\} \tag{A3}$$

where $P_\omega(C_k)$ and $P_\omega(S_k)$ are the power spectra of the cosine and sine coefficients, respectively, and $Q_\omega(C_k,S_k)$ is the quadrature spectrum of the cosine and sine coefficients.

For the computation of the eddy fluxes of heat and momentum we will use the cospectrum between travelling waves of two different parameters like the zonal and meridional wind component for the horizontal eddy momentum flux.

According to Hayashi (1971) the cospectrum between two different kinds of disturbances (W and W') can be calculated from the cospectrum and quadrature spectrum of the cosine and sine coefficients

$$K_{\pm\omega}(W_k,W'_k) = \frac{1}{2} R_{k,\pm\omega}R'_{k,\pm\omega} \cos(\phi'_{k,\pm\omega} - \phi_{k,\pm\omega})$$
$$= \frac{1}{4} \{K_\omega(C_k,C'_k) + K_\omega(S_k,S'_k) \qquad \text{(A4)}$$
$$\pm Q_\omega(C_k,S'_k) \mp Q_\omega(S_k,C'_k)\}$$

and the quadrature spectrum by

$$Q_{\pm\omega}(W_k,W'_k) = \frac{1}{2} R_{k,\pm\omega}R'_{k,\pm\omega}\sin(\phi'_{k,\pm\omega} - \phi_{k,\pm\omega})$$
$$= \frac{1}{4} \{\pm Q_\omega(C_k,C'_k) \pm Q_\omega(S_k,S'_k) \qquad \text{(A5)}$$
$$-K_\omega(C_k,S'_k)+K_\omega(S_k,C'_k)\}$$

With the knowledge of the cospectrum and quadrature spectrum between the two travelling waves we can compute their phase difference.

$$\phi'_{k,\pm\omega} - \phi_{k,\pm\omega} = \tan^{-1} \{Q_{\pm\omega}(W_k,W'_k)/K_{\pm\omega}(W_k,W'_k)\} \qquad \text{(A6)}$$

The quality of our phase calculation can be measured in terms of coherence between the two waves.

$$\text{coh}^2_{\pm\omega}(W_k,W'_k) = \frac{K^2_{\pm\omega}(W_k,W'_k) + Q^2_{\pm\omega}(W,W'_k)}{P_{\pm\omega}W_k)P_{\pm\omega}(W'_k)} \qquad \text{(A7)}$$

A value close to 1 for the coherence indicates a reliable determination of the phase difference.

In practice the time spectra were calculated by the Fast Fourier Transform method. The basic time-spectral interval for the analysis and forecast ensemble dataset is 1/112 days. For the discussion of the baroclinic waves the spectrum was integrated over two spectral bands. The medium frequency band contains 21 spectral intervals and the high frequency band 17 intervals. The limiting coherence to reject a null hypothesis of zero coherence at the 95% level can be calculated by a formula proposed by Julian (1975).

$$\beta^2 = 1 - (1-p)^{\frac{1}{n-1}} \qquad \text{(A8)}$$

When we assume that the actual coherence is zero we will find with a given probability p that a coherence of β or larger will be found depending on how many effective Fourier coefficients n (number of degrees of freedom) are present in the spectral band. The coherence between two disturbances in the medium frequency band should be above .37 and in the high frequency band above .41 in order to have significant spectral estimates. When the vertical structure of the baroclinic waves is looked at in a latitude band a further integration over 8 latitude circles is carried out. This increases the number of effective Fourier harmonics by a factor of 8 and the necessary coherence for significant results drops to 0.13 in the medium frequency and 0.15 in the high frequency band. Goodman (1957) showed that an estimate of the possible phase error can be calculated from

$$\sin^2(\Delta\phi) = \frac{1-\mathrm{coh}^2}{\mathrm{coh}^2} \left\{ (1-p)^{-\frac{2}{n}} - 1 \right\} \qquad \text{(A9)}$$

For an assumed coherence of 0.95 this calculation gives phase errors of 11 to 12 degrees in the frequency integrated bands and about 4 degrees in the case

where an additional averaging over 8 latitudes has been carried out. However, these error estimates seem to be too high, as we found a close agreement between the fluxes calculated from the mean amplitude and mean phase difference of two waves (first part of equation A4) and from the sum of the co- and quadrature spectra (second part of equation A4). An exception was found for the computation of the horizontal eddy momentum flux where a very low coherence between the zonal and meridional wind component makes it impossible to determine the phase difference between the two variables.

The spatial variation of the time amplitude of transient disturbances can be calculated by using a method proposed by Hayashi (1979). The space-time series of the data are filtered in space by a zonal Fourier decomposition. For the wavenumber range of interest the spatial values on the selected latitudes are calculated

$$C(x,t) = \sum_k C_k(t)\cos kx + S_k(t)\sin kx$$

$$= \sum_k A_k(t)\cos\,[-kx+\phi_k(t)] \qquad \text{(A10)}$$

$$S(x,t) = \sum_k -C_k(t)\sin kx + S_k(t)\cos kx$$

$$= \sum_k A_k(t)\sin[-kx + \phi_k(t)]$$

and a time cross-spectral analysis is carried out using the Fast Fourier Transform method at each gridpoint (x) on that latitude.

APPENDIX B

Diagnostic formulae

For the discussion of the vertical structure of the baroclinic waves some very useful diagnostic formulae have been derived which show the hydrostatic and geostrophic relationship of some variables. Assuming that the wave structure for a fixed time is given by

$$\psi(x,y,p) = \psi_o(y,p)\ \cos[kx - \phi_\psi(y,p)]$$

where $\psi_o(y,p)$ is the amplitude and $\phi_\psi(y,p)$ is the phase of either of the variables Z, T, u, v or ω. Substituting the wave form of the geopotential height and the temperature into the hydrostatic equation we get an equation

$$\frac{\partial Z_o}{\partial(\ell np)} = \frac{R}{g} T_o \cos(\phi_T - \phi_Z) \qquad \text{(B1)}$$

which relates the vertical change of the geopotential height wave to the amplitude of the temperature wave and to the cosine of the phase difference between Z and T.

From the thermal wind equation we find that the vertical change of the meridonal wind amplitude is proportional to the amplitude of the temperature wave and the sine of the phase difference between T and v.

$$f \frac{\partial V_o}{\partial(\ell np)} = -RT_o k \sin\ (\phi_T - \phi_V) \qquad \text{(B2)}$$

Any form of horizontal or vertical eddy flux can be written as

$$\overline{\beta'\gamma'} = \frac{1}{2} \beta_o \gamma_o \cos\ (\phi_\beta - \phi_\gamma) \qquad \text{(B3)}$$

Using the geostrophic wind approximation we find that the horizontal eddy momentum flux

$$\overline{v'_g u'_g} = \frac{kg^2}{2f^2} z_o^2 \frac{\partial \phi_Z}{\partial y} \tag{B4}$$

depends on the horozontal phase tilt of the geopotential wave and the horizontal eddy heat flux

$$\overline{v'_g T'} = \frac{kg^2}{2fR} \frac{\partial \phi_Z}{\partial (\ell np)} \tag{B5}$$

depends on the vertical tilt of the geopotential height wave.

ECMWF PUBLISHED TECHNICAL REPORTS

No. 1 A Case Study of a Ten Day Prediction

No. 2 The Effect of Arithmetic Precisions on some Meteorological Integrations

No. 3 Mixed-Radix Fast Fourier Transforms without Reordering

No. 4 A Model for Medium-Range Weather Forecasting - Adiabatic Formulation

No. 5 A Study of some Parameterizations of Sub-Grid Processes in a Baroclinic Wave in a Two-Dimensional Model

No. 6 The ECMWF Analysis and Data Assimilation Scheme - Analysis of Mass and Wind Fields

No. 7 A Ten Day High Resolution Non-Adiabatic Spectral Integration: A Comparative Study

No. 8 On the Asymptotic Behaviour of Simple Stochastic-Dynamic Systems

No. 9 On Balance Requirements as Initial Conditions

No.10 ECMWF Model - Parameterization of Sub-Grid Processes

No.11 Normal Mode Initialization for a multi-level Gridpoint Model

No.12 Data Assimilation Experiments

No.13 Comparison of Medium Range Forecasts made with two Parameterization Schemes

No.14 On Initial Conditions for Non-Hydrostatic Models

No.15 Adiabatic Formulation and Organization of ECMWF's Spectral Model

No.16 Model Studies of a Developing Boundary Layer over the Ocean

No.17 The Response of a Global Barotropic Model to Forcing by Large-Scale Orography

No.18 Confidence Limits for Verification and Energetics Studies

No.19 A Low Order Barotropic Model on the Sphere with the Orographic and Newtonian Forcing

No.20 A Review of the Normal Mode Initialization Method

No.21 The Adjoint Equation Technique Applied to Meteorological Problems

No.22 The Use of Empirical Methods for Mesoscale Pressure Forecasts

No.23 Comparison of Medium Range Forecasts made with Models using Spectral or Finite Difference Techniques in the Horizontal

No.24 On the Average Errors of an Ensemble of Forecasts

No.25 On the Atmospheric Factors Affecting the Levantine Sea

No.26 Tropical Influences on Stationary Wave Motion in Middle and High Latitudes

ECMWF PUBLISHED TECHNICAL REPORTS

No.27 The Energy Budgets in North America, North Atlantic and Europe Based on ECMWF Analyses and Forecasts

No.28 An Energy and Angular-Momentum Conserving Vertical Finite-Difference Scheme, Hybrid Coordinates, and Medium-Range Weather Prediction

No.29 Orographic Influences on Mediterranean Lee Cyclogenesis and European Blocking in a Global Numerical Model

No.30 Review and Re-assessment of ECNET - a private network with Open Architecture

No.31 An Investigation of the Impact at Middle and High Latitudes of Tropical Forecast Errors

No.32 Short and Medium Range Forecast Differences Between a Spectral and Grid Point Model. An Extensive Quasi-Operational Comparison

No.33 Numerical Simulations of a Case of Blocking: The Effects of Orography and Land-Sea Contrast

No.34 The Impact of Cloud Track Wind Data on Global Analyses and Medium Range Forecasts

No.35 Energy Budget Calculations at ECMWF: Part I: Analyses

No.36 Operational Verification of ECMWF Forecast Fields and Results for 1980-1981

No.37 High Resolution Experiments with the ECMWF Model: A Case Study

No.38 The Response of the ECMWF Global Model to the El-Nino Anomaly in Extended Range Prediction Experiments

No.39 On the Parameterization of Vertical Diffusion in Large-Scale Atmospheric Models

No.40 Spectral Characteristics of the ECMWF Objective Analysis System

No.41 Systematic Errors in the Baroclinic Waves of the ECMWF Model